CHARACTERIZATION OF THE [FEFE]-HYDROGENASE: TOWARD UNDERSTANDING AND IMPLEMENTING BIOHYDROGEN PRODUCTION

by

Kevin Daniel Swanson

A dissertation submitted in partial fulfillment
of the requirements for the degree

of

Doctor of Philosophy

in

Biochemistry

MONTANA STATE UNIVERSITY
Bozeman, Montana

November 2014

TABLE OF CONTENTS

TABLE OF CONTENTS CONTINUED

TABLE OF CONTENTS CONTINUED

LIST OF TABLES

LIST OF FIGURES

Figure Page

LIST OF FIGURES – CONTINUED

Figure Page

LIST OF FIGURES – CONTINUED

Figure Page

ABSTRACT

Hydrogen may provide an avenue for a clean renewable fuel source, yet the methods to produce hydrogen are either extremely energy intensive, rely on fossil fuels, or require expensive noble metal catalysts. Biology may hold the keys necessary to unlocking new technologies that could change how hydrogen is produced. Microbial processes also produce hydrogen and harbor enzymes that carryout the reversible reduction of protons to hydrogen gas. These enzymes are capable of producing hydrogen at high rates comparable to platinum catalysts, but biological hydrogen catalysts can produce hydrogen using abundant elements carbon, oxygen, nitrogen, sulfur, iron, nickel and selenium. Biological hydrogen catalysts are termed hydrogenases, and though hydrogenases use abundant elements they are extraordinarily complex. This has made it difficult to construct model complexes using inorganic synthesis that can replicate the activities of their biological counterparts. One way to circumvent this problem is to use microbial hydrogen production and let microbes produce and maintain these enzymes inside a cell. Microbial hydrogen production also has the added benefit that hydrogen production could be engineered to connect with other metabolic processes such as photosynthesis and fermentation. Engineering microbes for hydrogen production could eventually allow for the production of hydrogen using inexpensive energy inputs such as solar energy or waste materials. Yet, there are many barriers that need to be overcome in order to engineer a robust microbial organism. One of the primary difficulties of developing this technology has been the oxygen sensitivity of hydrogenases. Hydrogenases when exposed to atmospheric concentrations of oxygen either completely inactivate or their rates are significantly slowed. To engineer a hydrogenase that is more amenable for microbial hydrogen production, the optimization of expressing and purifying hydrogenase enzymes has been developed. Methodologies have been developed to characterize how oxygen inactivates hydrogenase enzymes, and a new methodology has been explored to help find novel hydrogenase gene sequences that may help in engineering oxygen tolerant enzymes.

CHAPTER 1

INTRODUCTION

Alternative Energy

Roughly 85% of the world's energy is supplied by some form of fossil fuel and 15% comes from alternative energy sources (Figure 1.1) (1, 2). An alternative energy source can be considered any source of energy that isn't a fossil fuel. In order to maintain a healthy world economy, alternatives to fossil fuels will need to be found and development of new technologies to improve the production and usage of alternative

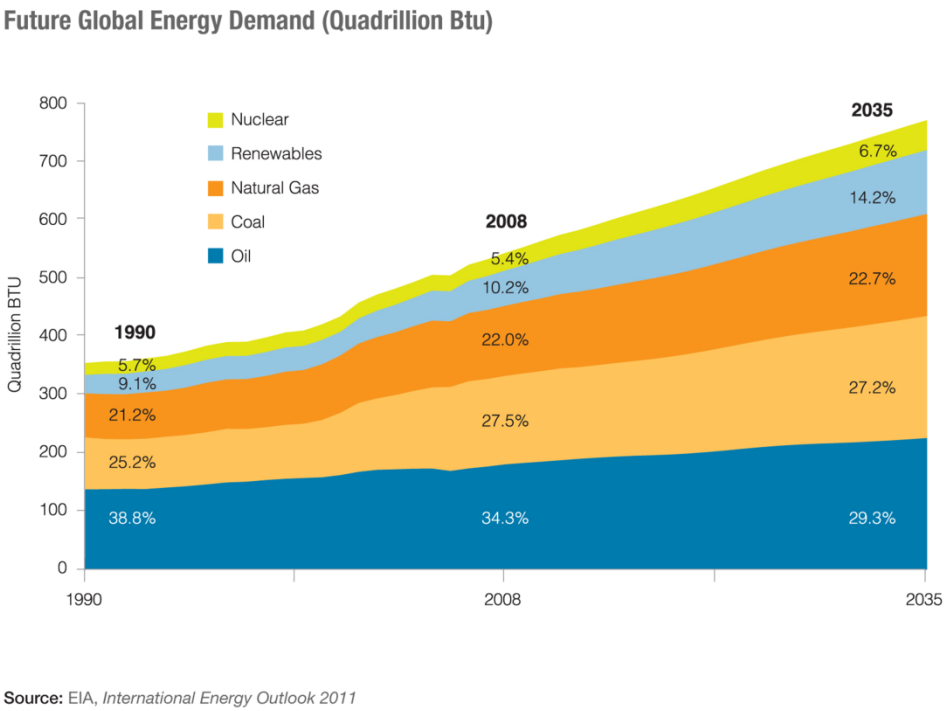

Figure 1.1. The trends in use of nuclear, renewable, natural gas, coal, and oil for energy. Alternative energy takes up roughly 15% of the total energy portfolio in 2008, including nuclear energy, with it projected to increase by ~7% in 2035. From (2).

energy sources will be necessary. The main alternatives to fossil fuels are hydroelectric, nuclear, geothermal, wind, solar, tidal, and bio-(diesel, ethanol, and hydrogen) with hydroelectric taking up the largest percentage of total renewable energy output, but with alternative energy only taking up 10-15 % of our current energy portfolio, it is evident that more technologies need to be developed and improved to increase this percentage (1, 2).

Out of the above mentioned alternative energy sources, solar energy is considered to be the most abundant energy source. It is estimated that in two weeks, the surface of the earth receives the energy that is equal to the total energy that is present in the entire world's fossil fuel deposits (10^{16} kW) (3). The Department of Energy (DoE), USA, predicted that if the solar irradiance of 1% of the Earth's surface is converted into storable energy with 10% efficiency, it would provide 105 TW of energy that is equal to the several times of the estimated world energy requirement in the year 2050 (3, 4). When comparing solar output to the other forms of alternative energy, the amount of energy that could be extracted in the same year 2050 from wind, tides, biomass, and geothermal would be 2–4 TW, 2–3 TW, 5–7 TW, and 3–6 TW, respectively, (4, 5). A large issue with the majority alternative energy forms is they aren't continuous forms of energy with the exception of geothermal. Even though, solar energy is a large enough supply of energy; it is not available in the nights and on the cloudy days. Hence, to supply solar energy continuously, a method to store it is required (6). However, most of the solar energy storage methods developed so far possess very low energy densities or are expensive (7). The energy density by mass of compressed air (200 atm), batteries,

flywheels, supercapacitors, H2O pumped 100 meters uphill are estimated to be ~0.1 $MJkg^{-1}$, ~0.1–0.5 $MJkg^{-1}$, ~0.5 $MJkg^{-1}$, ~0.01$MJkg^{-1}$, and ~0.005-0.007 $MJkg^{-1}$, respectively (7-9). Although several technologies including photovoltaic (PV) cells, Peltier (Seebeck) modules, Fresnel lenses, concentrated solar radiation, solar thermal energy, dye-sensitized solar cells (DSSCs), etc., have already been developed for converting solar light into electricity (10). There is a discontinuity between solar irradiation and power consumption during the year, and in terms of geographical distribution. The same is true even for wind and tide based energy resources. Therefore, it is required to find a suitable method to covert, store, and transport alternative energy in a suitable manner (7-9).

Hydrogen

Hydrogen is the most abundant element in the universe and is the simplest element consisting of one proton and one electron. Hydrogen (hydrogen gas or dihydrogen) is a colorless, odorless, and highly combustible diatomic gas. It is composed of two covalently bonded hydrogen atoms sharing two 1s electrons. This covalent bond has a high bonding energy of 436 kJ mol^{-1} and when hydrogen combusts it forms water and heat as a byproduct during combustion. Hydrogen gas is uncommon as it readily oxidizes and it can escape the atmosphere since it has a low molecular weight (11). Hydrogen atoms are more commonly found in molecules such as water and hydrocarbons. This means that to attain hydrogen gas it must be generated from chemical processes (12).

Hydrogen as an Energy Storage Molecule.

A possible solution to energy conversion and storage of alternative energy has been to store energy in the form of chemical energy such as converting alternative energy into hydrogen gas. Hydrogen has the highest energy content per unit mass than any other fuel owing to its high bond energy and low molecular weight. Hydrogen has ~2.8 times more energy per mass when compared to gasoline (3). Hydrogen is also relatively inert in pure form allowing storage for extended periods of time with little decomposition (12). Yet, using hydrogen as a means for energy storage currently faces significant drawbacks since it has a low ignition energy, it has a low energy density, it's prone to leak, and it brittles metals. These properties of hydrogen require it to have special storage considerations and make the infrastructure for hydrogen more expensive than standard liquid fuels like oil and gasoline (13-18).

Standard fuels such as gasoline, diesel, and natural gas have a larger and more developed infrastructure for storage and transport and their use is already been proven to be relatively safe. The benefits for hydrocarbon liquid fuels is they have a higher energy density, even compared to hydrogen in its liquid state, and they have the added benefit that they are simpler to store since they don't have to be maintained at cryogenic temperatures. Hydrogen's low molecular weight makes it a very low energy density fuel, and when compared to liquid methane and gasoline it is about a 2.5 times and 3.7 times less energy dense respectively (3). The energy densities of hydrogen and electrical storage are far lower than liquid fuels based on fossil or renewable (biomass) sources (3). Thus, it may be more practical to continue to -utilize liquid fuels with high energy

density. This makes sense because liquid fuels produced by green methods can be directly employed in place of fossil fuels used today (17).

Hydrogen Chemical Transformations for Energy Use.

Hydrogen will likely play a pivotal role in decreasing our reliance on fossil fuels, yet it is uncertain whether hydrogen itself will replace fossil fuels for use in transportation and electricity generation. Hydrogen can be transformed into chemical forms that may make more amenable for use as an energy storage agent and possible fuel (3). It is well known that hydrogen can react with metals and form metal hydrides converting gaseous hydrogen to a solid state. Metal hydride fuel cells have an advantage over storing hydrogen as liquid or compressed gas in that they have a lower operating energy, or it takes more energy to compress or liquefy hydrogen than it takes to make metal hydrides and later desorb the hydrogen using a small amount of heat (19). This technology is currently limited by the low percent weight ratio of hydrogen in the material. The amount of hydrogen absorbed in metal hydrides currently is much less than that in liquid hydrogen per weight (12, 19). Metal hydrides fuel cells of comparable energy content to a full tank of gas are also heavy about 2-3 times heavier (12).

Another alternative way to store energy captured in the form of hydrogen is to convert hydrogen into liquid fuels such as diesel, methanol, and gasoline. Hydrogen and carbon monoxide (syngas) can be converted to liquid fuel by the Fisher-Tropsch process $(2n + 1)H_2 + nCO \rightarrow C_nH_{(2n+2)} + nH_2O$ (Figure 1.2) (20). Diesel, methanol, and gasoline are obtained by refining a mixture of hydrocarbons that are produced from syngas in the

Fischer-Tropsch process. This process is currently used in several refineries where crude oil is scarce and carbon monoxide and hydrogen (syngas) can be obtained by coal gastrification (20). Methanol produced can be directly burned in gasoline powered engines as a gas methanol blend without any modifications or it can be further reacted to form gasoline (21, 22). The Mobil process converts methanol to gasoline by the conversion of methanol to dimethyl ether then dimethyl ether is converted to ethylene, and ethylene is converted to gasoline (Figure 1.2)(23).

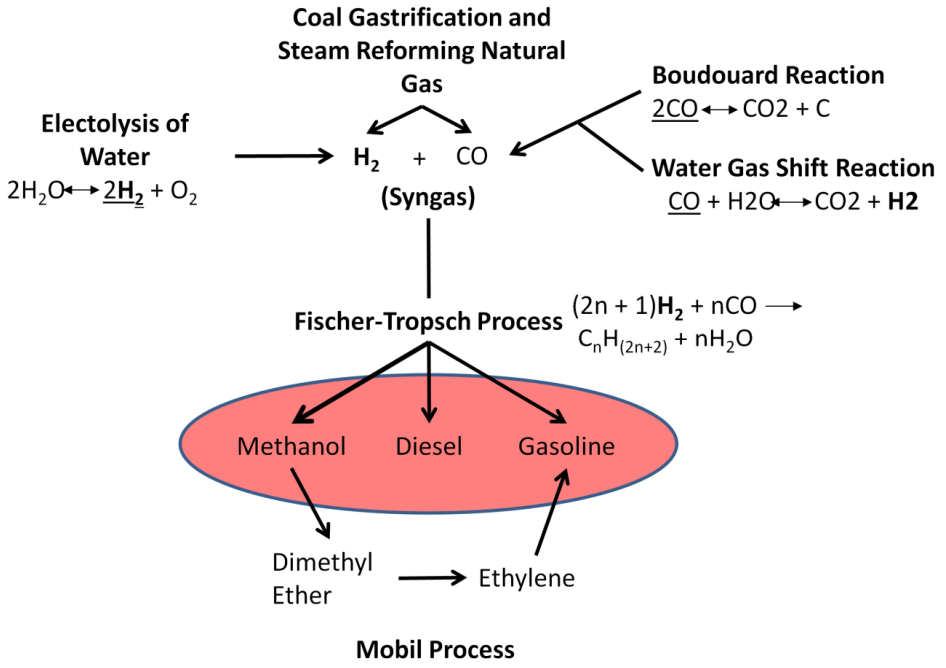

Figure 1.2. Important industrial chemical transformation processes involving hydrogen

Hydrogen Production

Approximately 449.3 billion m^3 of hydrogen is produced annually in the world (24). Hydrogen can be produced in a number of ways, but industrially the main and the most cost effective method is steam reformation of natural gas and is where ~50% of

hydrogen produced comes from (Figure 1.3) (25). This is an energy intensive process involving two reactions. The first reaction occurs between 700 °C and 1100 °C and is an endothermic reaction. Water vapor reacts with natural gas at high temperatures to produce syn gas (heat + CH_4 + $H_2O_{(g)}$ → CO + $3H_2$). The second reaction is exothermic and requires the temperature to be lowered to 360 °C, and water vapor reacts with CO producing CO_2 and H_2 (CO + $H_2O_{(g)}$→CO_2 + H_2) (Figure 1.2) (26). Some other methods that can produce hydrogen are solar gasification, thermo-chemical gasification, electrolysis of water and biohydrogen production (27). The ideal way to produce hydrogen would be from the splitting of water into hydrogen and oxygen, but the energy cost makes this method undesirable (Figure 1.3) (25). Biohydrogen production is recognized for possibly being a future low energy and carbon neutral method for

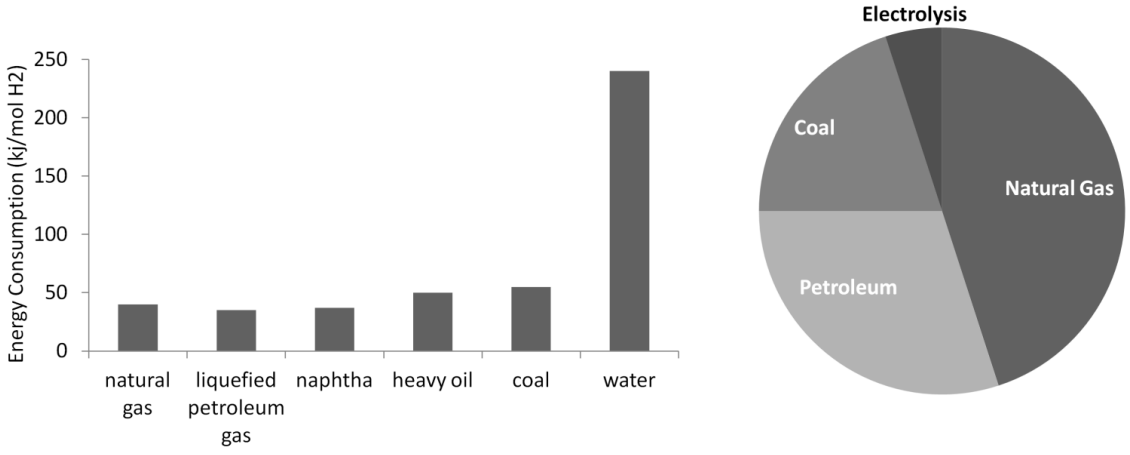

Figure 1.3. Bar graph shows a comparison of the energy input required to produce hydrogen from various feedstocks. Hydrogen production from water poorly competes with fossil fuels due to the high energy required to split water. Pie chart illustrates the percentage of use for each of the major feedstocks for hydrogen production. Adapted from (25).

producing hydrogen since biological enzymes can efficiently produce hydrogen by reducing dissociated protons in water (28-30).

Other Applications for Hydrogen

The majority of hydrogen produced is used in industrial processes. The primary applications for hydrogen are the production of ammonia, petroleum processing, and the production of methanol (31). The majority of hydrogen produced (50%) is used in the Haber Bosch process to fix nitrogen to produce ammonia primarily for use in fertilizers (31). Hydrogen is an important component of petroleum processing and it is used for processes such as hydrocracking that produces small chain saturated hydrocarbons to make jet fuel and diesel (31). The last main application for hydrogen is its use in methanol production. Hydrogen can be combined with carbon monoxide at high pressures and temperatures to produce methanol (31). Other noteworthy uses for hydrogen include oil and fat hydrogenation, shielding gas in welding, cyrogenics, rocket fuel, production of hydrochloric acid, and hydrogen fuel cells (19, 31, 32).

Biological Hydrogen Production

Biological hydrogen production is possible from microorganisms that harbor hydrogenase enzymes that are capable of catalyzing the reduction of protons to hydrogen gas. Hydrogenase enzymes are utilized in many different metabolic and regulatory roles in microorganisms, but significant interest has developed in microbes capable of evolving hydrogen gas. Two prominent modes of microbial hydrogen production are

biophotolysis and dark-fermentation. These processes are of interest since they provide a method to produce hydrogen from renewable resources. No commercial processes are available for microbial hydrogen production to date (30).

Biophotolysis

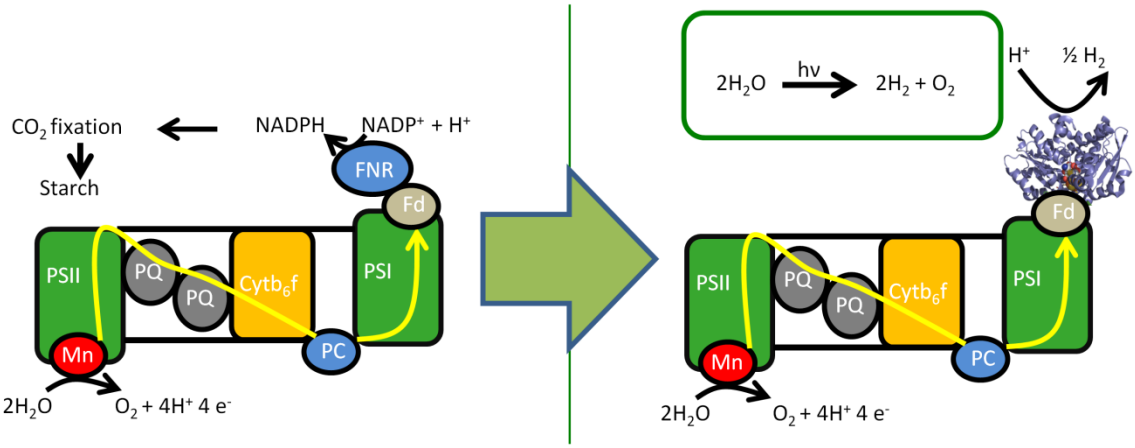

Figure 1.4. Schematics of photosynthesis in green algae used for carbon fixation left and hydrogen production right. Mn is the oxygen evolving complex, PSII is photosystem II, PQ is plastoquinone , $Cytb_6f$ is cytochrome b_6f complex, PC is plastocyanin, PSI is photosystem I, Fd is ferredoxin, FNR is ferredoxin $NADP^+$ reductase, and the cartoon figure represents the [FeFe]-hydrogenase. The schematic on the left represents the general pathway for photosynthesis in green algae e.g. *Clamydomonas reinhardtii*. The schematic on the right represents an idealized pathway for hydrogen production were electrons from water are energized by light and transferred onto protons to produce hydrogen. Modified from (33).

Green algae can carryout photobiological hydrogen production. They are capable of photosynthetically generating reductants using light and water by means of photosynthetic machinery to subsequently reduce protons to hydrogen gas using hydrogenase enzymes in the reaction: $2H_2O$ + light → $2H_2 + O_2$ (Figure 1.4) (30). Conversion efficiencies of up to 22% have been observed for thin films of the green algae *Chlamydomonas reinhardtii* under low light conditions and O_2 (34). In large batch

cultures light to hydrogen conversion efficiencies have only approached 1%, and for this process to be economically viable it has been proposed that efficiencies need to reach 10% (35). This type of system is limited due to the O_2 intolerance of the hydrogenase enzymes found in green algae and light saturation of the photosynthetic antennae causing low energy conversion efficiencies and self shading (34). These limitations may be overcome by developing mutants with reduced antenna sizes and engineering or finding an O_2 tolerant hydrogenase (36).

Darkfermentative

Dark-fermentative production of hydrogen may be a more viable method to produce hydrogen in the near future. Developing a fermentative process for hydrogen production may be easily adapted from industrial scale fermentative processes and from well developed bioreactor technologies that already exist. This process may also be more desirable since it can be done anaerobically, which would make the oxygen sensitivity of hydrogenase enzymes less of a concern (30).

In this process sugars are metabolized in glycolysis and electrons are shuttled into the pyruvate ferredoxin oxidoreductase pathway (PFOR), pyuvate formate lyase pathway (PFL), NADH ferredoxin oxidoreductase pathway (NFOR), to the H_2 bifurcating [FeFe]-hydrogenase (Fd-NADH [FeFe] Figure 1.5), or to the hnd [FeFe]-hydrogenase (NADH-[FeFe] Figure 1.5) depending on the organism (29, 30, 37, 38). *Clostridial* and some thermophilic bacteria contain all the above mentioned ways to produce H_2 except the PFL pathway (29). In the PFOR pathway, pyruvate is oxidized by pyruvate ferredoxin

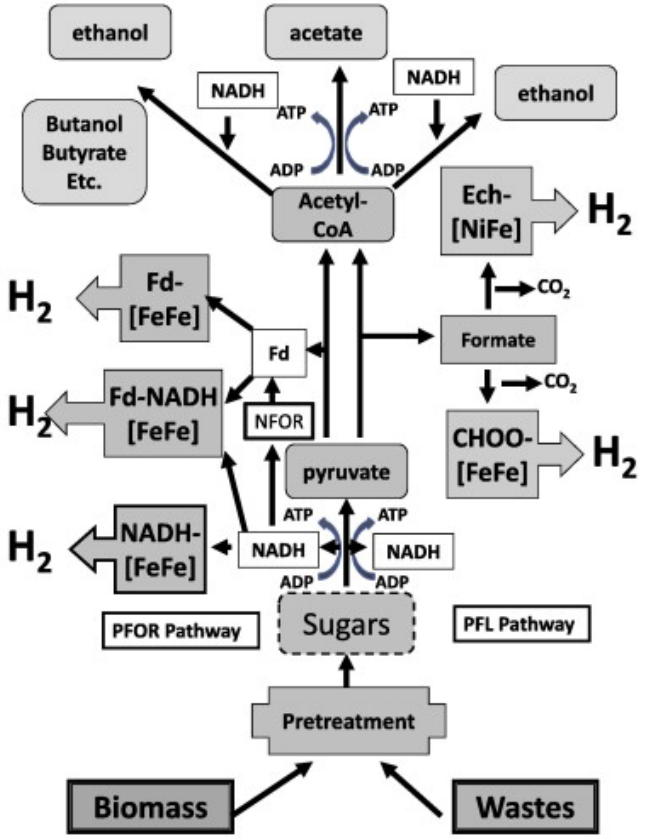

Figure 1.5. Schematic of anaerobic hydrogen producing fermentation pathways from (29). Waste material can be treated to produce sugars that can feed into central metabolism which can then feed into the PFOR pathway, PFL pathway, NADH be directly used to produce hydrogen, or NADH can be used to reduce ferredoxin by NFOR.

oxidoreductatse transferring electrons to ferredoxin, which subsequently reduces an [FeFe]-hydrogenase allowing hydrogen production. In the NFOR pathway, electrons are transferred from NADH to ferredoxin by ferredoxin oxidoreductase. The NADH bifurcating hydrogenase can obtain electrons from NADH and ferredoxin, and the hnd [FeFe]-hydrogenase can directly oxidze NADH and produce hydrogen (37). Lastly the PFL pathway found in facultative anaerobs such as *Escherichia coli*, pyruvate is converted to formate and acytel-CoA by pyruvate formate lyase (PFL). Then formate is

converted to CO_2 and H_2 by formate hydrogen lyase complex (FHL) (Figure 1.5) (29, 30).

Glucose has a theoretical yield of 12 mol of hydrogen per mol of glucose. Facultative anaerobs such as *E. coli* can only produce a maximum of 2 mol of hydrogen. *Clostridial* species can theoretically produce 4 mol of glucose since they can access electron in NADH for hydrogen production. These energy yields are comparatively low compared to other biofuel producing syetems, and in order for hydrogen production from dark fermentation to become a tractable biofuel producing system work needs to be done to increase the yield of hydrogen produced (29, 30).

Hydrogenase

Hydrogenases are enzymes that can catalyze the reversible production of hydrogen. These enzymes are often classified into three types based off their active site metal content (Figure 1.6), physiology, and phylogenetic history: [FeFe]-hydrogenase, [NiFe]-hydrogenase, and [Fe]-hydrogenase. [Fe]-hydrogenases are a unique class and will be discussed briefly (39). [Fe]-hydrogenases are only found in a small group of methanogenic archaea (40). The [Fe]-hydrogenase performs a different reaction than [NiFe]- and [FeFe]- hydrogenases in that it catalyzes the reversible reduction of N^5,N^{10}-methyltetrahydromethanopterin ($CH–H_4MPT^+$) with H_2 to N^5,N^{10}-methylenetetrahydromethanopterin ($CH_2=H_4MPT$) and a proton ($CH–H_4MPT^+ + H_2 \rightleftharpoons CH_2=H_4MPT + H^+$) (40). The [Fe]-hydrogenase class of enzymes has little significance

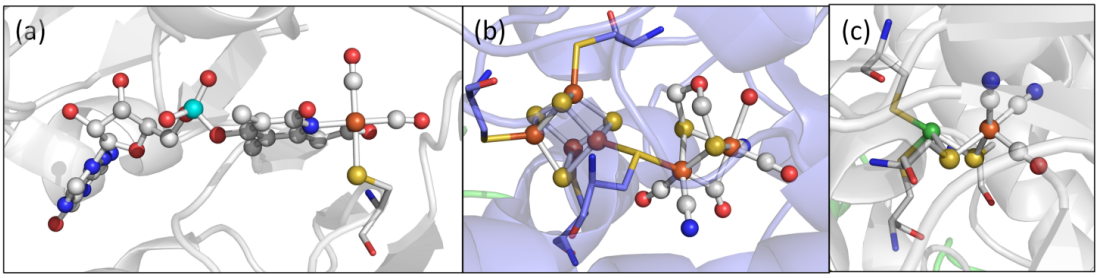

Figure 1.6. Close-up view of the active sites of the (a) [Fe]- (pdb 3F47), (b) [FeFe]- (pdb 3C8Y), and (c) [NiFe]-hydrogenase (pdb 1YRQ). Atoms labeled as: carbon (grey), oxygen (red), nitrogen (blue), sulfur (yellow), phosphorus (cyan), iron (rust), and nickel (green). For (b), the central atom of the dithiolate was later confirmed to be nitrogen since the submission of this crystal structure (41).

for hydrogen production applications (29, 30). [FeFe]-hydrogenases and [NiFe]-hydrogenases are considered true hydrogenases and are considered important for investigation for hydrogen production applications (30). These two classes enzyme carry out the reversible production of hydrogen from protons ($2H^+ + 2e^- \rightleftharpoons H_2$) (30). The hydrogenase enzyme classes are evolutionary unrelated and their primary amino acid sequences are distinct, yet similar structural features exist among the three enzyme classes (39). All three hydrogenase classes contain a redox inactive low-spin iron that is ligated by five or six ligands arranged as a distorted square pyramid or octahedron (Figure 1.6) (42, 43). The ligand found in hydrogenases enzymes include CO, CN^-, or pyridinol and these ligands are all π-accepting ligands oriented cis to each other (42, 43). Also a thiolate sulfur coordinates the iron trans to a diatomic molecule in all three classes of hydrogenase (42, 43). Each hydrogenase has one low spin iron center that interacts with a redox active substituent, which are methenyl-H4MPT+ in the [Fe]-hydrogenase, the distal iron in the [FeFe]-hydrogenase, and nickel in the [NiFe]-hydrogenase (42, 43). CO and CN^- active site ligands are required for hydrogen catalysis, and each class of

hydrogenase has evolved different biosynthesis pathways for incorporating these ligands (44).

[FeFe]-hydrogenases.

[FeFe]-hydrogenases are often found in bacteria (e.g. *Clostridium pasteurianum*) and lower eukaryotes (e.g. *Chlamydomonas reinhardtii*) (39). [FeFe]-hydrogenases can exist as either monomers or heteromers, and they typically contain a varying number of accessory iron-sulfur clusters (F-clusters) that shuttle electrons to or from the active site termed the H-cluster (Figure 1.7) (45, 46). [FeFe]-hydrogenase are classified based off their subunit composition due to hydrogen producing enzymes being the only form of [FeFe]-hydrogenase that has been characterized in depth structurally and biochemically. [FeFe]-hydrogenases are assigned M, D, TR, and TE, which represent monomeric, dimeric, trimeric, and tetrameric forms respectively (39, 47).

Four crystal structures are available for the mature form of the [FeFe]-hydrogenase class of enzymes. There are three structures for the four domain [FeFe]-hydrogenase from *Clostridium pasteurianum* (Cp1) and one structure for the heterodimeric *Desulfovibrio desulfuricans* (DdH) (45, 46, 48, 49). The crystal structure from *C. pasteurianum* was the first to elucidate the complex nature of the active site H-cluster of the [FeFe]-hydrogenase (46). Later crystal structure of Cp1and DdH helped in assignment of the complex arrangement of ligands associated with the H-cluster (45, 49). The active site of the [FeFe]-hydrogenase is composed of a [4Fe-4S] cubane bridged by a cysteine to a [2Fe] subcluster. The proximal iron of the [2Fe] subcluster is coordinated by one CN^- ligand and one CO ligand and is bridged by one carbon monoxide and a

dithiolate ligand to the distal Fe. The distal Fe is further coordinated by one CO ligand and one CN^- ligand in the oxidized state (Figure 1.6) (45, 46, 50). Hyperfine sublevel correlation spectroscopy (HYSCORE) and density functional theory (DFT) calculations indicate that the dithiolate bridge is dithiomethylamine (41). Further support for

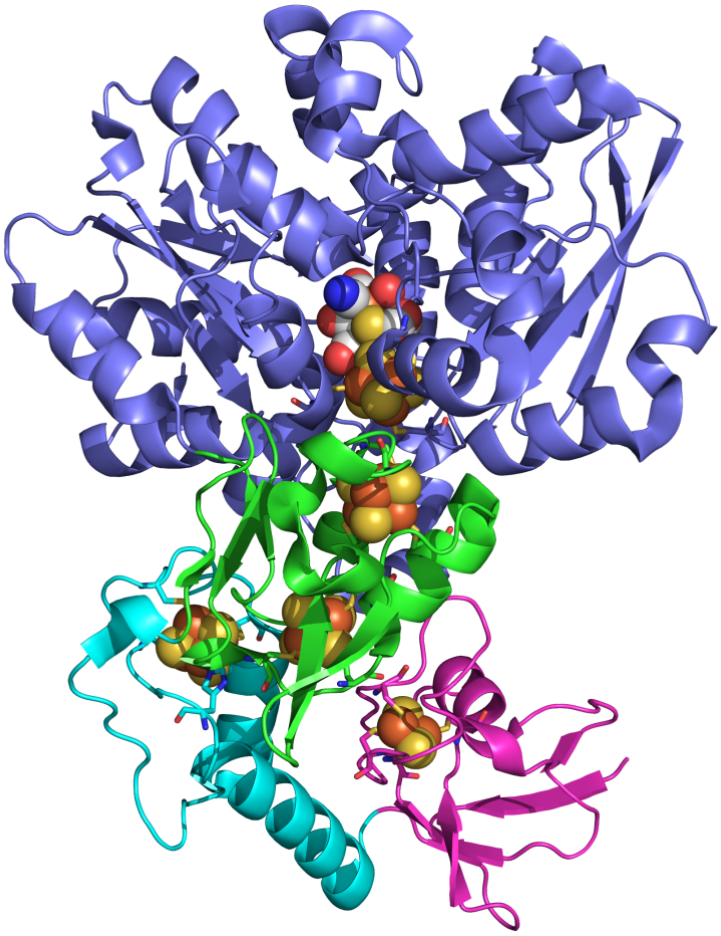

Figure 1.7. Cartoon representation of the [FeFe]-hydrogenase from *Clostridium pasteurianum* (PDB code 3C8Y). S, Fe, C, O, and N are colored yellow, rust, grey, dark grey, red, and blue respectively. Each domain is colored separately with the accessory FeS cluster domains being colored green, cyan, and magenta. The H-cluster domain is colored blue.

dithiomethylamine as the dithiolate bridging substituent comes from 2Fe subcluster model complexes with dithiomethylamine being inserted into immature [FeFe]-hydrogenase containing only the [4Fe-4S] subcluster resulting in biochemical and spectroscopic properties similar to that of wild type enzyme (Figure 1.6) (51).

[NiFe]-hydrogenases.

[NiFe]-hydrogenases are found in archaea, bacteria, and cyanobacteria. [NiFe]-hydrogenases in their simplest form are heterodimers of a large (60 kDa) and a small (30 kDa) subunit containing accessory iron-sulfur clusters (Figure 1.8) (44). Unlike [FeFe]-hydrogenases, [NiFe]-hydrogenases are categorized based off their physiological function. There are generally considered four groups of [NiFe]-hydrogenases and these are group 1-membrane associated hydrogen uptake, group 2-cyanobacterial hydrogen uptake or hydrogen sensing, group 3-bidirectional, and group 4-membrane bound hydrogen evolving.

Group 1 [NiFe]-hydrogenases are referred to as uptake hydrogenases and oxidize H2 to create reduced electron carriers to provide energy for cellular growth and metabolism. Group 1 enzymes are characterized by the presence of a 30-35 amino acid long signal peptide at the N terminus of their small subunit (39, 52). Group 1 enzymes are trimeric enzymes with the third subunit anchoring the [NiFe]-hydrogenase to the membrane, and these enzymes are connected to the electron transport chain with electrons obtained from H_2 oxidation being fed into the quinone pool (37, 39, 53). Feeding electrons into the quinine pool functions to link H_2 oxidation to the reduction of electron acceptors, which include CO_2, fumarate, O_2, NO_3, or SO_4 (37, 39, 53). The

group 2 [NiFe]-hydrogenases are referred to as H_2 sensing and are characterized by not containing a signal peptide on the N-terminus of their small subunit and having several amino acid deletions as compared to group 1(37, 39). Group 2 enzymes are cytoplasmic and are involved in regulating transcription in the presence of H_2 or are involved in recovering energy from H_2 produced during N_2 fixation (37, 39). The group 3 [NiFe]-hydrogenases are referred to as bidirectional hydrogenases and are multimeric, with

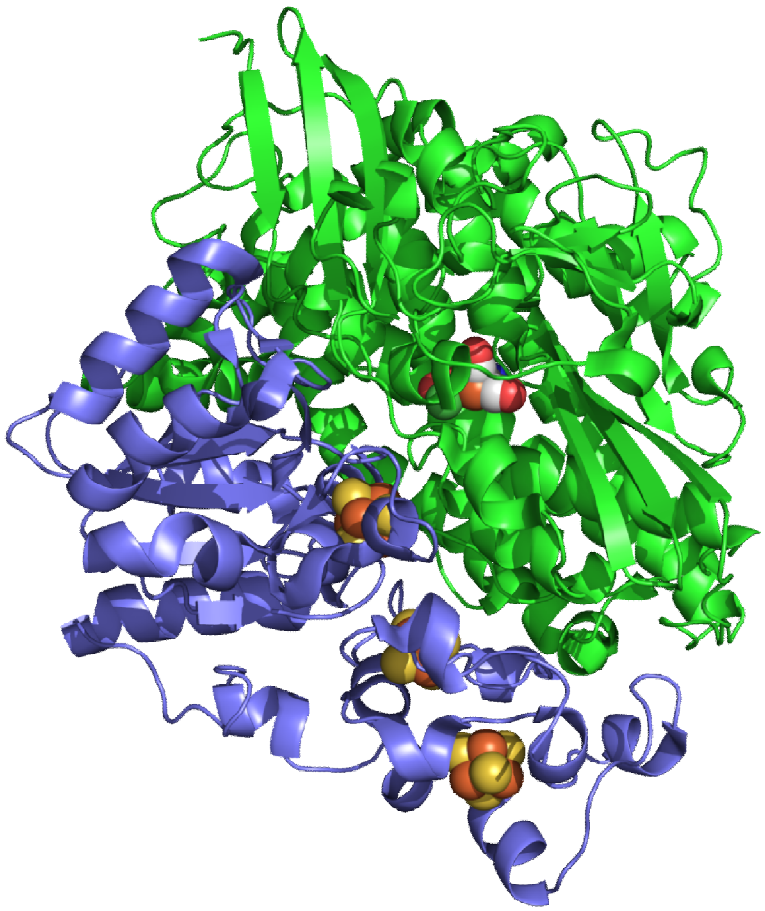

Figure 1.8. Cartoon representation of the NiFe]-hydrogenases from *Desulfovibrio fructosivorans* (pdb identifier 1YRQ). The large subunit is colored green and the small subunit is colored blue (42). S, Fe, Ni, C, O, and N are colored yellow, rust, green, grey, red, and blue respectively. The large subunit contains the active site and the small subunit contains accessory FeS clusters.

additional subunits that can mediate electrons to soluble cellular redox cofactors such as NAD, NADP or F420. Enzymes from group 3 are able to use electron from H_2 to reduce soluble redox cofactors, but they are also capable of oxidizing these cofactors to reduce protons and produce H_2 (37, 39). The group 4 H_2 evolving [NiFe]-hydrogenases are multimeric membrane associated enzymes with six or more subunits, and these enzymes produce H_2 consequently recycling reduced electron carriers produced by oxidation of C1 compounds formate and carbon monoxide (37).

There is a large abundance of structural data on [NiFe]-hydrogenase. X-ray crystal structures of [NiFe]-hydrogenase are more numerous than that of the [FeFe]-hydrogenase. Structures of [NiFe] *Desulfovibrio gigas* (54), *Desulfovibrio vulgaris* (55-57), *Desulfovibrio fructosivorans* (58), and *Desulfovibrio desulfuricans* (59), *Allochromatium vinosum* (60), *Hydrogenovibrio marinus* (61), *Escherichia coli (62, 63) Salmonella enterica (64), Ralstonia eutropha* (65, 66), and *Methanothermobacter marburgensis* (67) have been solved. The [NiFe]-hydrogenase from *D. fructosivorans* has a large subunit and small subunit with the small subunit ligating 3 FeS clusters two of which are [4Fe-4S] clusters and one [3Fe-4S] cluster (Figure 1.8). The [NiFe]-hydrogenase's active site is composed of a bimetallic Ni and Fe site with the Fe atom having two cyanide and one carbon monoxide ligand. The Fe atom is bridged to the Ni by two thiolate ligand that come from cysteine residues and the Ni atom is additionally coordinated by two more cysteines (Figure 1.6) (44).

Summary and Research Directions

Developing alternative forms of energy will help to ensure a viable future economy. Several forms of abundant alternative energy exist but are currently underutilized. To utilize alternative forms of energy more effectively it is important to develop chemical processes to help capture and store energy to allow a continual energy supply similar to that obtained from fossil fuels. Hydrogen may play an important role in reaching our future energy needs. Hydrogen is a versatile molecule and its properties may impart roles in energy use, energy storage, and chemical energy transformations. It is therefore, of interest to determine ways to efficiently produce hydrogen by renewable means. Biological hydrogen production may help contribute to future hydrogen production once barriers to implementation are overcome. Photosynthetic hydrogen production is severely limited by the O_2 sensitivity of [FeFe]-hydrogenases. This limitation has led to the need to develop a way to efficiently produce highly active [FeFe]-hydrogenase to allow enzyme characterization, explore methods to find or produce a more oxygen tolerant [FeFe]-hydrogenase, and to characterize the process of oxgen inactivation of the [FeFe]-hydrogenase.

Method for Heterologous Expression and Purification of the [FeFe]-hydrogenase

[FeFe]-hydrogenase structural and active site biosynthesis genes can be cloned into and expressed in *Escherichia coli*. Expression systems were used and developed for structural hydrogenase genes from *C. pasteurianum*, *C. reinhardtii,* and *Clostridium acetobutylicum* and to express the [FeFe]-hydrogenases maturase HydF from *C.*

acetobutylicum. Methods were determined for conditions that would allow expression of enzyme with wild type activities and spectroscopic properties. Purification procedures were determined to obtain highly pure enzyme.

Investigation of Biomarkers for O_2 Tolerance in the [FeFe]-hydrogenase

To address the oxygen sensitivity of the [FeFe]-hydrogenase, environmental sequences were surveyed from the solar saltern at Guerrero Negro, Mexico. This environment has factors that could provide selection pressure to evolve an oxygen tolerant enzyme. Sequence variations were determined that may have significant effects on enzyme properties. Variations that were determined from environmental sequences were created in the gene sequence of Cp1. Enzyme was then expressed oxygen sensitivity was assayed. An enzyme variant was determined that may be a signature for oxygen tolerant [FeFe]-hydrogenases.

[FeFe]-hydrogenase Oxygen Inactivation is Initiated by the Modification and Degradation of the H cluster 2Fe Subcluster

[FeFe]-hydrogenase was surveyed for effects when exposed to differential amounts of oxygen. Ultraviolet and Visible spectroscopy (UVvis), Fourier Transform Infrared spectroscopy (FTIR), X-ray crystallography, mass spectrometry, *in vitro* activation, and enzyme activity assays were used to characterize the effects of oxygen on the integrity of the enzyme. FTIR and activity assays demonstrated that the 2Fe subcluster is highly prone to degrade when exposed to oxygen. UVvis, X-ray

crystallography, activity assays, and *in-vitro* activation demonstrated that the [4Fe-4S] subcluster is more robust that the 2Fe subcluster when exposed to oxygen.

CHAPTER 2

METHODS FOR HETEROLOGOUS EXPRESSION AND PURIFICATION OF THE [FEFE]-HYDROGENASE AND MATURASE HYDF

Abstract

Heterologous expression of metallo-enzymes, such as the [FeFe]-hydrogenase, can be highly complex due to the biosynthesis of the inorganic cofactors that are necessary for catalysis; this has made expression of the [FeFe]-hydrogenase and related maturases challenging. Expression of the genes involved in the maturation process and the structural gene often yields a significant portion of enzyme that is incompletely formed and non-functional. It is, therefore, crucial to determine methodologies for the expression and purification of fully functional enzyme in order to allow reliable biochemical, biophysical, and structural studies of the [FeFe]-hydrogenase and enzymes involved in the maturation process. Enzyme was expressed in *Escherichia coli* in supplemented media that has been shown to favor the production of fully functional [FeFe]-hydrogenase enzyme. In addition, these conditions were also used to test expression of the [FeFe]-hydrogenase maturase HydF yielding high yields of fully formed HydF enzyme.

Introduction

[FeFe]-hydrogenase (HydA) catalyze the reversible reduction of protons to hydrogen gas. These enzymes are physiologically important to the microbial organisms that harbor them since they allow the recycling of reducing equivalent or they can oxidize hydrogen to provide energy for metabolic processes. These enzymes are of interest for use in biotechnological applications such as for microbial hydrogen production in dark fermentation or biophotolysis (30). The active site of the [FeFe]-hydrogenase allows for the seemingly simple chemistry of proton reduction to occur. This active site termed the H-cluster is extraordinarily complex and requires specialized enzymes and chemistry in order to create an active enzyme capable catalysis. The H-cluster is a [4Fe-4S] subcluster bridged to an organometallic, 2Fe subcluster through a protein cysteine thiolate. The 2Fe subcluster is coordinated by unique non-protein ligands including CO, CN, and dithiomethylamine (41, 45, 46, 51, 68).

The maturation process for the [FeFe]-hydrogenase has been shown to involve three enzymes HydE, HydF, and HydG (69). HydE and HydG are from the radical SAM class of enzymes and act to synthesize the ligands on the 2Fe subcluster (69-75). HydE and HydG likely carryout their chemistry on HydF, which has been shown to be solely be capable of transferring an intact 2Fe subcluster to immature [FeFe]-hydrogenase that has a preformed [4Fe-4S] subcluster (Figure 2.1) (70, 74, 75). The substrate for HydG is tyrosine and it has been demonstrated that HydG is capable of producing carbon monoxide and cyanide from this substrate which become the ligands on the fully matured

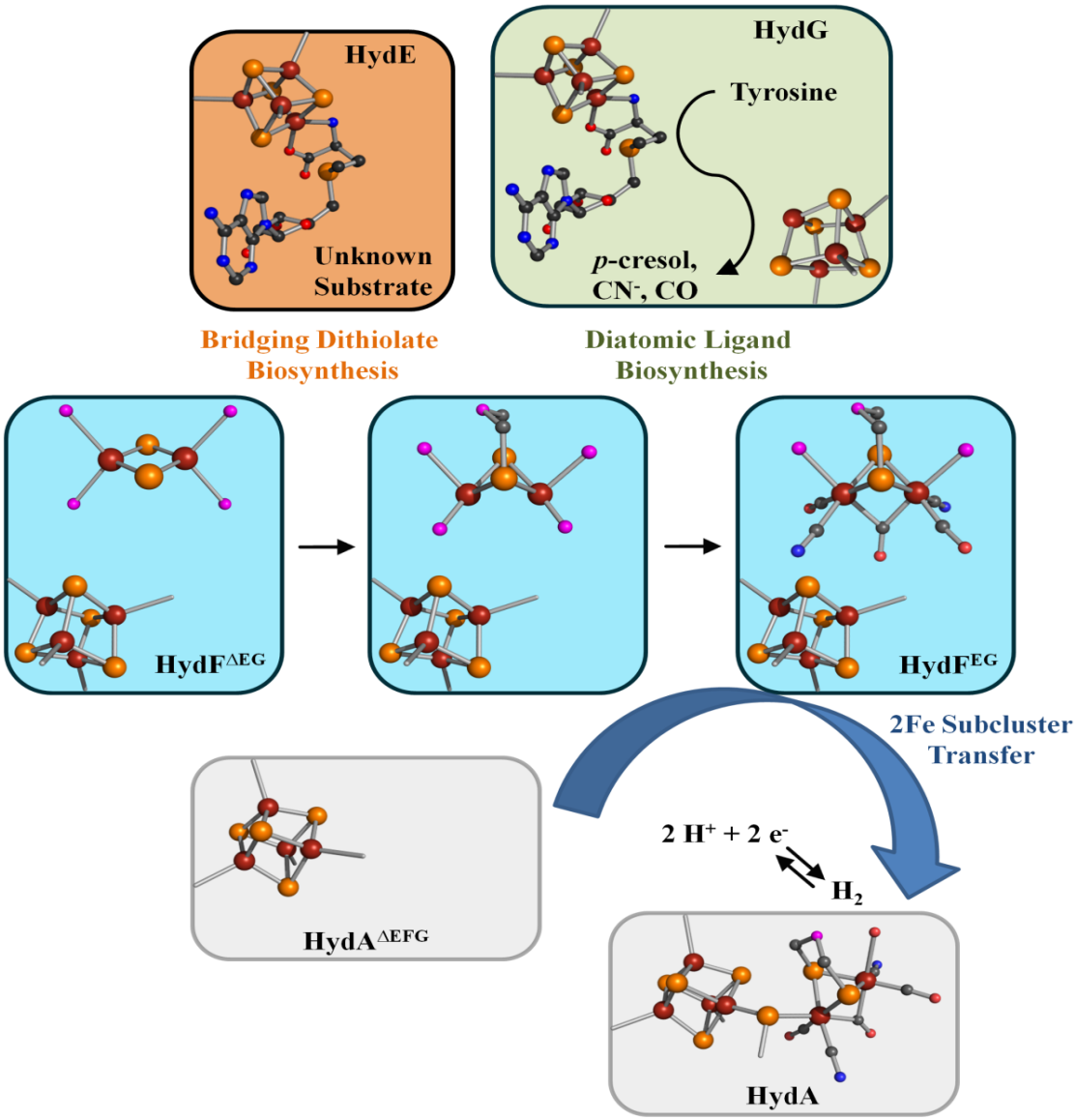

Figure 2.1. Schematic of the activation process of the [FeFe]-hydrogenase from (76). HydF acts as a scaffold and HydE and HydG build a 2Fe subcluster (star). The 2Fe subcluster is transferred to HydA creating a fully mature enzyme that is capable of catalysis.

[FeFe]-hydrogenase (72, 73). The substrate for HydE is yet to be determined but HydE has a role in synthesizing the dithiolate ligand.

Characterizing the [FeFe]-hydrogenase and the maturation process has suffered from difficulties in obtaining sufficient quantities of active enzyme (77). It has been necessary to develop an expression system that allows large yields both structural and *maturase enzymes that are fully functional. The overexpression of the [FeFe]-hydrogenase was first attempted in *Escherichia coli* and produced active enzyme but with low activity (77). It was later shown that the [FeFe]-hydrogenase could be overexpressed in *Clostridium acetobutylicum* and *Shewanella oneidensis* and produce enzyme with near wild type hydrogen production activities (78-80). Subsequently the conditions for high-yield expression of [FeFe]-hydrogenase in *E. coli* were also found (81, 82).

Expression of the maturase HydF has also been of interest due to it containing the fully formed precursor that is transferred to the [FeFe]-hydrogenase to form enzyme capable of catalysis (70). HydF is either a tetramer or dimer, which is likely dependent on the stage of the maturation process (83). Unlike HydE and HydG that contain simply [4Fe-4S] clusters, HydF containing the [FeFe]-hydrogenase active site 2Fe subcluster precursor has proven itself to be difficult to isolate in sufficient quantities for characterization. The first report of the isolation of HydF was of the inactive form of the enzyme heterologously expressed in *E.coli* in the absence of the other two maturases HydE and HydG (84). Later HydF was isolated and shown to be the activating component of the maturation process and was shown to contain the 2Fe subcluster with CO and CN ligands (70, 74, 75).

Methodologies have been reproduced and adapted in order to express and purify the [FeFe]-hydrogenase and similar methods were used express the maturase HydF to

yield highly active enzyme. [FeFe]-hydrogenases were heterologously expressed in and purified from *Escherichia coli* from *Clostridium pasteurianum* (Cp1), *Clostridium acetobutylicum* (Ca1), and *Clamydomonas reinhardtii* (CrHydA1). HydF from *C. acetobutylicum* was expressed in *E. coli* under similar conditions to that of the [FeFe]-hydrogenase and purified; CaHydF was found to have spectroscopic properties similar to that of wild type enzyme.

Methods

Expression

To express CrHydA1 and Ca1, plasmids with the genes Ca*hydE* and either Ca*hydA1* or Cr*hydA1* maintained in pET-Duet and genes for Ca*hydF* and Ca*hydG* maintained on pCDF-Duet were used (transformation set 1 chloramphenicol 30 mg/mL, carbenicillin 100 mg/mL, and streptomycin 50 mg/mL) (77). To express Cp1, plasmids pET-21b with Cp*hydA1* and pACYC-Duet with *Shewenella oneidensis hydGX and hydEF* were used (transformation set 2 chloramphenicol 30 mg/L, carbenicillin 100 mg/L, and kanamycin 30 mg/L) (81). For HydF expressions, the following plasmids were used: *hydF* maintained on pRSF-Duet, *hydE* maintained on pET-Duet, and *hydG* maintained on pCDF-Duet (transformation set 3 streptomycin 50mg/L, kanamycin 30 mg/L, and carbenicillin 100 mg/L) (70). Transformation set 1 for either Ca1 or CrHydA1 expression were independently transformed along with plasmids harboring maturases into *E. coli* BL21 (DE3) Rosetta2 cells (Novagen). Transformation set 2, for Cp1 expression,

was transformed into *E. coli* BL21 (DE3) ΔiscR. Transformation set 3, for HydF expression, was transformed into BL21-DE3 cells (Novagen).

Fresh transformations were used to inoculate overnight cultures by picking 5-10 colonies and transferring the selected colonies into 50-100 mL of terrific broth (TB) media for HydA or (50mM) phosphate buffered Luria-Bertani (PLB) media (pH 8) for HydF preheated to 37 °C. Each media composition was made to have the same antibiotic concentrations as that used for transformations. The following day, after ~16 hrs of growth, 5 mL of overnight was transferred into 37 °C preheated 1 L of TB broth in 2 L Erlenmeyer flasks for HydA or 1L PLB in 2 L Erlenmeyer flasks for HydF in 10 L batches. For HydA growths, TB was additionally supplemented with 0.5% w/v glucose before inoculation. For HydF growths, PLB was additionally supplemented with 0.5% w/v glucose and 2.5 mM ammonium ferric citrate. Cultures were left shaking at 250 rpm at 37 °C until culture reached an OD_{600} of 0.5. Cultures were then removed from shakers and cultures were combined to create 2L total volumes for sparging and sparging was carried out using ultrapure argon. Immediately after cultures began to sparge 25 mM sodium furmarate, 2.5 mM ammonium ferric citratate (except HydF expressions), 1.5 mM isopropyl β-D-1-thiogalactopyranoside (IPTG), and 2 mM cysteine were added in the order listed. Cultures were left to sparge overnight ~16 hrs and all manipulations after sparging overnight were carried out in an anaerobic chamber (Coy Labs, Grass Lake MI) except centrifugation. Cultures were tested for hydrogenase activity before harvesting and if cultures had expected activities, then cells were harvested by centrifugation. Gas tight bottles 1L were used for harvesting cells and cultures were

centrifuged at 8000 rpm for 8 min. Pelleted cells were scraped from the bottom of centrifugation bottles and flash frozen in liquid nitrogen. Cell pellets were stored in a -80 °C freezer for later purification of enzyme.

Lysis and Purification

Cells were lysed by resuspension in buffer composed of 50 mM Tris, pH 8, 0.3 M NaCl, 5% glycerol, 5 mM sodium dithionite (NaDT) dithiothreitol, 1 protease inhibitor tablet (Roche), 1% Triton X-100, 140 μg ml^{-1} DNAse and RNAse, and 120 μg ml^{-1} lysozyme. The cell lysate was stirred for 1 h at room temp, and centrifuged in gas tight bottles at 38,000 x *g* for 30 min. HydA (either Cp1, Ca1, or CrHydA1) was purified under anaerobic conditions using septa sealed and argon flushed vials. All buffers were degassed under vacuum before purification. CrHydA1 isolation from cell extracts was performed using a two-step chromatography process of ion-exchange over diethylaminoethanol (DEAE, GE Lifesciences) Sepharose followed by affinity capture on Strep-Tactin (IBA) resin (82). Strep-Tactin bound enzyme was eluted in 50 mM Tris buffer (pH 8.0) containing 300 mM NaCl, 5% glycerol, 5 mM NaDT, and 2 mM desthiobiotin. Purity was verified by sodium dodecyl sulfate polyacrylamide gel electrophoresis (SDS-PAGE), and the concentration determined by Bradford assay.

$HydF^{EG}$ was purified in an anaerobic chamber (Coy Labs, Grass Lake MI) similar to as previously described (70). Cells were harvested by centrifugation and cell pellets stored at -80 °C. Cells were lysed by resuspension in buffer composed of 10 mM HEPES, pH 7.4, 0.5 M KCl, 5% glycerol, 1 mM dithiothreitol, 20 mM imidazole, 20 mM $MgCl_2$, 1 mM PMSF, 1% Triton X-100, 140 μg ml^{-1} DNAse and RNAse, and 120 μg ml^{-1}

lysozyme. The cell lysate was stirred for 1 h at room temp, and centrifuged in gas tight bottles at 38,000 x *g* for 30 min. The His-$HydF^{EG}$ was purified from the supernatant by immobilized metal chromatography on a TALON cobalt column (GE Life Sciences). The column was loaded and washed with 15 column volumes of 20 mM HEPES pH 7.4, 0.5 M KCl, 5% glycerol, 1 mM dithiothreitol, and 20 mM imidazole. Purified $HydF^{EG}$ was eluted with wash buffer containing 200 mM imidazole. $HydF^{EG}$ was collected and concentrated anaerobically with 30 kDa Amicon Ultra-15 centrifugal concentrators (Millipore). The $HydF^{EG}$ was loaded onto a G25 PD-10 desalting column (GE Life Sciences) to remove imidazole and eluted with 50 mM HEPES pH 7.4, 0.5 M KCl, 5% glycerol, and 1 mM dithiothreitol. Purity was verified by sodium dodecyl sulfate polyacrylamide gel electrophoresis (SDS-PAGE), and the concentration determined by Bradford assay.

$HydF^{EG}$ was flash frozen in liquid N_2 and stored at –80 °C or in liquid N_2 until further use.

Fourier Transform Infrared Spectroscopy

Spectra were collected as described previously with a Nicolet 6700 FTIR spectrometer (Thermo Fisher Scientific) equipped with a Globar IR source, a CaF_2 beam splitter, and a liquid-nitrogen-cooled mercury cadmium telluride (MCT) detector (85). All of the spectra were collected at room temperature (21 °C). The custom-built sample chamber consists of a covered aluminum box designed to minimize external light interference with the sample. The OMNIC software was configured to report absorbance spectra, and absorbance baselines were fit to these data using a manually adjusted spline.

Activity Assays

Activities were assayed by H_2 evolution from reduced methyl viologen. Reaction volumes of 0.6 or 2 ml were placed in 3 or 10 ml Wheaton vials, respectively, which contained 5 mM methyl viologen (MV), 10 mM NaDT, 50 mM Tris, 300 mM NaCl, 5% glycerol, and between 25 ng-4 µg of enzyme per assay. Hydrogen production was detected by gas chromatography (Shimadzu GC-8A).

Whole cell activities were measured by sampling 20 µl of culture after overnight expression and measuring hydrogen production activities. Assays were carried out in 20 mL Wheaton vial containing the buffer conditions above plus 0.1% triton.

In vitro Activation of CrHydA1

Activation of CrHydA1 was performed by the addition of N-terminal His tagged-$HydF^{EG}$ at different molar ratios to obtain a 300 µl total volume in 3 ml crimp sealed anaerobic Wheaton vials. CrHydA1 was allowed to reactivate at 37 °C in a water bath for 1 h, and reactivation was followed by measuring the H_2 production activity as described above.

Results/Discussion

Recombinant Expression of [FeFe]-hydrogenase and $CaHydF^{EG}$ and Purification

It was important due to the high oxygen sensitivity of the [FeFe]-hydrogenase system that adequate methods be developed for maintaining enzyme in anaerobic conditions after expression. It was found necessary to use ultra pure argon that was run through an oxygen scrubbing trap when making buffers or cultures anaerobic. When carrying out purifications, it was also critical to maintain positive pressure in buffers with an over pressure of argon and collect fractions in septum sealed vials thoroughly flushed with argon. All other manipulations were of enzyme during purification had to be carried out in an anaerobic coy chamber that was maintained at 0 ppm oxygen.

Cultures were IPTG induced under strict anoxic conditions produced by sparging with argon gas. By using the electron acceptor fumarate, it allowed cultures to continue to grow after being switched to anaerobic conditions. After overnight expression culture densities were found to be around an OD_{600} of 2-3. Whole cell activities allowed the assessment of the viability of growths. Cp1 and Ca1 growths were used for enzyme purification if they had whole cell activities at 1000 nmol H_2 min^{-1} mL^{-1} or greater and CrHydA1 growths were used if they had whole cell activities of 3000 nmol H_2 min^{-1} mL^{-1} or greater. It was found that growth conditions were highly dependent on the source of reagents used for expression. Ammonium Fe(III) citrate (sigma 09714-250G), D-glucose (sigma 68270-5kg), L-cysteine HCl monohydride sigma (C7880-100G), IPTG (goldbio 12481 C500), and TB media (EMD 1.01629.9010) yielded the best expression conditions

as determined by whole cell activities. CaHydF was expressed under similar conditions as described by Kuchenreuther et al (81). Enzyme's quality could only be assessed after purification by *in vitro* activation of CrHydA1 expressed in the absence of maturases and FTIR making determination of culture conditions more difficult.

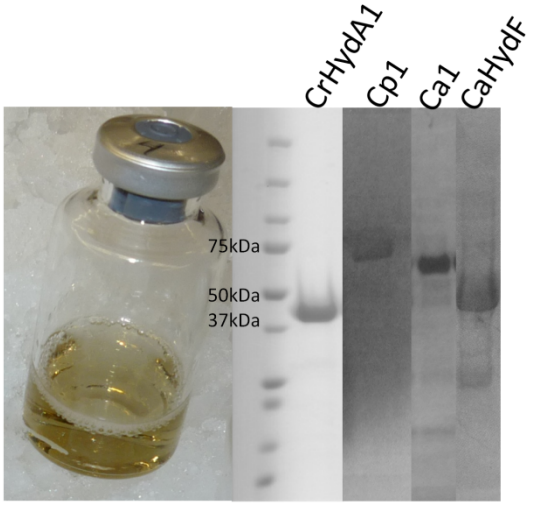

Figure 2.2. Picture is of purified CrHydA1 and SDS-PAGE gels of CrHydA1, Cp1, Ca1, and CaHydF

The two step column purification of the [FeFe]-hydrogenases produced pure protein verified by SDS-PAGE (Figure 2.2) with specific activities near wild type levels (Table 2.1) (81). Enzyme yields for CrHydA1 were ~3 mg/L of culture, for Ca1 were ~1 mg/L of culture, and for Cp1 were 0.5 mg/L of culture. Due to the expense of Strep-Tactin, DEAE sepharose was used as an initial purification step to help remove contaminates that decrease the life of the Strep-Tactin column. Enzyme eluted off the

Table 2.1. Specific activities determined for [FeFe]-hydrogenases heterologously expressed in *E. coli*.

	Specific Activity $\mu mol \cdot min^{-1} \cdot mg^{-1}$	Standard Deviation
Ca1	2347	±130
Cp1	1646	±200
CrHydA1	609	±66

DEAE column at 30% buffer B (50 mM Tris buffer (pH 8.0) containing 1 M NaCl, 5% glycerol, and 5 mM NaDT.) and [FeFe]-hydrogenase containing fractions would produce hydrogen and were a dark brown color which is characteristic of Fe containing enzymes. Strep-Tactin resin was efficient at binding the strep tag cloned onto the C-terminus of the [FeFe]-hydrogenase enzymes expressed and enzyme was easily eluted with buffer containing 2 mM desthiobiotin as a single dark brown band. This purification method allowed for efficient isolation of a solution of golden brown and highly pure and active enzyme. CrHydA1 due to it lacking accessory electron transfer FeS clusters was lighter in color when compared to isolated Cp1 and Ca1 of a similar concentration. Due to enzyme being easily contaminated by oxygen the majority of the enzyme preparations were flash frozen by pelleting into liquid nitrogen. Freezing as pellets by dripping the proteins solution into liquid nitrogen allowed for ease of use when doing small scale experiments; this allowed for removal of single pellets (20-50µL/pellet) thawing only a small amount of protein at a time.

Purification of CaHydF by immobilized metal chromatography on a Co^{2+} column produced pure enzyme (Figure 2.2) that was capable of activating purified [FeFe]-

hydrogenase expressed in the absence of maturases (Figure 2.3). Co^{2+} resin was chosen since it doesn't bind 6xhistidine tags as

tightly as Ni^{2+} resulting in lower concentrations of imidazole being needed for elution. This was taken as an important consideration since the imidazole can chelate metal ions. Co^{2+} resin resulted in protein that was highly pure and was a dark brown color and eluted of the column in a single band, and the protein was immediately concentrated and

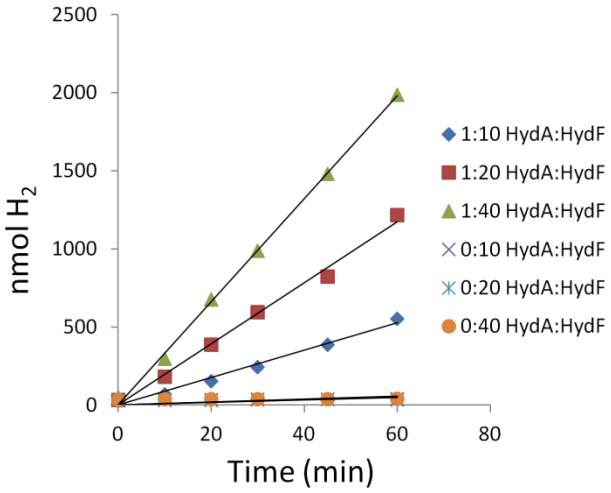

Figure 2.3. Titration of CrHydA that was expressed in the absence of maturases HydE, HydF, and HydG (86). Ratios presented are molar ratios of HydA to HydF.

exchanged into imidazole free buffer before being flash frozen as pellets in liquid N_2. CaHydF had a yield of ~11 mg/L of culture.

Fourier Transform Infrared Spectroscopy

The CO and CN^- ligands provide a means to easily assess the quality of purified enzyme by FTIR. As isolated CrHydA1 heterologously expressed in *E. coli* produced a strong FTIR signal that was consistent of enzyme that was in mostly the Hox form with a small amount of reduced signal. H_{ox} state is observed at 1804, 1940, 1964, 2071 and

2089 cm^{-1} (Figure 2.4). As isolated CaHydF heterologously expressed in *E.coli* also produced strong FTIR features with peaks at 1877, 1907, 1943, 1967, 2027, 2044, and 2069 cm^{-1} (Figure 2.4). This signal is most consistent with the enzyme being in the reduced form. The reduced signal is observed at 1877, 1907, 1943, 1967, 2044, and 2069 cm^{-1} (75). The observed 2027 cm^{-1} peak maybe a result of the expression system causing incomplete cluster formation, the purification method introducing artifacts, a mixture of

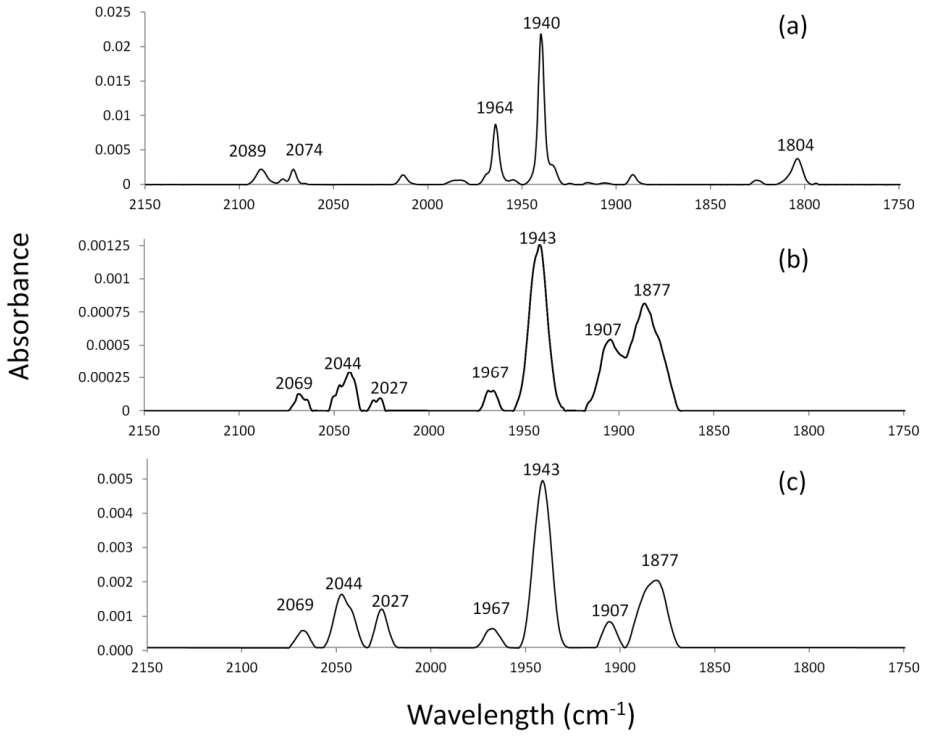

Figure 2.4. (a) FTIR spectra of as isolated CrHydA1 at 75 mg/mL. (b) FTIR spectra of as isolated CaHydF at 56 mg/mL. (c) FTIR spectra of as isolated HydF at 336 mg/mL.

oxidized and reduced states, or the use of dithiothreitol as a reductant. The FTIR features of CaHydF heterologously expressed in *E. coli* are highly similar to that found in wild

type preparations of homologously expressed CaHydF(75) and the spectra attained from this method of preparation is different than that previously shown for heterologously expressed CaHydF in *E. coli* that had peak wave numbers of 1881, 1940, 2027, and 2046 cm^{-1} (74).

Conclusion

Methods discussed here allowed for the efficient preparation of [FeFe]-hydrogenase structural enzyme and the maturase CaHydF. Developing methods for isolating components of the [FeFe]-hydrogenase system is important as it allows the production of sufficient quantities of enzyme for biochemical, biophysical, and structural studies. The [FeFe]-hydrogenase system is a challenging system to characterize since it is extremely oxygen sensitive. It has been crucial to develop methods to maintain strict anaerobic conditions while handling preparations. Enzyme was isolated and shown to be highly active for hydrogen production and FTIR was further used to verify the quality of enzyme produced. The expression and purification of CaHydF resulted in enzyme sufficient for activating immature [FeFe]-hydrogenase and it also had FTIR features consistent with that of wild type CaHydF. Additional features were also seen that may be novel and a result of the expression system or conditions used. In addition, the expression and purification method presented resulted in heterologously expressed CaHydF from *E. coli* that may be more similar to wild type enzyme than what has previously been shown for CaHydF expressed in *E. coli* (74).

CHAPTER 3

INVESTIGATION OF BIOMARKERS FOR O_2 TOLERANCE IN THE [FEFE]-HYDROGENASE

Abstract

The [FeFe]-hydrogenase O_2 sensitivity is a limiting factor in applying it in scaled up hydrogen producing technologies. There is a large natural sequence diversity for [FeFe]-hydrogenases and the natural variation in sequence of [FeFe]-hydrogenases may encode the information necessary for structural modifications that would allow the folding and maturation of an O_2 tolerant [FeFe]-hydrogenase. In order for O_2 tolerance to evolve, environmental factors would be necessary to create the selection pressure that would lead to the evolution of O_2 tolerance, and environments that contained these environmental factors that promote selection pressure would be the best to probe for biomarkers of O_2 tolerance. The hypersaline environment of the salterns in Guerrero Negro, Mexico have characteristics that make it an ideal place to explore the sequence space of [FeFe]-hydrogenases for O_2 tolerance. The sequence space obtained from the Guerrero Negro was analyzed for [FeFe]-hydrogenase sequence variation that would promote O_2 tolerance. Variants were made based off the environmental sequences and enzyme activity was tested for increased tolerance in the presence of O_2.

This section was coauthored by Kevin D. Swanson, Spencer White, Eric S. Boyd and John W. Peters and was prepared for submission to the International Journal of Molecular Sciences

Introduction

[FeFe]- and [NiFe]-hydrogenases are the principle enzymes responsible for hydrogen cycling in the environment. [FeFe]- and [NiFe]-hydrogenases function in organisms by recycling reduced electron carriers by mediating the transfer of electrons from the reduced electron carriers to protons forming hydrogen. Alternatively they can oxidize hydrogen and reduce oxidized electron carriers that can then provide the energy to carryout energy utilizing metabolic processes. These enzymes are ubiquitous in nature and [FeFe]-hydrogenases are found in an array of species of bacteria and unicellular green algae and [NiFe]-hydrogenases are found in bacteria and archaea (39). These two enzyme classes differ in their metal active site composition and are phylogenetically unrelated (39).

Localized hydrogen produced by hydrogenase enzymes can create an interspecies metabolic dependence. Hydrogen is produced mainly through fermentative processes and [FeFe]-hydrogenases are more efficient for hydrogen production and result in the majority of hydrogen produced in microbial communities (87). The monomeric form of [FeFe]-hydrogenases have been the best characterized structurally (45, 46, 49, 86). The monomeric forms of the [FeFe]-hydrogenase can vary by domain composition which is likely due to the redox partner of the enzymes (88, 89). The accessory domains often harbor accessory FeS clusters to mediate electron transfer to and from the active site (46) [FeFe]-hydrogenases also exist in multimeric forms being dimer, trimers, and tetramers (47). The multimeric forms of the [FeFe]-hydrogenase are capable of utilizing NADH or NADPH as a source of reducing equivalents for hydrogen production (47, 90).

To date no oxygen tolerant [FeFe]-hydrogenases have been found. There has been a large degree of effort in engineering oxygen tolerance into the [FeFe]-hydrogenase with production of variants with only small increases in O_2 tolerance (91-95). A rational design approach was used to target residues to create single site substitutions within one of the gas channels of the [FeFe]-hydrogenase in order to limit diffusion of O_2 over that of hydrogen. O_2 tolerance was increased in variant enzyme and the gas channel was indicated as the primary site for O_2 diffusion (Figure 3.1) (91, 93-95). Random mutagenesis of the [FeFe]-hydrogenase sequence yielded variants with increased O_2 tolerance and it was shown that multiple sequence variations provided an additive

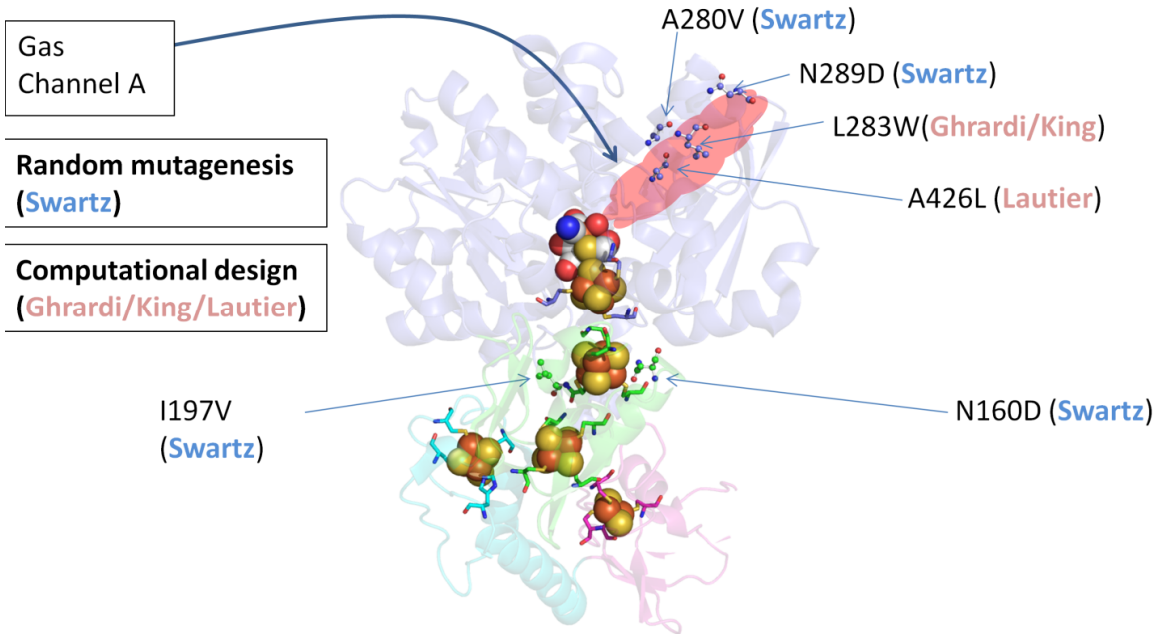

Figure 3.1. Transparent cartoon representation of the [FeFe]-hydrogenase from *C. pasteurianum* with FeS clusters and the H-cluster shown as spheres. Gas channel is highlighted in red. Residues that were mutated in the designated studies are shown as ball and sticks other residues ligating clusters are shown as sticks. Computational based design of Cp1 variants with increased O_2 tolerance was reported in (91, 93). Random mutagenesis base variant with multiple site substitutions N160D, I197V, A280V, and N289D with increased oxygen tolerance was reported in (92).

effect to increasing the O_2 tolerance (Figure 3.1) (92). The variant enzyme that was produced in the random mutagenesis study produced a variation in the gas channel with additional site changes around the accessory FeS cluster closest to the active site. The results of these studies suggest traditional enzyme engineering routes may not yield an enzyme with O_2 tolerance. The additive effect of the multi-site substituted variant demonstrated that it may be difficult to target single sites and that in order to find an O_2 tolerant enzyme a larger degree of sequence variation would be necessary for an enzyme to confer O_2 tolerance.

Natural sequence variation in the environment provides the ideal sequence space to test [FeFe]-hydrogenase O_2 tolerance. Hypersaline environments contain O_2 gradients that could provide an increased selection pressure when moving up the gradient to higher O_2 concentrations. Partial sequences recovered from the saltern in Guerrero Negro (GN), Baja California Sur, Mexico were analyzed for sequence variation in regions in the gas channels and near the active site (96). Single site directed variants were created based off the environmental sequences found in the [FeFe]-hydrogenase from *Clostridium pasteurianum* (Cp1). Enzyme was then expressed and tested for any increases in O_2 tolerance. A single site variant was found with an increased tolerance to O_2. This variant could be considered a biomarker for O_2 tolerance and may provide impetus to isolate and culture organisms that harbor this [FeFe]-hydrogenase gene sequence.

Methods

[FeFe]-hydrogenase Sequence Isolation from the Guerrero Negro Solar Saltern

Procedures for isolation of [FeFe]-hydrogenase gene sequencesare described in (96), but briefly mat core samples that were 1 cm by 6 cm were taken from Pond 4 at the Exportadora de Sal saltworks, GN. Cores were section in 1 mm sizes and flash frozen in liquid nitrogen. Genomic DNA was isolated and quantified on DNA agarose gels. Degenerate primers were used to amplify ~500 bp fragments of [FeFe]-hydrogenase sequence. The primers that were used were FeFe-272F (5'-GCHGAYMTBACHATWATGGARGA-3' H=A, C, T; Y=C, T; M=A, C; B=C, G, T; W=A, T; R=A,G} and FeFe-427R (5'GCNGCYTCCATDACDCCDCCNGT-3' where N=A, C, T, G; Y=C, T; D=A, G, T). [FeFe]-hydrogenase sequences were amplified using 35 cycles with an annealing temperature of 56.6 °C, $MgCl_2$ concentration of 1.5 mM and primer concentration of 1 mM for each. Reactions had a total volume of 50 µL and contained 10 ng of isolated template DNA. DNA fragments were purified and cloned into pGEM-T (promega). pGEM-T harboring environmental sequences were then sequenced.

Consensus Sequence Construction

In order to simplify sequences to represent key site variations consensus sequences were constructed for GN [FeFe]-hydrogenase sequences. Sequences recovered from GN where obtained from GenBank accession numbers FJ623894-FJ623958. The sequences from GN group into 7 clusters (96). Four consensus sequences were made to

represent the most abundant sequence variations to help target site directed variants for biochemical testing. Consensus sequences were created with BioEdit (Version 7.0.5).

Subcloning and Site Directed Mutagenesis

To remove the 6x histidine tag Cp1 was digested from pET14b (originally cloned by John W Peters-unpublished) with Nde1 and BamHI. The resulting DNA fragment was ligated into pET-3a digested with Nde1 and BamHI. Mutagensis was performed to make L283A, L283F, I287A, I287F, C300A, C300D, C300H, C300S, F293A, and F293L. The primers used are as follows:

L283F fwd, GCTACAGAATTTGTTCAAAGAATAGAGAATAATGG

L283F rev, CTATTCTTTGAACAAATTCTGTAGCCTCTTCC

L283A fwd, GCTACAGAAGCAGTTCAAAGAATAGAGAATAATG

L283A rev, CTTTGAACTGCTTCTGTAGCCTCTTC

L287F fwd, GTTCAAAGATTTGAGAATAATGGACCTTTC

L287F rev, CCATTATTCTCAAATCTTTGAACTAATTCTGTAG

L287A fwd, GTTCAAAGAGCAGAGAATAATGGACCTTT

L287A rev, CCATTATTCTCTGCTCTTTGAACTAATTCTGTAG

F293L fwd, GGACCTTTACCAATGTTTACATCTTGC

F293L rev, GATGTAAACATTGGTAAAGGTCCATTATTCTC

F293A fwd, GGACCTGCCCCAATGTTTACATCTT

F293A rev, CATTGGGGCAGGTCCATTATTCTCT

C300S fwd, ATCTTGCTCCCCAGGTTGGGTAA

C300S rev, ACCTGGGGAGCAAGATGTAAACATTG

C300A fwd, TCTTGCGCCCCAGGTTG

C300A rev, CCTGGGGCGCAAGATGTAAACA

C300D fwd, TCTTGCGACCCAGGTTGGGTAA

C300D rev, CCTGGGTCGCAAGATGTAAACATTG

C300H fwd, TCTTGCCACCCAGGTTGGGTAA

C300H rev, CCTGGGTGGCAAGATGTAAACATTG

Polymerase chain reaction conditions were set up with the following components: 40 µL nuclease free water, 5 µL 10x Pfu AD buffer, 1 µL 10 mM DNTPs, 1 µL pET-3a-Cp1, 1 µL of each fwd and rev 10 µM primer, and 1 µL Pfu turbo AD (Agilent). The thermocycler was set to cycle 95°C for 1 min, then cycle 18 times 95°C for 50 sec→50°C for 50 sec → 68°C for 7 min, and a final extension was performed at 68°C for 7 min. All mutations were verified by DNA sequencing (Davis Sequencing) (Figure 3.2).

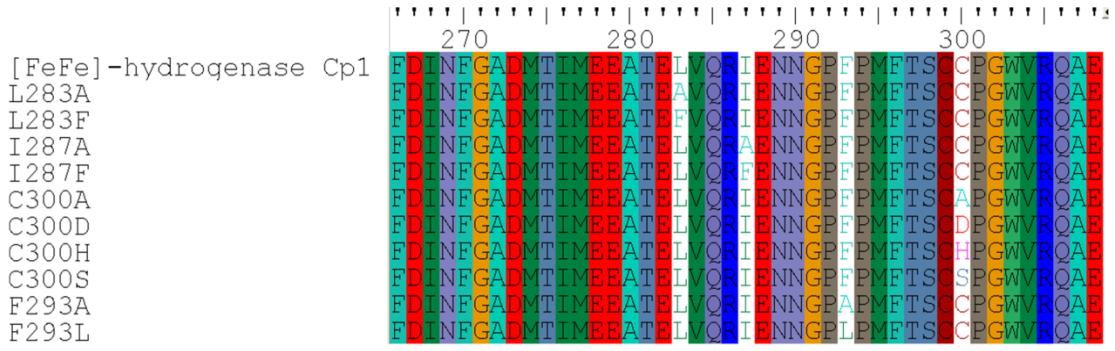

Figure 3.2. Alignment of contigs obtained from samples sent for sequencing. Sequencing confirmed mutagenesis occurred for each of the variants made.

Recombinant Cp1 Expression

Cp1 WT and variants in pET-3a and pACYC-Duet with *Shewenella oneidensis hydGX and hydEF* were transformed into *E. coli* BL21 (DE3) ΔiscR chemically competent cells. Fresh transformations were used to inoculate overnight cultures by picking 5 colonies and transferring the selected colonies into 5mL of Terrific Broth (TB) media (pH 8) 100 µg/mL carbenicillin, 30 µg/mL kanamycin, and 30 µg/mL Chloramphenicol preheated to 37 °C. The following day, after ~16 hrs of growth, 1 mL of overnight was used to inoculate 37 °C preheated 1 L TB in a 500 mL Erlenmeyer flasks. TB was additionally supplemented with 0.5% w/v glucose before inoculation. Cultures were left shaking at 250 rpm at 37 °C until culture reached an OD_{600} of 0.5. Cultures were then removed from shakers and were sparged using ultrapure argon. Immediately after cultures began to sparge 25 mM sodium furmarate, 2.5 mM ammonium ferric citrate, 1.5 mM isopropyl β-D-1-thiogalactopyranoside (IPTG), and 2 mM cysteine were added in the order listed. Cultures were left to sparge overnight ~16 hrs and all manipulations after sparging overnight were carried out in an anerobic chamber (Coy Labs, Grass Lake MI) except centrifugation. Cultures were tested for hydrogenase activity before harvesting and if cultures had expected activites, then cells were harvested by centrifugation. Gas tight bottles 250 mL were used for harvesting cells and cultures were centrifuged at 8000 rpm for 8 min. Pelleted cells were scraped from the bottom of centrifugation bottles and flash frozen in liquid nitrogen. Cell pellets were stored in a -80 °C freezer until later use.

O_2 Inactivation and Enzyme Activity Assays

All reactions were performed at 37°C. To determine the quality of growths, whole cell activities were measured by sampling 20 µl of culture after overnight expression and measuring hydrogen production activities in 20 mL Wheaton vials in 2 mL total volume containing 5 mM methyl viologen (MV), 10 mM Na Dithionite, 300 mM NaCl, 5% glycerol, 0.1% triton-X and 50 mM Tris pH 8. Reactions were initiated by the addition of 1 mL of 10 mM MV, 10 mM Na Dithionite, 300 mM NaCl, 5% glycerol, 0.2% triton, and 50 mM Tris pH 8 to 1 mL of diluted lysate in buffer.

Lysate was used for characterization of oxygen tolerance of Cp1 and cells were lysed by resuspension in buffer at a 1:5 ratio of grams of cell paste to mL of lysis buffer composed of 10 mM HEPES, pH 7.4, 0.5 M KCl, 5% glycerol, 1 mM dithiothreitol, 20 mM imidazole, 20 mM $MgCl_2$, 1 mM PMSF, 1% Triton X-100, 140 µg ml^{-1} DNAse and RNAse, and 120 µg ml^{-1} lysozyme. The cell lysate was stirred for 1 h at room temp, and centrifuged in gas tight bottles at 38,000 x *g* for 30 min.

O_2 inactivation was carried out in 4.5 mL Wheaton vials. 100 µL of lysate was added to 900 µl of buffer and 2 mL of 100% O_2 was added to the vial. Samples of 50 µL of the O_2 inactivation were taken at 0, 0.5, 1, 3, and 5 minutes and added to 450 µL activity assay buffer in a separate 4.5 mL Wheaton vial (10 mM Na Dithionite, 300 mM NaCl, 5% glycerol, and 50 mM Tris pH 8). Activities were assayed by H_2 evolution after the addition of 0.5 mL of 10 mM MV, 10 mM Na Dithionite, 300 mM NaCl, 5% glycerol, 0.2% triton, and 50 mM Tris pH 8 by gas chromatography (Shimadzu GC-8A).

Results/Discussion

To simplify analysis of the 65 sequences recovered from GN, four consensus sequences were generated (Figure3.4). These consensus sequences were made based off the clusters designated when the phylogenetic analysis was performed (Figure 3.3) (96).

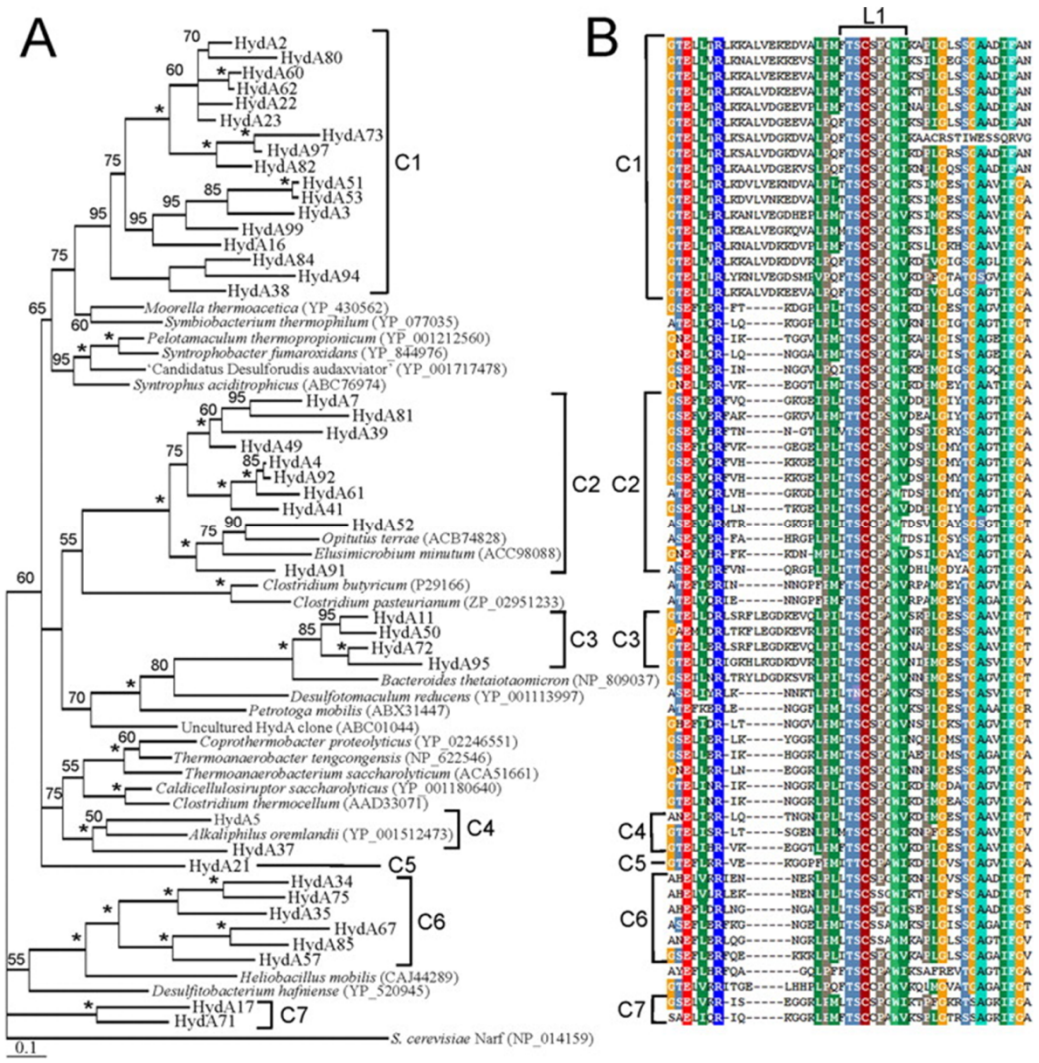

Figure 3.3. Phylogenetic tree (A) and sequence alignment (B) of [FeFe]-hydrogenase fragments isolated from Guerrero Negro, MX. [FeFe]-hydrogenase sequences were found to cluster in 7 different groups. Figure from (96).

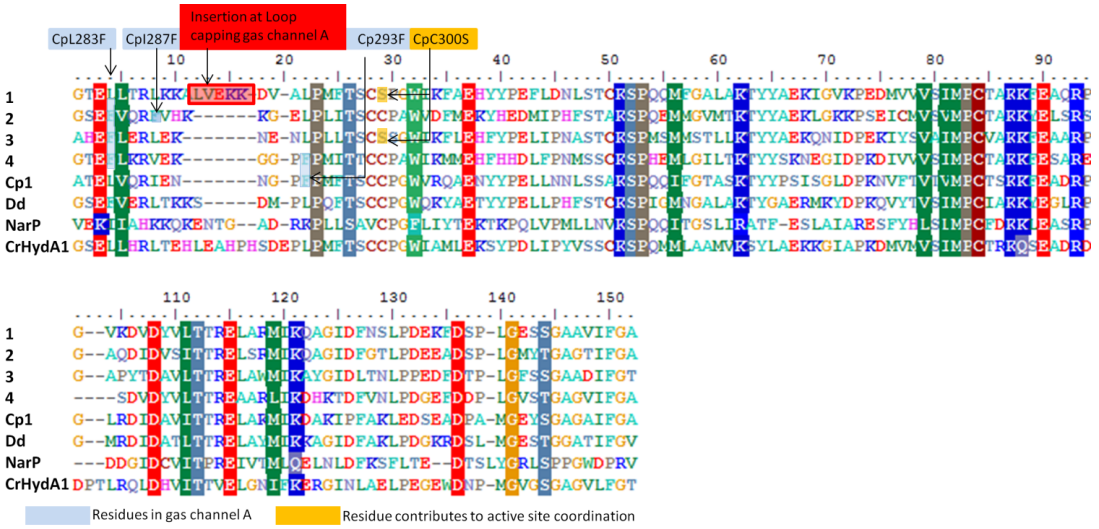

Figure 3.4. Consensus sequences generated from sequences recovered from Guerrero Negro, as well as, [FeFe]-hydrogenase sequences from *Clostridium pasteurianum* (Cp), *Desulfovibrio desulfuricans* (Dd), and *Chlamydomonas reinhardtii* (CrHydA). Also shown is *narP* from *Saccharomyces cerevisiae* (NarP). Alignment was performed with Clustle W. Residues are highlighted according to whether they are in gas channel A or coordinating the active site.

Consensus sequence 1 represents cluster 1 and it was found to have a C300S variation and this residue is involved in the coordination of Cp1's metalo-cofactor. Consensus sequence 1 also shows an insertion of 6 amino acid insertion between N289 and N290 a loop that caps Cp1's gas channel. Consensus sequence 2 represents cluster 2 and it was found to have L283F and I287F both these residues line the gas channel that links the active site of Cp1 to the outside of the enzyme. Consensus sequence 3 represents cluster 6 and it was found to have L283F and C300S. Consensus sequence 4 represents group 5 and was found to have C283F. Other clusters were excluded from this study because no useful targets for mutagenesis near the active site, in the gas channel, or in the proton transfer pathway were found in them.

Residues in the gas channel of the [FeFe]-hydrogenase have already been demonstrated to be functionally important for O_2 sensitivity of the [FeFe]-hydrogenase from creation of site directed variants (91-94). Though C283F and I287F variants are in the gas channel, these exact mutations have not been tested in any other study for their affect in oxygen tolerance. C300S is an interesting variation since serine coordination of FeS clusters is uncommon in nature. The only well-characterized enzyme displaying such coordination is the P-cluster of the nitrogenase where serine is thought to stabilize the cluster in its oxidized state (97, 98). It's possible that the C300S variant observed in GN HydA sequences may also have a stabilizing effect on the H-cluster, functioning to stabilize a more oxidized state of the active site in the presence of O_2.

Mutant	Whole Cell H_2 Production ($nmol \cdot min^{-1} ml^{-1}$ cell culture)	Lysate H_2 Production Activity ($nmol \cdot min^{-1} mg^{-1}$)	H_2 Production Half Life (min)
1) L283A	1584	1950	1.67
2) L283F*	3493	1930	7.88
3) I287A	4405	2784	5.46
4) I287F*	0	25	n/a
6) C300S*	0	15	n/a
5) WT	3145	4275	5.06

*different than previous work involving single site substitutions – based on real environmental variance

Table 3.1 Table comparing activities of whole cells, lysate, and half lives for each of the natural sequence variation observed in Guerrero Negro. Variants colored light blue represent gas channel variants, variant highlighted yellow is an active site coordinating residue variant, and wild type is white.

L283F, L283A, and I287A were the only variation made in Cp1 that showed significant levels of hydrogen production when compared to wild type (Table 3.1). Other variants may have activity that is too low to detect in lysate. L283A decreased the half

life of Cp1 in O_2 by more than half of wild type value, L283F increased the half life by half of the wild type value, and C300S had no detectable hydrogen production activity above background (Table 3.1). Since L283F showed a large increase in tolerance to oxygen and L283A showed a large decrease in oxygen tolerance it may be possible that this mutation is a biomarker for O_2 tolerance in a hydrogen producing rather than hydrogen oxidizing [FeFe]-hydrogenase since the enzyme maintained significant hydrogen production capabilities. I287A showed no significant variation from wild type levels of hydrogen production, and I287F was inactive (Table 3.1). All variants had about half the wild type level of lysate hydrogen production activities when compared to wild type (Table 3.1).

Conclusion

The complete environmental sequence space for [FeFe]-hydrogenases has only been explored to a small degree for O_2 tolerance. Through bioprospecting efforts aimed at finding [FeFe]-hydrogenase gene sequences in environments that have selection pressure for O_2 tolerance, it may be possible to discover the sequence for an O_2 tolerant [FeFe]-hydrogenase. Making [FeFe]-hydrogenase variants based off of environmental sequences could be a useful tool for narrowing down environmental sequence space to those gene sequence that could confer O_2 tolerance. Phenylalanine corresponding to site 283 in Cp1 may in fact be a biomarker for O_2 tolerance in [FeFe]-hydrogenases since it appears to possibly play a significant role in modulating O_2 diffusion to the active site of Cp1 and this may also be the case in the uncharacterized [FeFe]-hydrogenases with this

variation in hypersaline environments. In addition, if an entire [FeFe]-hydrogenase sequence that had this variation could be isolated and biochemically characterized from a hypersaline environment such as GN, then it could be that additive effects from the entire protein sequence could confer complete O_2 tolerance. It is still uncertain why C300S occurs in these environmental samples. This variant could play a role in O_2 tolerance, modulating hydrogen uptake activity, or stabilizing the active site in saline environments. In order to test whether C300S and the other variants (L283F and I287F) are biomarkers for O_2 tolerance it will be necessary to isolate complete gene sequences for sequences containing these variations from a hypersaline environment.

-

CHAPTER 4

[FEFE]-HYDROGENASE OXYGEN INACTIVATION IS INITIATED BY THE MODIFICATION AND DEGRADATION OF THE H-CLUSTER 2FE SUBCLUSTER

Abstract

The [FeFe]-hydrogenase catalytic site H cluster is a complex iron sulfur cluster assembly that is sensitive to oxygen (O_2). The O_2 sensitivity is a significant barrier for production of hydrogen as an energy source in water-splitting, oxygenic systems. Oxygen reacts directly with the H cluster, which results in rapid enzyme inactivation and eventual degradation. To investigate the progression of O_2-dependent [FeFe]-hydrogenase inactivation and the process of H cluster degradation, the highly O_2 sensitive [FeFe]-hydrogenase HydA1 from the green algae *Chlamydomonas reinhardtii* was exposed to defined concentrations of O_2 while monitoring the loss of activity and accompanying changes in H cluster spectroscopic properties. The results indicate that H cluster degradation proceeds through a series of reactions, the rate and extent of which depend on the initial enzyme reduction/oxidation state. The degradation process begins with O_2 binding and reacting with the 2Fe subcluster, leading to degradation of the 2Fe subcluster and leaving an inactive [4Fe-4S] subcluster state. In addition, Cys 169 that has been implicated as part of the proton transfer pathway was observed to have reacted with a reactive oxygen species to form sulfenic acid. This final inactive degradation product could be reactivated *in vitro* by incubation with 2Fe subcluster maturation machinery, specifically $HydF^{EG}$, which was observed by recovery of enzyme activity.

This section was coauthored by Kevin D. Swanson, Michael W. Ratzloff, David W. Mulder, Jacob H. Artz, Shourjo Ghose, Andrew Hoffman, Spencer White, Oleg A. Zadvornyy, Joan B. Broderick, Brian Bothner, Paul W. King, and John W. Peters and submitted to the Journal of the American Chemical Society

Introduction

[FeFe]-hydrogenases are found in bacteria and lower eukaryotes, and are commonly involved in the recycling of reduced electron carriers that accumulate during anaerobic metabolism (39). [FeFe]-hydrogenases catalyze reversible H_2 activation at very high rates and thus are attractive targets for bioengineering efforts aimed at coupling microbial H_2 production to oxygenic photosynthesis (30, 99). However, [FeFe]-hydrogenases are rapidly inactivated upon exposure to O_2, the byproduct of water oxidation (100, 101). In [FeFe]-hydrogenases, proton reduction occurs at a complex bridged FeS cluster termed the H cluster. The H cluster exists as a regular [4Fe-4S] subcluster bridged to an organometallic 2Fe subcluster through a protein cysteine thiolate. The 2Fe subcluster is coordinated by unique non-protein ligands including CO, CN, and dithiomethylamine (Figure4.1) (41, 45, 46, 51, 68). The O_2 sensitivity has been attributed to redox reactions with O_2, and subsequent destruction of the H cluster by reactive oxygen species (ROS), rendering the enzyme irreversibly inactivated (102).

Although all of the characterized [FeFe]-hydrogenases have been shown to be sensitive to O_2 inactivation, enzymes from different sources have varying sensitivity to O_2, which has been attributed largely to differences in the access of the active sites to O_2 (91, 94, 101, 103-105). Computational studies have revealed putative channels that are proposed to function in the diffusion of gases, including O_2, to and from the active site

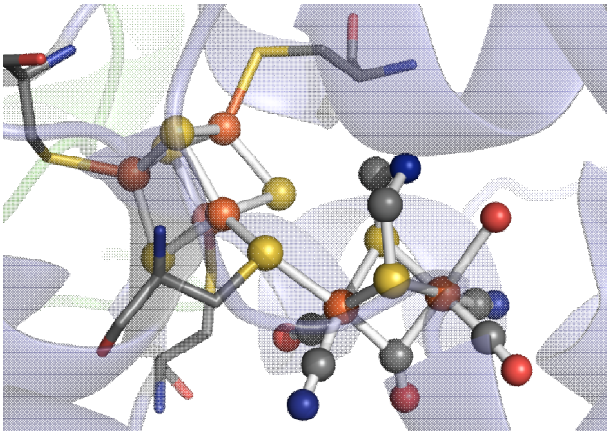

Figure 4.1. H cluster ball-and-stick representation with carbon, nitrogen, oxygen, sulfur, and iron atoms colored grey, blue, red, yellow, and rust respectively (PDB 3C8Y).

(94). It was also discovered through computational analysis and enzymatic assays of site-directed variants that constricting the gas channels can decrease the sensitivity of the [FeFe]-hydrogenase to O_2 but not to a significant enough degree to be useful for applications in technology (91, 94, 104, 105). A random mutagenesis approach was used to screen thousands of [FeFe]-hydrogenase variants leading to isolation of a more O_2 tolerant variant with several site substitutions. The effect of each mutation was individually tested, and showed that each contributed to an additive effect on the overall O_2 tolerance of the [FeFe]-hydrogenase (105).

Theoretical studies of inactivation have measured the thermodynamics of O_2 binding and reactivity with the H cluster, and probed the subsequent reaction steps that ultimately lead to enzyme degradation. The models suggest that initiation of O_2 interaction with hydrogenase catalysis is dependent on the oxidation state, coordination environment and redox activity of the Fe sites (106-109). In the H cluster reaction models, O_2 binds at the distal Fe, which is assigned to the (I) oxidation state for H_{ox} with a “loosely” bound water. Reaction of the bound O_2 with Fe(I) leads to formation of a

terminally bound -OOH or $-O_2^-$ species. Further reaction cycles of the terminal "O" species with H^+ generates H_2O_2 or iron-peroxide as end-products (108). Alternatively, 2Fe subcluster oxidation, or O atom insertion into the distal Fe terminal CO ligand can release CO_2 (108). The exact chemical nature of the O-species produced from O_2 reactions at the H cluster remain to be experimentally validated. A recent experimental and theoretical study of anaerobic, oxidative inactivation of CrHydA1(110) proposed that the inactivation mechanism proceeds *via* reversible, and slower irreversible inactivation processes. Reversible inactivation involved H_2 binding to different thermally available conformers of the H-cluster, with ligand rearrangements on Fe_d that led to protection from O_2 inactivation. Irreversible inactivation occurred at high (positive) potentials and was modeled as a slow oxidation of H_{ox}, rendering the H cluster susceptible to nucleophilic attack and subsequent H cluster disruption (110).

Structural and biophysical studies on how O_2 reacts with the H cluster to cause inactivation are challenging, and there are limited experimental studies on this process (100, 111). A mechanism of H cluster degradation by O_2 has been proposed from the results of X-ray absorption spectroscopy (XAS) studies in which reactive O_2 species produced at the 2Fe subcluster result in enzyme inactivation by destruction of the [4Fe-4S] subcluster (102, 112). Those results contrast with previous models whereby O_2 accesses and binds to the 2Fe subcluster to form ROS or other end-products that can readily degrade the 2Fe subcluster followed by loss of enzyme activity (108). It has been observed earlier that exposure of [FeFe]-hydrogenases to either O_2 or light (photolysis) led to the formation of an H_{ox}-CO like EPR or IR signal (113-115). The photolytic effect

is known to lead to CO release, which can re-bind to the same enzyme, or another enzyme in a process termed "cannibalization" (114, 115). O_2 caused both irreversible and reversible inactivation, where reversible inactivation was proposed to occur *via* formation of an "O"-adduct with an EPR signal similar to H_{ox}-CO. A mechanism for the O_2 induced formation of the O-adduct has not been determined.

In order to reexamine the mechanistic process of O_2 inactivation of [FeFe]-hydrogenases, we have exposed the [FeFe]-hydrogenase from *Chlamydomonas reinhardtii* (CrHydA1) to low titers of O_2 while monitoring changes in the biochemical activity and changes in Fourier transform infrared (FTIR) and Ultraviolet–visible (UV-Vis) spectroscopic properties. The FTIR results indicate that H cluster reacts with O_2 and undergoes a series of reactions to produce a mixture of intermediates, the populations of which depend on the initial reduction/oxidation state of the H cluster. Ultimately, oxidative destruction results in the loss of the 2Fe subcluster and formation of a [4Fe-4S] subcluster state observed with UV-Vis and in the X-ray crystal structure. This inactivation/degradation end product could be reactivated *in vitro* by incubation with the 2Fe subcluster specific maturation machinery, as observed by enzyme activity assays.

Methods

Protein Preparation

Heterologous expression and purification of CrHydA1 in *Escherichia coli* was done as previously described (77, 82). The protein was purified under anaerobic conditions in a MBraun anaerobic chamber (MBraun USA). All buffers were degassed

under vacuum before purification. CrHydA1 isolation from cell extracts was performed using a two-step chromatography process of ion-exchange over diethylaminoethanol (DEAE, GE Lifesciences) Sepharose followed by affinity capture on Strep-Tactin (IBA) resin (82). Strep-Tactin bound enzyme was eluted in 50 mM Tris buffer (pH 8.0) containing 300 mM NaCl, 5% glycerol, 5 mM sodium dithionite (NaDT), and 2 mM desthiobiotin. Purity was verified by sodium dodecyl sulfate polyacrylamide gel electrophoresis (SDS-PAGE), and the concentration determined by Bradford assay. CrHydA1 was prepared in the H_{ox} state by serial concentration and dilution in NaDT-free buffer until the FTIR spectra consisted primarily of H_{ox}. CrHydA1 was prepared in the H_{ox}-CO state by brief sparging under 100% CO gas, and 10 min incubation, in a sealed serum vial. Aliquots of CrHydA1 were prepared in H_{red}-H_2 by 10 evacuation flush cycles with 100% H_2 on a Schlenk line fitted with an O_2 trap.

HydF was obtained by expression of *hydF* in the background of HydE and HydG ($HydF^{EG}$) in *E. coli* strain BL21 (DE3). The *hydE*, *hydF*, and *hydG* from *Clostridium acetobutylicum* were individually cloned into pET-Duet, pRSF-Duet, and pCDF-Duet, respectively (70). The cloned copy of *hydF* contained a N-terminal 6xHis tag (70). Cells were grown in LB Miller growth medium supplemented with streptomycin (50 mg L^{-1}), kanamycin (30 mg L^{-1}), ampicillin (100 mg L^{-1}), 0.5% w/v glucose (~25 mM), 2 mM ferric ammonium citrate and 50 mM phosphate buffer (final pH of medium was 7.4). All cultures were grown aerobically at 25 °C until an OD_{600} of 0.5. Cultures were sparged with 100% argon for 20 min, and induced with 1.5 mM isopropyl β-D-1-thiogalactopyranoside (IPTG). Cysteine (2 mM) and sodium fumarate (25 mM) were

added immediately after IPTG addition. Cultures were sparged with argon at 25°C overnight.

$HydF^{EG}$ was purified in an anaerobic chamber (Coy Labs, Grass Lake MI) as previously described (70). Cells were harvested by centrifugation and cell pellets stored at -80 °C. Cells were lysed by resuspension in buffer composed of 10 mM HEPES, pH 7.4, 0.5 M KCl, 5% glycerol, 1 mM dithiothreitol, 20 mM imidazole, 20 mM $MgCl_2$, 1 mM PMSF, 1% Triton X-100, 140 μg ml^{-1} DNAse and RNAse, and 120 μg ml^{-1} lysozyme. The cell lysate was stirred for 1 h at room temp, and centrifuged in gas tight bottles at 38,000 x *g* for 30 min. The His-$HydF^{EG}$ was purified from the supernatant by immobilized metal chromatography on a TALON cobalt column (GE Life Sciences). The column was loaded and washed with 15 column volumes of 20 mM HEPES pH 7.4, 0.5 M KCl, 5% glycerol, 1 mM dithiothreitol, and 20 mM imidazole. Purified $HydF^{EG}$ was eluted with wash buffer containing 200 mM imidazole. $HydF^{EG}$ was collected and concentrated anaerobically with 30 kDa Amicon Ultra-15 centrifugal concentrators (Millipore). The $HydF^{EG}$ was loaded onto a G25 PD-10 desalting column (GE Life Sciences) to remove imidazole and eluted with 50 mM HEPES pH 7.4, 0.5 M KCl, 5% glycerol, and 1 mM dithiothreitol. $HydF^{EG}$ was flash frozen in liquid N_2 and stored at – 80 °C or in liquid N_2 until further use.

Preparation of Oxygen Treated CrHydA1

O_2 gas standards were prepared using septum-sealed 123 ml Wheaton vials. Dilutions were prepared using a gas-tight syringe (Hamilton) to remove gas from a 100% O_2 standard (equilibrated to atmospheric pressure) and injecting the O_2 into vials

containing 100% N_2 at atmospheric pressure. Standards of 100%, 4%, 1%, and 0.1% O_2 were used for all of the O_2 additions. Samples used to measure the FTIR spectra of O_2 treated CrHydA1 were prepared as follows: H_{ox} (Figures 4.2 and 4.3), O_2 was injected by gas-tight syringe into the headspace above an aliquot of 75 µL of 45 mg mL^{-1} CrHydA1 in a septum-sealed 825 µL conical vial; H_{ox}-CO (Figure 4.2, Figure S1), a 15 µL aliquot of 70 mg mL^{-1} H_{ox} CrHydA1 was injected via gas-tight syringe into a septum-sealed 825 µL conical vial that had previously been flushed with 100% CO. O2 was then injected by gas-tight syringe into the headspace of the conical vial; H_{red}-H_2 (Figure 4.2), 70 µL of 30 mg mL^{-1} H_{ox} CrHydA1 in a septum-sealed 825 µL conical vial, along with 3 similar empty conical vials, underwent 10 vacuum/100% H_2 exchanges on a Schlenk line, and incubated for 1 h at 4 °C in the Mbraun. A 10 µL aliquot of this enzyme sample was transferred to each one of the empty, H_2-treated vials via gas-tight syringe. O_2 was then injected by a gas-tight syringe into the headspace of each vial; H_{red}-DT (Figures 2 and s2) was prepared in the MBraun glovebox by adding NaDT (20 mM final) to 50 µL of 50 mg mL^{-1} H_{ox} CrHydA1 (45 mg mL^{-1} final) and mixed via pipetting for 30 s. A 15 µL aliquot was transferred to a 825 µL conical vial, and then sealed with a septum. O_2 was injected by gas-tight syringe into the headspace of the conical vials. In all cases, the conical vials contained a micro stir bar, and stirred while on an ice bath, Final O2 concentrations ranged from 0.01-24.7% (v/v). In order to minimize pressure increases due to gas injection, the appropriate standard was used to keep the injection volume less than 5% of the vial volume (with the exception of the 24.7% CO sample shown in Figure S1). An aliquot of CrHydA1 was removed from the septum-sealed vial using gas-tight syringe

and loaded in a custom gas-tight FTIR sample cell (85). A summary of the O_2 concentration and molar ratios is given in Table S1. Control experiments were performed to estimate the repeatability of O_2 injections, with O_2 concentrations determined by GC (Agilent Technologies). The standard deviation for O_2 injections is estimated to be SD= +/-(% O_2 x 0.15) or +/- 15% of each individual injection (Table S2).

FTIR Spectroscopy

Spectra were collected as described previously with a Nicolet 6700 FTIR spectrometer (Thermo Fisher Scientific) equipped with a Globar IR source, a CaF_2 beam splitter, and a liquid-nitrogen-cooled mercury cadmium telluride (MCT) detector (85). All of the spectra were collected at room temperature (21 °C). The custom-built sample chamber consists of a covered aluminum box designed to minimize external light interference with the sample. The OMNIC software was configured to report absorbance spectra, and absorbance baselines were fit to these data using a manually adjusted spline.

Ultraviolet-Visible Spectroscopy

A 100 µl aliquot of 3 mg mL^{-1} H_{ox} CrHydA1 was prepared in the glove box under 100% N_2, transferred into low volume 1 cm path-length quartz cuvette and septum sealed. The O_2 reaction was initiated by injecting O_2 (at 0.001%, 17% or 300%) with a gas-tight syringe into the headspace of cuvette with the enzyme solution at 4°C, cooled with a peltier cooler. A micro-stir bar provided agitation of the solution in the cuvette. The reaction of CrHydA1 with O_2 was monitored by UV-Vis every min for 200-300 min,

by scanning over a 250-750 nm range at 1 nm intervals. UV-Vis spectra were recorded on a Cary 4000 UV-Visible spectrophotometer.

Activity Assays

Activities of CrHydA1 were assayed by H_2 evolution from reduced methyl viologen. Reaction volumes of 0.6 or 2 ml were placed in 3 or 10 ml Wheaton vials, respectively, which contained 5 mM methyl viologen (MV), 10 mM NaDT, 50 mM Tris, 300 mM NaCl, 5% glycerol, and between 25 ng-4 μg of enzyme per assay. Hydrogen production was detected by gas chromatography (Agilent Technologies).

Mass Spectrometry

Protein digests were performed with 1.5 mg ml^{-1} CrHydA1, 12.5 ug ml^{-1} Trypsin Gold (Promega), 50 mM Tris-HCl pH 8, 300 mM NaCl, and 5% glycerol. Reactions were allowed to proceed overnight in a 37 °C heat block, and complete digestion was verified by sodium dodecyl sulfate polyacrylamide gel electrophoresis (SDS-PAGE). Reactions were transferred into septum sealed vials with a N_2 headspace. The digestion product was diluted up to a 1000 fold in 50/50 water/Acetonitrile and transferred to screw capped auto sampler vials for LCMS.

An Agilent 1100 series HPLC system coupled to an Agilent Chip Cube integrated microfluidics reverse-phase nano-HPLC system was used. Trapping and analytical separations were performed with an Agilent C18 HPLC-Chip (G4240-62001, 40 nl trap column and 75 μm x 43 mm analytical). Chromatography solvents were H_2O with 0.1% (v/v) formic acid for channel "A" and acetonitrile for channel "B". The HPLC program

was held at 7% B from 0.0 to 2.0 min, then ramped from 7 to 35% B from 2.0 to 20.0 min. The gradient was then ramped from 35 to 95% B from 22 to 27 min. The mass spectrometer was an Agilent 6520 Q-TOF with a dual-ESI source: resolution approximately 20,000 and accuracy 3 ppm. Spectra were collected in positive mode from 50 to 1700 m/z at 2 Hz for both MS and MS/MS, with adaptive acquisition time for highly-abundant ions.

The resulting MS/MS data were analyzed using the PEAKS 6.0 software package and searching the CrHydA1 protein sequence. Peptide mass tolerance was 10 ppm and fragment mass tolerance 0.5 Da. Variable modifications were set to sulfonic acid 47.97, sulfinic acid 31.98, and oxidation or hydroxylation of cysteine 15.99.

Crystallization and Structure Determination

CrHydA1 (1 mL at 10 mg mL^{-1}) in NaDT free buffer was exposed to 0.01% O2 for 2 hrs in a 4.5 mL Wheaton vial. Enzyme activity was measured at the end of the 2 hr period (50 μmol $min^{-1}mg^{-1}$). An aliquot of the sample was set aside for trypsin digest and MS analysis, and the rest of the sample was concentrated to 30 mg mL^{-1} for crystallization. CrHydA1 was crystallized anaerobically in a MBraun glove box at room temperature using micro-capillary batch diffusion with a precipitation solution of 25.5% polyethylene glycol 8000 as precipitate and 0.085 M sodium cacodylate (pH 6.5), 0.17 M sodium acetate trihydrate, and 1 mM dithionite. After allowing the crystals to form for 2-3 weeks, they were mounted on cryo-loops and flash frozen in liquid nitrogen. Data were collected at the Stanford Synchrotron Radiation Lightsource (SSRL) on beam line BL12-1 at 1.75 Å wavelength. The data was processed using XDS,(116) and scaled with

Pointless and Aimless (117). The structure was solved using molecular replacement using AutoMR (CCP4 suite of programs) with CrHydA1 (PDB ID, 3LX4) (118). The structure was built using COOT with further refinement using REFMAC5 using NCS and B factor restraints. The final model was solved to 2.23 Å with an R factor of 24.1% and an R free of 27.7% (Table S4, Table S5). Atomic coordinates were deposited in the PDB (code 4ROV).

In vitro Reactivation of O_2 Inactivated CrHydA1

Reactivation of the O_2 inactivated CrHydA1 was performed with the addition of N-terminal His tagged-$HydF^{EG}$ at different molar ratios to obtain a 300 µl total volume in 3 ml crimp sealed anaerobic Wheaton vials. CrHydA1 was allowed to reactivate at 37 °C in a water bath for 1 h, and reactivation was followed by measuring the H_2 production activity as described above.

Results

FTIR Analysis and Comparison of H_{ox}, H_{red}-NaDT, H_{red}-H_2 and H_{ox}-CO

To investigate how differences in the oxidation state and/or site occupancy of the 2Fe subcluster of CrHydA1 affect the process of O_2 damage, reducing agents NaDT and H_2, and the competitive inhibitor CO were each added to oxidized (H_{ox}) CrHydA1. These enzyme samples were then exposed to O_2 and monitored by FTIR. CrHydA1 was initially prepared in the H_{ox} state with major peaks observed at 1804, 1940, 1964, 2071 and 2089 cm^{-1} (Figure 4.2a, red). Exposure of the H_{ox} CrHydA1 to ~0.01% O_2 (Figure

4.2a black spectrum) for 2 h resulted in the loss of H_{ox} features and an increase in features assigned to H_{ox}-CO and the O_2-damaged cluster, discussed in more detail in the time course discussion. A control experiment (Figure S3) on a duplicate sample in the absence of O_2 showed only slight change in the accumulation of H_{ox} signal due to auto-oxidation.

CrHydA1 in the H_{ox} state was exposed to CO to make H_{ox}-CO (Figure 4.2b, red spectrum). The expected shift of *ν*CO and *ν*CN peaks to higher wavenumbers were observed as previously reported for CO-inhibited [FeFe]-hydrogenases, with *ν*CO peaks at 1809, 1963, 1969, 2013, and *ν*CN peaks at 2082, and 2091 cm^{-1} (50, 115, 119). The enzyme was then exposed to ~2.4% O_2. H_{ox}-CO was exposed to larger percentages of oxygen in order to see if any attenuation of FTIR signal could be observed. After approximately 2 h of O_2 exposure, the FTIR spectrum indicated the peaks assigned to H_{ox}-CO remained relatively unchanged (Figure 4.2b, red vs. black spectrum). Small peaks appeared, which are attributed to degradation of some residual H_{ox} species, and this may have also contributed to the slight increase in H_{ox}-CO signal intensity after O_2 exposure. Enzyme in the H_{ox}-CO state was also treated with higher amounts of O_2 (up to ~24.7%, Figure S1), and the resulting FTIR spectra again showed significantly less degradation compared to oxidized and reduced preparations, consistent with other observations that H_{ox}-CO is stable to oxidative reactions with O_2 (100-102, 120).

Equilibration of H_{ox} CrHydA1 under 100% H_2 led to a collective shift in the *ν*CO peaks, consistent with ligand exchange and electronic transitions at the H cluster associated with H_2 activation (85, 121). Figure 4.2c shows the spectrum of H_2-reduced

CrHydA1 with principle *ν*CO peaks, assigned to a mixed population of reduced intermediates, observed at 1792, 1882, 1891, 1916, 1933, 1953, and 1963 cm^{-1}

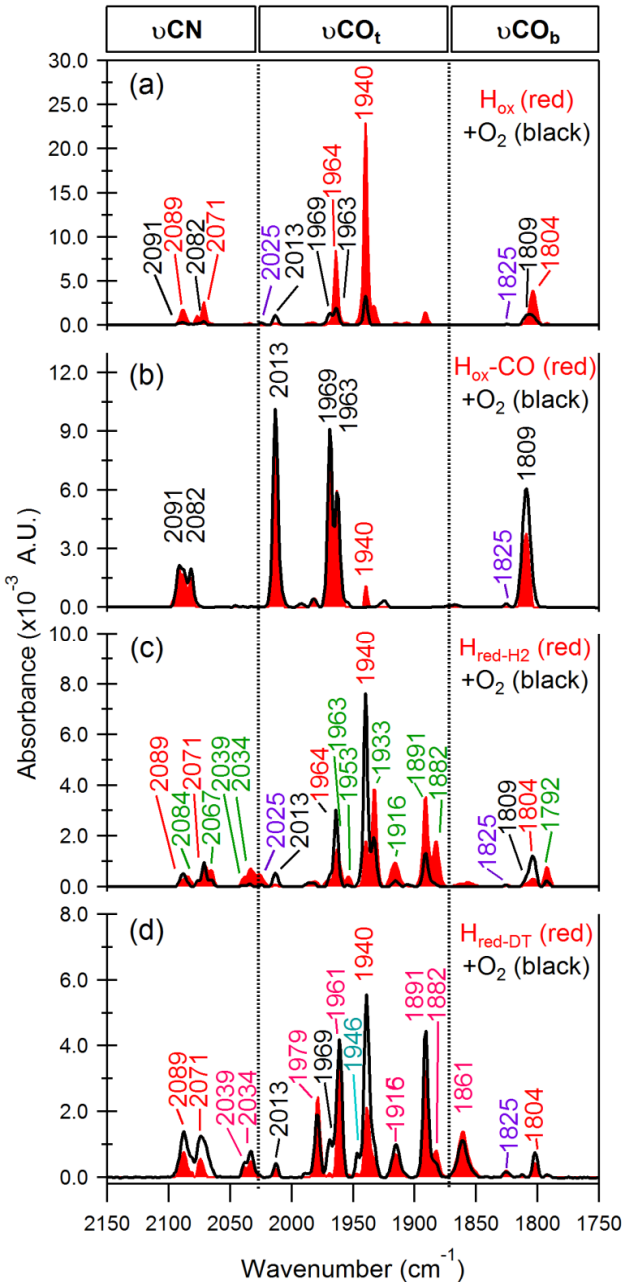

Figure 4.2. FTIR spectra of CrHydA1 samples exposed to O_2. The solid red spectra are prior to O_2 injection, and black traces after 2 h exposure to O_2. (a) H_{ox}, ~0.01% O_2; (b) H_{ox}-CO, ~2.4% O_2; (c) H_{red}-H_2, ~0.01% O_2; (d) H_{red}-NaDT, ~0.01% O_2. Wavenumbers in red, H_{ox}; black, H_{ox}-CO; green, H_{red}-H_2; magenta H_{red}-NaDT; purple, oxidative damage and cyan, unassigned.

(Figure 4.2c, red spectrum) (85, 121, 122). Additional peaks associated with H_{ox}-CO were also seen in the starting sample, possibly arising from a slight amount of O_2 exposure during H_2 treatment. Exposure of H_{red}-H_2 CrHydA1 to ~0.01% O_2 for 2 h, in the presence of 100% H_2 atmosphere led to attenuation of the 1792, 1882, 1891, 1916, and 1933 cm^{-1} peaks (Figure 4.2c, red vs. black spectrum). This was accompanied by an increase in peak intensities assigned to H_{ox} at 1804, 1940, and 1964 cm^{-1} together with a small increase in peak intensities assigned to H_{ox}-CO at 1969 and 2013 cm^{-1}. Thus, degradation of the H_2-reduced CrHydA1 is likely to involve initial formation of $H_{ox,}$ with subsequent interaction with O_2 leading to formation of H_{ox}-CO and eventual 2Fe subcluster degradation.

When H_{ox} CrHydA1 was treated with NaDT (20 mM final concentration, a 20-fold excess), the initial spectrum (Figure 4.2d, red spectrum) showed *ν*CO peaks previously assigned to reduced intermediates at 1861, 1882, 1891, 1916, 1961, and 1979 cm^{-1} (85). Compared to H_{ox} (Figure 4.2a), the NaDT-treated CrHydA1 showed less signal attenuation after exposure to O_2 (Figure 4.2d, red vs. black spectra), with only a small loss of 2Fe subcluster signal after 2 h of exposure to ~0.05% O_2. Regarding *ν*CO peak intensities, the O_2 treatment produced new peaks at 1946 cm^{-1} and 1969 cm^{-1}, a slight increase in peak intensities at 1916, and 2013 cm^{-1}, and larger increases in peak intensities at 1804 and 1940 cm^{-1}. The increases at 1804 and 1940 cm^{-1} are assigned to an increase in the population of H_{ox}, and the changes at 1969 and 2013 cm^{-1} are assigned to an increase in the population of H_{ox}-CO. The appearance of H_{ox} is similar to the sequence observed for O_2 exposure of H_2-reduced CrHydA1, again consistent with O_2

inactivation involving at least one H_{ox}-dependent reaction pathway. It should be noted that the presence of NaDT complicates conclusions drawn from this experiment, as it both reduced CrHydA1 and scavenged O_2. NaDT also reacts with O_2 to form ROS, which in turn reacts with CrHydA1 to exact inactivation. However, titrations of the NaDT-reduced CrHydA1 with increasing amounts of O_2, led to similar transitions observed for H_{ox} CrHydA1, that is formation of both the H_{ox}-CO and O_2 damage signals (Figure S2).

FTIR Time Series of O_2 exposed H_{ox} CrHydA1

In order to observe O2-induced transitions in the 2Fe subcluster by FTIR on the timescales of full spectral collection (512 scans, ~8 min), CrHydA1 prepared in the Hox state (with νCO modes at 1804, 1940, 1964 cm 1) was incubated under a low (~0.01%) O2 partial pressure at 4 °C, and FTIR spectra were collected at approximately ~25 min intervals (Figure 4.3). Based on an O2 titration series (Figure S4) we selected 0.01% O2

Table 4.1. Rate constants for O2 induced changes in CrHydA1 and CaI Hox νCO peak intensities, and H2 evolution activities.

Enzyme	[1] $k_{\Delta Hox}$ ΔIR signal, (s^{-1} μM^{-1})		[1] k_{inact} H_2 evolution activity (s^{-1} μM^{-1})	[2] Ref. k_{inact} (s^{-1} μM^{-1})
CrHydA1	(Δ1940) 3.0×10^{-4}	(Δ1964) 2.0×10^{-4}	2.0×10^{-4}	4.3×10^{-4} (a) 2.2×10^{-3} (b)
CaI	(Δ1945) 9.0×10^{-6}	(Δ1800) 1.2×10^{-6}	6.4×10^{-6}	5.1×10^{-6} (b)

1 $k = -[\ln(y/y_0)]/t$ (s^{-1} μM^{-1})

2 (a) Goldet, G., et al. 2009. *JACS*. 131:14979; (b) Stripp, S.T., et al. 2009. *PNAS*. 106(41):17331.

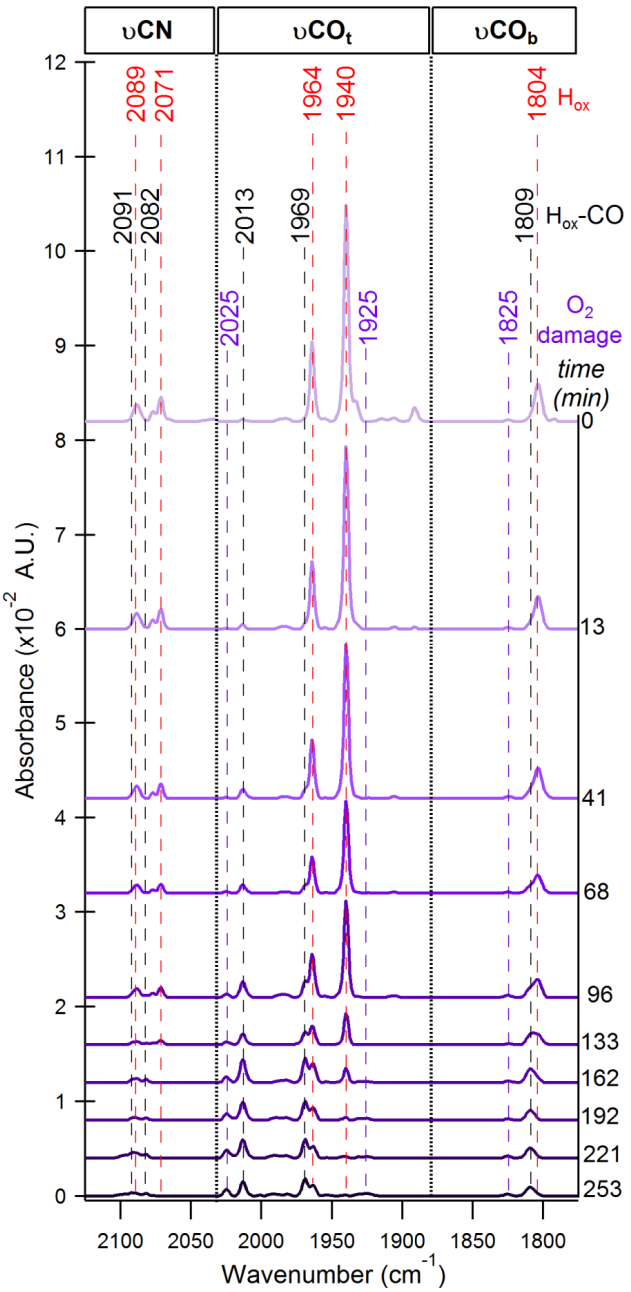

Figure 4.3. Time course of the FTIR spectra of H_{ox} CrHydA1 exposed to ~0.01% O_2. The initial H_{ox} signal (1804, 1940, 1964, 2071, and 2089 cm^{-1}) gradually decays, and the spectrum transitions to a characteristic H_{ox}-CO signal with *ν*CO peaks at 1809, 1963, 1969, and 2013 cm^{-1}. Signals assigned to O_2 damaged clusters are shown in purple.

for the time-course experiment in order to allow the timescales of oxidative transitions to match the timeframe of IR sampling and data collection. Under 0.01% O_2, the H_{ox} signal gradually attenuated and transitioned to H_{ox}-CO, with primary *ν*CO peaks at 1809, 1963, and 2013 cm^{-1}. A near complete transition of H_{ox} to H_{ox}-CO was observed after ~200 min of O_2 exposure. The decay rates of H_{ox} specific *ν*CO signals at 1940 and 1964 cm^{-1} were calculated from normalized absorbance measurements to be $k_{Hox} \approx 10^{-4}$ s^{-1} μM^{-1} (Table 4.1, see also Table S3). These rates matched well to the inactivation rates $k_{inact} \approx 10^{-4}$ s^{-1} μM^{-1} of H_2 evolution activity (Table 4.1). We also measured the change in the FTIR spectra of *Clostridium acetobutylicum* HydA (CaI) prepared in H_{ox} and exposed to a ~30-fold higher concentration (~0.28%) of O_2. This enzyme is ~100-fold less sensitive to O_2 inactivation than CrHydA1,(101) thus was expected to have slower kinetics of O_2-induced changes in FTIR spectral features. A time-course spectrum (Figure S5) of CaI exposed to ~0.28% O_2 shows a slower decay rate of H_{ox} peak intensities, and subsequent appearance of H_{ox}-CO signals, than for CrHydA1 (Table 4.1, see also Table S3). These differences match to the comparatively slower (~100-fold) inactivation rate of CaI versus CrHydA1 (Table 4.1, see also Table S3). As observed for CrHydA1 there is good agreement between the rate of loss of H_{ox} signal intensity, $k_{Hox} \approx 10^{-6}$ s^{-1} μM^{-1} O2, and the inactivation rate of H_2 evolution activity by O_2, $k_{inact} \approx 10^{-5}$ to 10^{-6} s^{-1} μM^{-1} O2. For both enzymes, prolonged periods of O2 exposure appeared to have led to higher order effects on *ν*CO signal decay. These components were not included in the fitting parameters of Tables 4.1 and S3 used to calculate k_{Hox}.

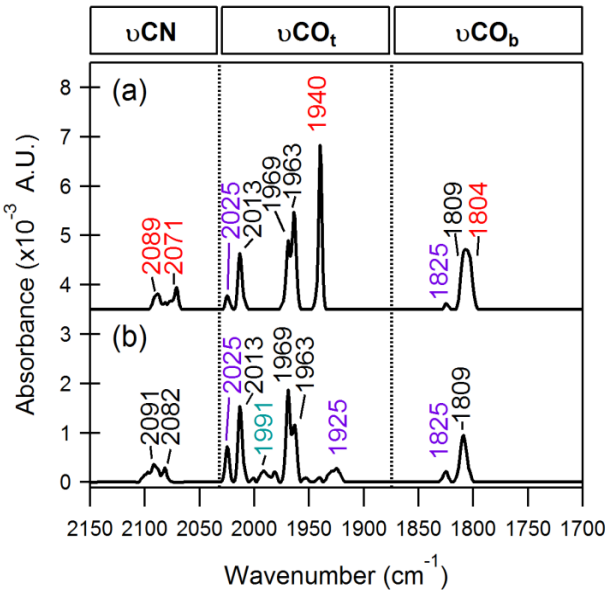

Figure 4.4. FTIR spectra of H_{ox} CrHydA1 after long-term exposure to 0.01% O_2. Scans taken at (a) 133 min, and (b) 253 min, after exposure to O_2. Wavenumber coloring is as described in Figure 4.2.

The percentage of H_{ox}-CO formed after O_2 exposure of H_{ox} (change in primary *ν*CO peaks from 1804, 1940, and 1964 cm^{-1} to 1809, 1963 and 1969 cm^{-1}) was estimated by using standardized values for *ν*CO peak heights, normalized to mg of enzyme, for an anaerobically prepared CrHydA1 H_{ox}-CO sample (Figure 4.2b, red spectrum). The amount of O_2-treated H_{ox} CrHydA1 that converted to H_{ox}-CO was determined based on normalizing the *ν*CO peak intensities in the O_2-treated sample to the H_{ox}-CO standard. The amount of CrHydA1 that converted to H_{ox}-CO was ~20% after 133 min (Figure 4.4a) of ~0.01% O_2 exposure, where the rest of the signal loss is likely due to complete degradation of the 2Fe subcluster, which is observed at 253 min (Figure 4.4b). The O_2-induced H_{ox}-CO signal appeared simultaneously with the loss of H_{ox}, and slowly decreased in intensity after 133 min (Figure 4,3). After a longer period of exposure, the loss of H_{ox}-CO was accompanied by the appearance of new *ν*CO peaks at 1825, 1925 and

2025 cm^{-1} (Figure 4.4b). These peaks were specific for oxidatively damaged H cluster, but since the overall 2Fe subcluster signal is degrading and other states are growing in (H_{ox}-CO) and decaying (H_{ox}), it is not currently possible to determine whether these peaks arise from a single or multiple H cluster state(s). These putative *ν*CO bands at 1825, 1925 and 2025 cm^{-1} might arise from oxygenation of a bridging thiolate, which was observed to induce a 6-19 cm^{-1} upshift of the νCO IR bands (123). It is possible that O2 or a byproduct of O2 led to a similar effect on CrHydA1 *ν*CO bands (see Figures 4.4a and 4.4b) (123). In depth DFT calculations on O_2 binding to the H cluster propose reaction pathways that include both oxygenation of Fe_d and oxidation of 2Fe (124, 125). In this case, the resulting oxidation of the 2Fe subcluster would also cause an upshift in the νCO bands, again consistent with the observed upshifts in CrHydA1 H_{ox} spectrum after O2 exposure.

UV-Vis of O2 Exposed CrHydA1

Ultraviolet visible (UV-Vis) spectroscopy was employed to monitor the [4Fe-4S] cluster during O2 exposure. The absorption spectra of holo-CrHydA1, CrHydA1 expressed in the absence of HydE, HydF and HydG and lacking the 2Fe subcluster (CrHydA1ΔEFG), and the O2 inactivated CrHydA1 all showed a broad 415-420 nm absorbance feature associated with S to Fe charge transfer bands of FeS clusters. CrHydA1ΔEFG contains only a [4Fe-4S] subcluster inserted by E. coli's FeS cluster assembly machinery (86, 126). The difference between the spectra of CrHydA1ΔEFG and holo-CrHydA1 (Figures 4.5b and 4.5c, red and blue trace, respectively) shows that

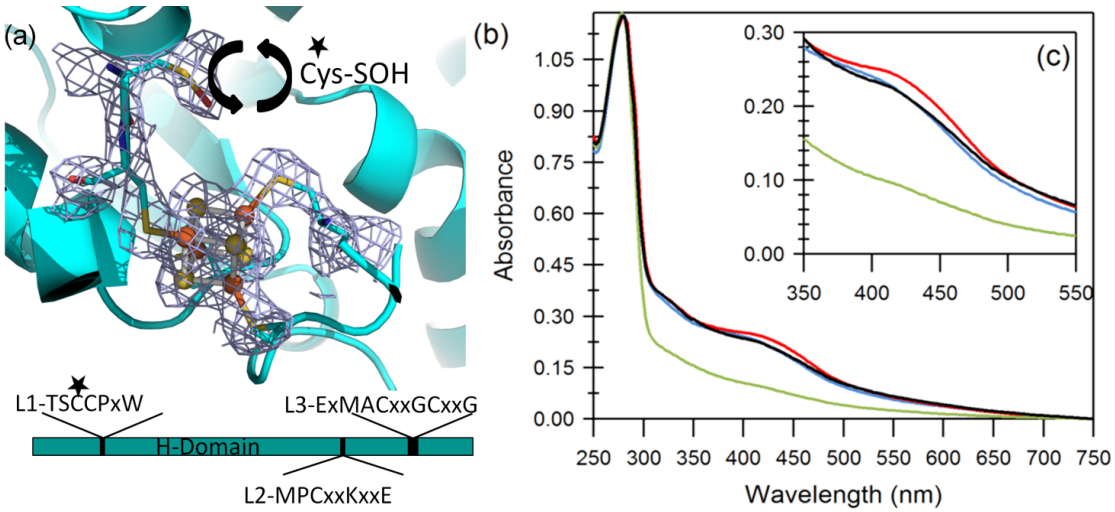

Figure 4.5. Crystal structure and UV-Vis of O_2 inactivated CrHydA1. (a) Electron density map contoured at 2σ showing extra electron density in the H cluster environment including oxidized Cys 169. The conserved [FeFe]-hydrogenase motifs are depicted below the ribbon diagram with Cys 169 (starred). (b) The full spectrum of reduced immature CrHydA1$^{\Delta EFG}$ (—), and of holo-CrHydA1 (—) after inactivation with 0.001% O_2 2 h (—), or with 3 atm of 100% O_2 for 3 h (—). (c) A close-up view of the 350-550 nm region.

the spectra for CrHydA1$^{\Delta EFG}$ appears to be red-shifted and the difference in signal at 450 nm accounts for 11% of the total absorbance. This absorbance difference could be due to CrHydA1$^{\Delta EFG}$ being in a more oxidized state, differences in Fe-loading per-mol of enzyme, or the presence of the 2Fe subcluster causing a blue shift of the 450 nm absorbance peak in holo-CrHydA1.

Inactivation of CrHydA1 by exposure to ~0.001% and 17% O_2 for 2 h was monitored by H_2 evolution activity and UV-Vis spectroscopy. The initial activity was 500 µmol min^{-1}mg^{-1}, which declined after the 2 h O_2 treatment to 12 µmol min^{-1} mg^{-1}. CrHydA1 that was not exposed to O_2 did not show a decrease in specific activity, nor any change in the UV-vis spectra. The blue trace in Figure 4.5b and 4.5c is the starting spectrum of holo-CrHydA1, and the black trace is after 2 h incubation with 0.001% O_2,

the orange trace is after 2 h incubation with 17% O_2. The difference spectra between holo-CrHydA1 (Figures 4.5b and 4.5c, blue trace) and O_2 inactivated CrHydA1 (Figures 4.5b and 4.5c, black and orange traces) did not reveal significant differences (data not shown), suggesting that most of the S→Fe charge transfer absorption is maintained after O_2 inactivation This result is consistent with stability of the [4Fe-4S] cluster against O_2 damage. CrHydA1 that was exposed to large amounts of O_2 (3 atm of 100% O_2 for 3 h) exhibited a significant decay in the peak at 420 nm (Figures 4.5b and 4.5c, green trace).

In-vitro Activation of O2 Inactivated CrHydA1

CrHydA1 that had been O2 inactivated could be in vitro activated with HydFEG (Figure S7) and activity could be recovered to ~80% 0f as purified activity. The remaining population of enzyme that was inactivateable is likely due to degradation products that were further degraded to possibly [3Fe-4S] cluster, [2Fe-2S] cluster, or completely stripped of cluster (123). This data suggests there is a significant population of enzyme containing intact [4Fe-4S] after O_2 exposure. It had been previously shown that $HydF^{EG}$ is sufficient for activating $CrHydA1^{\Delta EFG}$,(70) and that activation of $CrHydA1^{\Delta EFG}$ requires the assembly of a preformed [4Fe-4S] cluster (86).

Structural Characterization of O_2 Inactivated CrHydA1

CrHydA1 inactivated by O_2 readily crystallized and the structure was determined to 2.3Å resolution. The resulting structure was very similar to the previously characterized structure of purified CrHydA1 expressed in the absence of [FeFe]-hydrogenase maturases HydE, HydF, and HydG with an overall r.m.s. deviation between the two structures of 0.29 Å (86). The structure revealed a vacant 2Fe subcluster site and

an intact [4Fe-4S] subcluster (Figure 4.5a) and an open channel leading from the surface to the site left vacant in absence of the 2Fe subcluster. This suggests that the O_2 inactivated CrHydA1 is the appropriate conformation and is consistent with the observation that oxygen inactivated CrHydA1 can be reactivated by the H cluster maturation machinery. In addition, the structure revealed three Cys residues (amino acids 88, 169, and 238) to have additional electron density around the sulfur atoms which can be modeled and refined suggesting sulfenic acid (R-SOH) at positions Cys 169 (which functions in proton-transfer to the H-cluster(124)) and Cys 238 (surface localized) and sulfinic acid (R-SOOH) at position Cys 88 (surface localized). No modifications of the four Cys residues that function to coordinate the H cluster (Cys 170, 225, 417, and 421) were detected. The extra electron density at Cys 169 is best explained as a reaction product of the sulfur group with ROS, which might arise from O_2 binding at the 2Fe subcluster. It is possible that the modifications of the surface Cys 88 and 238 might arise from diffusion of ROS out of the catalytic site. Due to the importance of Cys 169, we used MS analysis to confirm the presence of sulfenic acid at the Cys 169 position observed in the X-ray structure (Figure S6). Thus this residue may also play an important role in inactivation. Although O_2 damage is evident from the X-ray and analytical structures, the [4Fe-4S] subcluster was intact with no evidence of O2 damage.

Discussion

The results of recent studies in which X-ray Absorption Spectroscopy (XAS) was used to monitor O_2 damage of CrHydA1 were interpreted to indicate that after O_2 binding and reaction with the 2Fe subcluster, the initial target of H cluster degradation was the [4Fe-4S] subcluster (102, 112). These studies were conducted with high concentrations of O_2 and in one study with the additional presence of high concentrations of NaDT. For example, Stripp *et al.* exposed ~ 30 nmol of CrHydA1 equilibrated in the H_{ox} state to ~20% O_2 over a period of 15 min,(102) whereas in Lambertz *et al.* exposed 8 nmol of NaDT reduced CrHydA1 to air saturated buffer (~330 μM or 21% O_2) for ~17 min (112). In contrast, for the comparative study with FTIR (Figure 4.3), we monitored H_{ox} 2Fe subcluster degradation with slightly more enzyme (~68 nmol), but exposed to ~2500x less (~0.137 μM in solution as determined by Henry's Law or ~0.01% headspace partial pressure) concentrated O_2 in solution over a ~17x longer time period. As mentioned above, several experiments were conducted with different amounts of O_2 in order to determine the amount that caused inactivation on timescales that allowed for detection of intermediates. Thus, the amount of O_2 used extended the time-frame of inactivation, and allowed for a combined use of FTIR and UV-Vis spectroscopies to monitor the integrity of both the 2Fe and [4Fe-4S] subclusters. Higher amounts of O_2 led to faster inactivation times and more rapid loss of 2Fe IR signals (Figure S4), whereas [4Fe-4S] signals persisted longer (Figures 4.5b and 4.5c). Similar experimental setups were performed to allow the use of additional analytical techniques (biochemical assays, and UV-Vis

spectroscopies, mass spectrometry, and X-ray crystallography) to follow the fate of the 2Fe subcluster and [4Fe-4S] subcluster during the inactivation process.

FTIR analysis of CrHydA1 incubated in the presence of ~0.01% O_2 in the absence of exogenously added reducing agents exhibited attenuation of the H_{ox} state. The attenuation of the H_{ox} signal tracked nearly 1:1 with loss of enzyme hydrogen production activity and is strong evidence that the 2Fe subcluster of the H cluster is the initial site of O_2 inactivation. In addition to the loss of H_{ox} signal due to O2, signals commonly associated with H_{ox}-CO state appeared. This observation suggests that O_2 degrades the 2Fe subcluster, liberating CO, and that the proportion of H cluster that transitions to the H_{ox}-CO state is a result of the free CO binding to remaining intact clusters. CO liberation and CO binding to intact enzyme in H_{ox} is also thought to occur during photoillumination of the [FeFe]-hydrogenases (50). These observations are consistent with free CO being a potent inhibitor (K_i≈0.1 μM) (101) of [FeFe]-hydrogenases.

The changes that occur when CrHydA1 is exposed to O_2 appear to occur to a greater extent and at a higher rate when poised in the H_{ox} state. Enzyme poised in H_{ox}-CO, H_{red}-H_2, and H_{red}-NaDT were less prone to O_2-dependent decay. CrHydA1 equilibrated under H_2 or NaDT reduced also showed limited degradation compared to H_{ox}, with a majority of 2Fe subcluster signal being maintained at 1.2% to 2% O_2 respectively after 2 h (NaDT data shown in Figure S2). The data suggests that an H cluster that is coordinately saturated with an occupied distal Fe ligand exchangeable site is more resistant to O_2 damage and provide strong support of this site as the initial site of O_2 binding and attack along the pathway of H cluster degradation (100-102, 108-111).

The addition of CO had the greatest protective effect with no observable decay of H_{ox}-CO up to 24.7% O_2 (Figure S1) over 2 h of exposure, consistent with previous electrochemical observations (100-102). The H_2 and NaDT treated CrHydA1 exposed to O_2 initially transitions into H_{ox} prior to degradation indicated by the observed appearance of the 1940 cm^{-1} feature. Subsequently, similar degradation products are observed in the NaDT- and H_2-treated CrHydA1 samples as were observed with H_{ox} samples, with the transient appearance of H_{ox}-CO specific FTIR features.

The O_2 inactivated CrHydA1 was capable of being reactivated by the addition of $HydF^{EG}$ suggesting that the inactivated enzyme has a damaged or absent 2Fe subcluster. Further, as described above, both UV-Vis spectroscopy and structural characterization indicated the presence of an intact [4Fe-4S] subcluster that was stable long after activity attenuated. Interestingly, the X-ray crystal structure and UV-Vis of O_2 inactivated CrHydA1 strongly resembled CrHydA1 expressed in the absence of maturases ($CrHydA1^{\Delta EFG}$). Previous studies probing H cluster degradation using comparatively higher concentrations of O_2 either with(112) or without(102) NaDT proposed that the degradation of the [4Fe-4S] subcluster preceded 2Fe subcluster degradation, whereby ROS was generated by O_2 binding and reaction at the 2Fe subcluster. Under the conditions of our study in which CrHydA1 was exposed to O_2 in the absence of NaDT, the [4Fe-4S] subcluster seems fairly resistant to degradation. We do however see evidence for the oxidation of the non-coordinating active site Cys (Cys 169) perhaps through the formation of ROS (125). Exposure of either the O_2 degradation intermediate observed here or $CrHydA1^{\Delta EFG}$ to high concentrations of O_2 resulted in the eventual

destruction of the [4Fe-4S] subcluster, as evidenced by reduction and eventual loss of the S→Fe charge transfer bands at ~420 nm.

Thus, based on the experimental evidence presented here, we propose that the mechanism of O_2 attack on CrHydA1 first involves degradation of the more labile 2Fe subcluster, followed by attack on the more robust [4Fe-4S] subcluster. The titration data suggests that the reaction sequence is independent of O_2 concentration, but occurs at a concentration dependent rate. High (>1%) O2 levels led to fast 2Fe subcluster degradation and did not allow for the reliable detection of inactivation intermediates by our FTIR set-up.

Conclusion

The inactivation of [FeFe]-hydrogenase by O_2 is defined by steps that involve the diffusion of gases into close proximity of the catalytic site, followed by redox/chemical steps of O_2 reaction with the H cluster. Our results are consistent with theoretical models(108) and indicate that the latter process proceeds *via* oxidative breakdown of the 2Fe subcluster, initially releasing CO that can bind to secondary targets (e.g., other enzymes). Further exposure results in the eventual formation of a stable break-down product with an intact [4Fe-4S] subcluster and a vacant 2Fe subcluster site capable of being reactivated by 2Fe subcluster specific maturation machinery. Long-term and/or high concentration O_2 exposure is required for oxidative damage of the [4Fe-4S] subcluster and complete H cluster degradation as evidenced by the previous XAS/EXAFS studies. Based on our results, [FeFe]-hydrogenase inactivation from O_2

exposure essentially reverses the maturation pathway of H cluster insertion into immature CrHydA1, and suggests that H clusters inactivated by low concentration O_2 exposure *in vitro* could be substrates for reactivation by $HydF^{EG}$.

CHAPTER 5

CONCLUDING REMARKS

Developing alternative energy technologies to replace fossil fuels is one of the biggest fundamental problems that face humanity. The continual burning of fossil fuels releases CO_2 into the atmosphere which may lead to irreversible effects that negatively impacting our environment and economy. In order to supplant fossil fuel use, methods for efficient energy capture, conversions, and storage must be found for our alternative energy sources (i.e. wind, hydro, solar, tidal, etc.). Hydrogen has properties that will likely make it a key player in developing technologies to capture, convert, and store alternative energy.

To effectively use energy from alternative sources on a continual basis, it will be necessary to capture and transfer energy into chemical bonds for long term energy storage and utilization. Hydrogen may be a useful intermediary in energy capture and transfer steps due to its high energy bond. Energy captured in the form of hydrogen could be used in industrial processes allowing transfer of energy into products such as liquid hydrocarbon fuels and ammonia in the Fisher-Tropsch process and Haber-Bosch process respectively. Alternatively, hydrogen can be used as an energy storage molecule itself or used directly as a fuel source in hydrogen fuel cells.

The demand for the production of hydrogen is growing and will likely continue to grow as alternative energy technologies develop and with its need for methanol production, ammonia production, and refinery processes. The increasing demand for

hydrogen means new ways need to be developed to produce hydrogen that decrease our reliance on the fossil fuel based feedstocks that are primarily used for hydrogen production. Hydrogen produced from biological sources may eventually be a real solution for decreasing this reliance, and microbes would be the biological source since there are species that contain the extremely efficient [FeFe]-hydrogenase hydrogen producing catalyst. Furthermore, the [FeFe]-hydrogenase can be linked to processes such as photosynthesis and anaerobic fermentation to produce hydrogen from renewable sources with those being sunlight and carbohydrate containing waste materials respectively. The [FeFe]-hydrogenase is limited by its O_2 sensitivity in many applications, and it has been of great interest to improve and understand its O_2 sensitivity in order to help realize a solution for biological hydrogen production on a large scale.

This work presented demonstrates new insight into understanding and addressing the problem of [FeFe]-hydrogenase O_2 sensitivity. In the 2nd chapter, methods were described on how to heterologously express the [FeFe]-hydrogenase and maturase HydF in *E. coli* and purify both proteins. Sufficient enough quantity and quality of enzyme was obtained to allow collection of FTIR spectra with properties similar to that of HydF isolated from *C. acetobutylicum* and CrHydA1 isolated from *C. reinhardtii*. These methods to obtain hydrogenase enzyme were also used in both chapter 3 and chapter 4 to produce material for characterization.

In the 3rd chapter, sequences recovered from the solar saltern mats in Guerrero Negro, MX were used as a guide to search for biomarkers that may suggest oxygen tolerance in the [FeFe]-hydrogenase. The large sequence set that was obtained from

Guerrero Negro was simplified by making consensus sequences. The resulting consensus sequences helped target sequence variations that could be made in the model [FeFe]-hydrogenase Cp1 by site directed mutagenesis. Several sequence variations were found in gas channel A, and the most interesting was found at site 283which increased the size of the side chain by varying from a leucine to a phenylalanine causing an increase in the half life of inactivation. Large occluding residues at this site may in fact suggest an [FeFe]-hydrogenase that has evolved O_2 tolerance suggesting it as a possible biomarker. An interesting site change from cysteine to serine was also observed for a residue that coordinates the H-cluster, and the serine variant was inactive for hydrogen production in Cp1. This may suggest that the gene products for enzymes containing this variation may have larger structural differences in order for them to be active, or in order to observe activity in the Cp1 variant, it may require conditions not typical for standard [FeFe]-hydrogenase activity assays.

Lastly, in the 4th chapter, it was explained how the [FeFe]-hydrogenase active site reacts with oxygen in a modular fashion were the 2Fe subcluster is the first site of O_2 related degradation. This was in contrast to a previous study that proposed the degradation of the [4Fe-4S] subcluster occurred first. It was demonstrated using FTIR that the 2Fe subcluster's IR signatures would attenuate under low concentrations of oxygen when in the H_{ox} state, and it was further demonstrated that enzyme in $H_{red\text{-}DT}$, $H_{red\text{-}H2,}$ and H_{ox}-CO states were protected from inactivation likely due occupation of the open coordination site of the distal Fe. It was also observed that CO liberated from inactivation could bind intact enzyme forming H_{ox}-CO, and from UVvis and X-ray

crystallography experiments it appeared that the [4Fe-4S]-subcluster remained largely intact after O_2 exposure. Additionally, the formation of sulfenic acid at site 169 as observed in the O_2 inactivated crystal structure and mass spectra of peptide fragments suggests formation of ROS since sulfenic acid only forms due to cysteine reacting with ROS. This data is suggestive that the [4Fe-4S] cluster doesn't decay in the presence of ROS as previously proposed.

REFERENCES CITED

1. Panwar, N. L., Kaushik, S. C., and Kothari, S. (2011) Role of renewable energy sources in environmental protection: A review, *Renewable and Sustainable Energy Reviews 15*, 1513-1524.

2. EIA, U. (2011) International energy outlook 2011, *US Energy Information Administration*.

3. Centi, G., and Perathoner, S. (2011) CO2-based energy vectors for the storage of solar energy, *Greenhouse Gases: Science and Technology 1*, 21-35.

4. Centi, G., and Perathoner, S. (2010) Towards Solar Fuels from Water and CO2, *ChemSusChem 3*, 195-208.

5. Lewis, N. S., and Crabtree, G. (2005) Basic Research Needs for Solar Energy Utilization: report of the Basic Energy Sciences Workshop on Solar Energy Utilization, April 18-21, 2005.

6. Lewis, N. S., and Nocera, D. G. (2006) Powering the planet: Chemical challenges in solar energy utilization, *P Natl Acad Sci Usa 103*, 15729-15735.

7. Evans, A., Strezov, V., and Evans, T. J. (2012) Assessment of utility energy storage options for increased renewable energy penetration, *Renewable and Sustainable Energy Reviews 16*, 4141-4147.

8. Züttel, A., Remhof, A., Borgschulte, A., and Friedrichs, O. (2010) Hydrogen: the future energy carrier, *Philosophical Transactions of the Royal Society A: Mathematical, Physical and Engineering Sciences 368*, 3329-3342.

9. Cook, T. R., Dogutan, D. K., Reece, S. Y., Surendranath, Y., Teets, T. S., and Nocera, D. G. (2010) Solar Energy Supply and Storage for the Legacy and Nonlegacy Worlds, *Chemical Reviews 110*, 6474-6502.

10. Roy, S. C., Varghese, O. K., Paulose, M., and Grimes, C. A. (2010) Toward Solar Fuels: Photocatalytic Conversion of Carbon Dioxide to Hydrocarbons, *ACS Nano 4*, 1259-1278.

11. Tian, F., Toon, O. B., Pavlov, A. A., and De Sterck, H. (2005) A Hydrogen-Rich Early Earth Atmosphere, *Science 308*, 1014-1017.

12. Schlapbach, L., and Zuttel, A. (2001) Hydrogen-storage materials for mobile applications, *Nature 414*, 353-358.

13. Krajačić, G., Martins, R., Busuttil, A., Duić, N., and da Graça Carvalho, M. (2008) Hydrogen as an energy vector in the islands' energy supply, *International Journal of Hydrogen Energy 33*, 1091-1103.

14. Edwards, P. P., Kuznetsov, V. L., and David, W. I. F. (2007) Hydrogen energy, *Philosophical Transactions of the Royal Society A: Mathematical, Physical and Engineering Sciences 365*, 1043-1056.

15. Sartbaeva, A., Kuznetsov, V. L., Wells, S. A., and Edwards, P. P. (2008) Hydrogen nexus in a sustainable energy future, *Energy & Environmental Science 1*, 79-85.

16. Vlachos, D. G., and Caratzoulas, S. (2010) The roles of catalysis and reaction engineering in overcoming the energy and the environment crisis, *Chemical Engineering Science 65*, 18-29.

17. Muradov, N. Z., and Veziroğlu, T. N. (2008) "Green" path from fossil-based to hydrogen economy: An overview of carbon-neutral technologies, *International Journal of Hydrogen Energy 33*, 6804-6839.

18. Mueller-Langer, F., Tzimas, E., Kaltschmitt, M., and Peteves, S. (2007) Techno-economic assessment of hydrogen production processes for the hydrogen economy for the short and medium term, *International Journal of Hydrogen Energy 32*, 3797-3810.

19. Sakintuna, B., Lamari-Darkrim, F., and Hirscher, M. (2007) Metal hydride materials for solid hydrogen storage: A review, *International Journal of Hydrogen Energy 32*, 1121-1140.

20. van Vliet, O. P. R., Faaij, A. P. C., and Turkenburg, W. C. (2009) Fischer–Tropsch diesel production in a well-to-wheel perspective: A carbon, energy flow and cost analysis, *Energy Conversion and Management 50*, 855-876.

21. Moon, G., Lee, Y., Choi, K., and Jeong, D. (2010) Emission characteristics of diesel, gas to liquid, and biodiesel-blended fuels in a diesel engine for passenger cars, *Fuel 89*, 3840-3846.

22. Olah, G. A. (2005) Beyond Oil and Gas: The Methanol Economy, *Angewandte Chemie International Edition 44*, 2636-2639.

23. Grimmer, H. R., Thiagarajan, N., and Nitschke, E. (1988) Conversion of Methanol to Liquid Fuels by the Fluid Bed Mobil Process (A commercial concept), In *Studies in Surface Science and Catalysis* (D.M. Bibby, C. D. C. R. F. H., and Yurchak, S., Eds.), pp 273-291, Elsevier.

24. Abbasi, T., and Abbasi, S. A. (2011) 'Renewable' hydrogen: Prospects and challenges, *Renewable and Sustainable Energy Reviews 15*, 3034-3040.

25. Nazim, Z. M. (2008) Production of Hydrogen from Hydrocarbons, In *Hydrogen Fuel*, pp 33-101, CRC Press.

26. Dicks, A. L. (1996) Hydrogen generation from natural gas for the fuel cell systems of tomorrow, *Journal of Power Sources 61*, 113-124.

27. Holladay, J. D., Hu, J., King, D. L., and Wang, Y. (2009) An overview of hydrogen production technologies, *Catalysis Today 139*, 244-260.

28. Hallenbeck, P. C., and Benemann, J. R. (2002) Biological hydrogen production; fundamentals and limiting processes, *International Journal of Hydrogen Energy 27*, 1185-1193.

29. Hallenbeck, P. C., Abo-Hashesh, M., and Ghosh, D. (2012) Strategies for improving biological hydrogen production, *Bioresource Technology 110*, 1-9.

30. Turner, J., Sverdrup, G., Mann, M. K., Maness, P. C., Kroposki, B., Ghirardi, M. L., Evans, R. J., and Blake, D. (2008) Renewable hydrogen production, *Int. J. Hydrogen Energ. 32*, 379-407.

31. Ramachandran, R., and Menon, R. K. (1998) An overview of industrial uses of hydrogen, *International Journal of Hydrogen Energy 23*, 593-598.

32. Cecere, D., Giacomazzi, E., and Ingenito, A. (2014) A review on hydrogen industrial aerospace applications, *International Journal of Hydrogen Energy 39*, 10731-10747.

33. Yacoby, I., Pochekailov, S., Toporik, H., Ghirardi, M. L., King, P. W., and Zhang, S. (2011) Photosynthetic electron partitioning between [FeFe]-hydrogenase and ferredoxin:NADP+-oxidoreductase (FNR) enzymes in vitro, *Proceedings of the National Academy of Sciences 108*, 9396-9401.

34. Greenbaum, E. (1988) Energetic Efficiency of Hydrogen Photoevolution by Algal Water Splitting, *Biophysical Journal 54*, 365-368.

35. Ghirardi, M. L., Posewitz, M. C., Maness, P.-C., Dubini, A., Yu, J., and Seibert, M. (2007) Hydrogenases and hydrogen photoproduction in oxygenic photosynthetic organisms, *Annu. Rev. Plant Biol. 58*, 71-91.

36. Srirangan, K., Pyne, M. E., and Perry Chou, C. (2011) Biochemical and genetic engineering strategies to enhance hydrogen production in photosynthetic algae and cyanobacteria, *Bioresource Technology 102*, 8589-8604.

37. Vignais, P. M., Billoud, B., and Meyer, J. (2001) Classification and phylogeny of hydrogenases, *FEMS Microbiol. Rev. 25*, 455-501.

38. Malki, S., Saimmaime, I., De Luca, G., Rousset, M., Dermoun, Z., and Belaich, J. P. (1995) Characterization of an operon encoding an NADP-reducing hydrogenase in Desulfovibrio fructosovorans, *Journal of Bacteriology 177*, 2628-2636.

39. Vignais, P. M., and Billoud, B. (2007) Occurrence, classification, and biological function of hydrogenases: An overview, *Chem. Rev. 107*, 4206-4272.

40. Shima, S., and Thauer, R. K. (2007) A third type of hydrogenase catalyzing H-2 activation, *Chem. Rec. 7*, 37-46.

41. Silakov, A., Wenk, B., Reijerse, E., and Lubitz, W. (2009) N-14 HYSCORE investigation of the H-cluster of [FeFe] hydrogenase: evidence for a nitrogen in the dithiol bridge, *Phys. Chem. Chem. Phys. 11*, 6592-6599.

42. Siegbahn, P. E. M., Tye, J. W., and Hall, M. B. (2007) Computational studies of [NiFe] and [FeFe] hydrogenases, *Chem. Rev. 107*, 4414-4435.

43. Shima, S., Pilak, O., Vogt, S., Schick, M., Stagni, M. S., Meyer-Klaucke, W., Warkentin, E., Thauer, R. K., and Ermler, U. (2008) The crystal structure of [Fe]-hydrogenase reveals the geometry of the active site, *Science 321*, 572-575.

44. Fontecilla-Camps, J. C., Volbeda, A., Cavazza, C., and Nicolet, Y. (2007) Structure/function relationships of [NiFe]- and [FeFe]-hydrogenases, *Chem. Rev. 107*, 4273-4303.

45. Nicolet, Y., Piras, C., Legrand, P., Hatchikian, C. E., and Fontecilla-Camps, J. C. (1999) Desulfovibrio desulfuricans iron hydrogenase: the structure shows unusual coordination to an active site Fe binuclear center, *Struct. Fold. Des. 7*, 13-23.

46. Peters, J. W., Lanzilotta, W. N., Lemon, B. J., and Seefeldt, L. C. (1998) X-ray crystal structure of the Fe-only hydrogenase (Cpl) from Clostridium pasteurianum to 1.8 angstrom resolution, *Science 282*, 1853-1858.

47. Meyer, J. (2007) [FeFe] hydrogenases and their evolution: a genomic perspective, *Cell. Mol. Life. Sci. 64*, 1063-1084.

48. Lemon, B., and Peters, J. (1999) Binding of exogenously added carbon monoxide at the active site of the iron-only hydrogenase (CpI) from Clostridium pasteurianum, *Biochemistry 38*, 12969-12973.

49. Pandey, A. S., Harris, T. V., Giles, L. J., Peters, J. W., and Szilagyi, R. K. (2008) Dithiomethylether as a Ligand in the Hydrogenase H-Cluster, *Journal of the American Chemical Society 130*, 4533-4540.

50. Pierik, A. J., Hulstein, M., Hagen, W. R., and Albracht, S. P. J. (1998) A low-spin iron with CN and CO as intrinsic ligands forms the core of the active site in [Fe]-hydrogenases, *Eur. J. Biochem. 258*, 572-578.

51. Berggren, G., Adamska, A., Lambertz, C., Simmons, T. R., Esselborn, J., Atta, M., Gambarelli, S., Mouesca, J. M., Reijerse, E., Lubitz, W., Happe, T., Artero, V., and Fontecave, M. (2013) Biomimetic assembly and activation of [FeFe]-hydrogenases, *Nature 499*, 66-69.

52. Weiner, J. H., Bilous, P. T., Shaw, G. M., Lubitz, S. P., Frost, L., Thomas, G. H., Cole, J. A., and Turner, R. J. (1998) A Novel and Ubiquitous System for Membrane Targeting and Secretion of Cofactor-Containing Proteins, *Cell 93*, 93-101.

53. Wu, L. F., and Mandrand, M. (1993) Microbial hydrogenases: Primary structure, classification, signatures and phylogeny, *FEMS Microbiology Letters 104*, 243-270.

54. Volbeda, A., Charon, M.-H., Piras, C., Hatchikian, E. C., Frey, M., and Fontecilla-Camps, J. C. (1995) Crystal structure of the nickel-iron hydrogenase from Desulfovibrio gigas, *Nature 373*, 580-587.

55. Ogata, H., Hirota, S., Nakahara, A., Komori, H., Shibata, N., Kato, T., Kano, K., and Higuchi, Y. (2005) Activation process of [NiFe] hydrogenase elucidated by high-resolution X-ray analyses: Conversion of the ready to the unready state, *Structure 13*, 1635-1642.

56. Ogata, H., Mizoguchi, Y., Mizuno, N., Miki, K., Adachi, S., Yasuoka, N., Yagi, T., Yamauchi, O., Hirota, S., and Higuchi, Y. (2002) Structural studies of the carbon monoxide complex of [NiFe]hydrogenase from Desulfovibrio vulgaris Miyazaki F: Suggestion for the initial activation site for dihydrogen, *J. Am. Chem. Soc. 124*, 11628-11635.

57. Higuchi, Y., Ogata, H., Miki, K., Yasuoka, N., and Yagi, T. (1999) Removal of the bridging ligand atom at the Ni-Fe active site of [NiFe] hydrogenase upon

reduction with H-2, as revealed by X-ray structure analysis at 1.4 angstrom resolution, *Structure 7*, 549-556.

58. Volbeda, A., Montet, Y., Vernede, X., Hatchikian, E. C., and Fontecilla-Camps, J. C. (2002) High-resolution crystallographic analysis of Desulfovibrio fructiosovorans [NiFe] hydrogenase, *Int. J. Hydrog. Energy 27*, 1449-1461.

59. Matias, P., Soares, C., Saraiva, L., Coelho, R., Morais, J., Le Gall, J., and Carrondo, M. (2001) [NiFe] hydrogenase from Desulfovibrio desulfuricans ATCC 27774: gene sequencing, three-dimensional structure determination and refinement at 1.8 angstrom and modelling studies of its interaction with the tetrahaem cytochrome c(3), *J. Biol. Inorg. Chem. 6*, 63-81.

60. Ogata, H., Kellers, P., and Lubitz, W. (2010) The Crystal Structure of the [NiFe] Hydrogenase from the Photosynthetic Bacterium Allochromatium vinosum: Characterization of the Oxidized Enzyme (Ni-A State), *Journal of Molecular Biology 402*, 428-444.

61. Shomura, Y., Yoon, K.-S., Nishihara, H., and Higuchi, Y. (2011) Structural basis for a [lsqb]4Fe-3S[rsqb] cluster in the oxygen-tolerant membrane-bound [lsqb]NiFe[rsqb]-hydrogenase, *Nature 479*, 253-256.

62. Volbeda, A., Amara, P., Darnault, C., Mouesca, J.-M., Parkin, A., Roessler, M. M., Armstrong, F. A., and Fontecilla-Camps, J. C. (2012) X-ray crystallographic and computational studies of the O2-tolerant [NiFe]-hydrogenase 1 from Escherichia coli, *Proceedings of the National Academy of Sciences 109*, 5305-5310.

63. Volbeda, A., Darnault, C., Parkin, A., Sargent, F., Armstrong, Fraser A., and Fontecilla-Camps, Juan C. (2013) Crystal Structure of the O2-Tolerant Membrane-Bound Hydrogenase 1 from Escherichia coli in Complex with Its Cognate Cytochrome b, *Structure 21*, 184-190.

64. Bowman, L., Flanagan, L., Fyfe, P. K., Parkin, A., Hunter, W. N., and Sargent, F. (2014) How the structure of the large subunit controls function in an oxygen-tolerant [NiFe]-hydrogenase, *Biochemical Journal 458*, 449-458.

65. Frielingsdorf, S., Fritsch, J., Schmidt, A., Hammer, M., Löwenstein, J., Siebert, E., Pelmenschikov, V., Jaenicke, T., Kalms, J., Rippers, Y., Lendzian, F., Zebger, I., Teutloff, C., Kaupp, M., Bittl, R., Hildebrandt, P., Friedrich, B., Lenz, O., and Scheerer, P. (2014) Reversible [4Fe-3S] cluster morphing in an O2-tolerant [NiFe] hydrogenase, *Nat Chem Biol 10*, 378-385.

66. Fritsch, J., Scheerer, P., Frielingsdorf, S., Kroschinsky, S., Friedrich, B., Lenz, O., and Spahn, C. M. T. (2011) The crystal structure of an oxygen-tolerant hydrogenase uncovers a novel iron-sulphur centre, *Nature 479*, 249-252.

67. Vitt, S., Ma, K., Warkentin, E., Moll, J., Pierik, A. J., Shima, S., and Ermler, U. (2014) The F420-Reducing [NiFe]-Hydrogenase Complex from Methanothermobacter marburgensis, the First X-ray Structure of a Group 3 Family Member, *Journal of Molecular Biology 426*, 2813-2826.

68. Pandey, A. S., Harris, T. V., Giles, L. J., Peters, J. W., and Szilagyi, R. K. (2008) Dithiomethylether as a Ligand in the Hydrogenase H-Cluster, *J. Am. Chem. Soc. 130*, 4533-4540.

69. Posewitz, M. C., King, P. W., Smolinski, S. L., Zhang, L. P., Seibert, M., and Ghirardi, M. L. (2004) Discovery of two novel radical S-adenosylmethionine proteins required for the assembly of an active [Fe] hydrogenase, *J. Biol. Chem. 279*, 25711-25720.

70. McGlynn, S. E., Shepard, E. M., Winslow, M. A., Naumov, A. V., Duschene, K. S., Posewitz, M. C., Broderick, W. E., Broderick, J. B., and Peters, J. W. (2008) HydF as a scaffold protein in [FeFe] hydrogenase H-cluster biosynthesis, *FEBS Lett. 582*, 2183-2187.

71. Rubach, J. K., Brazzolotto, X., Gaillard, J., and Fontecave, M. (2005) Biochemical characterization of the HydE and HydG iron-only hydrogenase maturation enzymes from Thermatoga maritima, *FEBS Lett. 579*, 5055-5060.

72. Driesener, R. C., Challand, M. R., McGlynn, S. E., Shepard, E. M., Boyd, E. S., Broderick, J. B., Peters, J. W., and Roach, P. L. (2010) [FeFe]-Hydrogenase Cyanide Ligands Derived From S-Adenosylmethionine-Dependent Cleavage of Tyrosine, *Angew. Chem. Int. Ed. 49*, 1687-1690.

73. Shepard, E. M., Duffus, B. R., George, S. J., McGlynn, S. E., Challand, M. R., Swanson, K. D., Roach, P. L., Cramer, S. P., Peters, J. W., and Broderick, J. B. (2010) [FeFe]-Hydrogenase Maturation: HydG-Catalyzed Synthesis of Carbon Monoxide, *J. Am. Chem. Soc. 132*, 9247-9249.

74. Shepard, E. M., McGlynn, S. E., Bueling, A. L., Grady-Smith, C. S., George, S. J., Winslow, M. A., Cramer, S. P., Peters, J. W., and Broderick, J. B. (2010) Synthesis of the 2Fe-subcluster of the [FeFe]-hydrogenase H-cluster on the HydF scaffold, *P. Natl. Acad. Sci. U.S.A. 107*, 10448-10453.

75. Czech, I., Silakov, A., Lubitz, W., and Happe, T. (2010) The [FeFe]-hydrogenase maturase HydF from Clostridium acetobutylicum contains a CO and CN- ligated iron cofactor, *FEBS Lett. 584*, 638-642.

76. Shepard, E. M., Byer, A. S., Boyd, E. S., Swanson, K. D., Peters, J. W., and Broderick, J. B. (2011) [FeFe]-Hydrogenase Cofactor Assembly, In *Encyclopedia of Inorganic and Bioinorganic Chemistry*, John Wiley & Sons, Ltd.

77. King, P. W., Posewitz, M. C., Ghirardi, M. L., and Seibert, M. (2006) Functional studies of [FeFe] hydrogenase maturation in an Escherichia coli biosynthetic system, *J. Bacteriol. 188*, 2163-2172.

78. Girbal, L., von Abendroth, G., Winkler, M., Benton, P., Meynial-Salles, I., Croux, C., Peters, J., Happe, T., and Soucaille, P. (2005) Homologous and heterologous overexpression in Clostridium acetobutylicum and characterization of purified clostridial and algal Fe-only hydrogenases with high specific activities, *Appl Environ Microb 71*, 2777-2781.

79. von Abendroth, G., Stripp, S., Silakov, A., Croux, C., Soucaille, P., Girbal, L., and Happe, T. (2008) Optimized over-expression of [FeFe] hydrogenases with high specific activity in Clostridium acetobutylicum, *Int. J. Hydrog. Energy 33*, 6076-6081.

80. Sybirna, K., Antoine, T., Lindberg, P., Fourmond, V., Rousset, M., Mejean, V., and Bottin, H. (2008) Shewanella oneidensis: a new and efficient system for expression and maturation of heterologous [Fe-Fe] hydrogenase from Chlamydomonas reinhardtii, *Bmc Biotechnol. 8*, 73.

81. Kuchenreuther, J. M., Grady-Smith, C. S., Bingham, A. S., George, S. J., Cramer, S. P., and Swartz, J. R. (2010) High-Yield Expression of Heterologous [FeFe] Hydrogenases in <italic>Escherichia coli</italic>, *PLoS ONE 5*, e15491.

82. Yacoby, I., Tegler, L. T., Pochekailov, S., Zhang, S., and King, P. W. (2012) Optimized Expression and Purification for High-Activity Preparations of Algal [FeFe]-Hydrogenase, *PLoS ONE 7*, e35886.

83. Cendron, L., Berto, P., D'Adamo, S., Vallese, F., Govoni, C., Posewitz, M. C., Giacometti, G. M., Costantini, P., and Zanotti, G. (2011) Crystal structure of HydF scaffold protein provides insights into [FeFe]-hydrogenase maturation, *Journal of Biological Chemistry*.

84. Brazzolotto, X., Rubach, J. K., Gaillard, J., Gambarelli, S., Atta, M., and Fontecave, M. (2006) The [Fe-Fe]-hydrogenase maturation protein HydF from

Thermotoga maritima is a GTPase with an iron-sulfur cluster, *J. Biol. Chem. 281*, 769-774.

85. Mulder, D. W., Ratzloff, M. W., Shepard, E. M., Byer, A. S., Noone, S. M., Peters, J. W., Broderick, J. B., and King, P. W. (2013) EPR and FTIR Analysis of the Mechanism of H2 Activation by [FeFe]-Hydrogenase HydA1 from Chlamydomonas reinhardtii, *J. Am. Chem. Soc. 135*, 6921-6929.

86. Mulder, D. W., Ortillo, D. O., Gardenghi, D. J., Naumov, A. V., Ruebush, S. S., Szilagyi, R. K., Huynh, B., Broderick, J. B., and Peters, J. W. (2009) Activation of HydA(Delta EFG) Requires a Preformed [4Fe-4S] Cluster, *Biochemistry 48*, 6240-6248.

87. Cammack, R. (1999) Bioinorganic chemistry - Hydrogenase sophistication, *Nature 397*, 214-215.

88. Winkler, M., Kuhlgert, S., Hippler, M., and Happe, T. (2009) Characterization of the Key Step for Light-driven Hydrogen Evolution in Green Algae, *Journal of Biological Chemistry 284*, 36620-36627.

89. Demuez, M., Cournac, L., Guerrini, O., Soucaille, P., and Girbal, L. (2007) Complete activity profile of Clostridium acetobutylicum [FeFe]-hydrogenase and kinetic parameters for endogenous redox partners, *FEMS Microbiology Letters 275*, 113-121.

90. Calusinska, M., Happe, T., Joris, B., and Wilmotte, A. (2010) The surprising diversity of clostridial hydrogenases: a comparative genomic perspective, *Microbiology 156*, 1575-1588.

91. Ghirardi, M. L., Cohen, J., King, P., Schulten, K., Kim, K., and Seibert, M. (2006) [FeFe]-hydrogenases and photobiological hydrogen production, In *SPIE*, pp 63400X-63400X-63406.

92. Bingham, A. S., Smith, P. R., and Swartz, J. R. (2012) Evolution of an [FeFe] hydrogenase with decreased oxygen sensitivity, *International Journal of Hydrogen Energy 37*, 2965-2976.

93. Lautier, T., Ezanno, P., Baffert, C., Fourmond, V., Cournac, L., Fontecilla-Camps, J. C., Soucaille, P., Bertrand, P., Meynial-Salles, I., and Leger, C. (2011) The quest for a functional substrate access tunnel in FeFe hydrogenase, *Faraday Discussions 148*, 385-407.

94. Cohen, J., Kim, K., King, P., Seibert, M., and Schulten, K. (2005) Finding Gas Diffusion Pathways in Proteins: Application to O2 and H2 Transport in CpI [FeFe]-Hydrogenase and the Role of Packing Defects, *Structure 13*, 1321-1329.

95. Cohen, J., Kim, K., Posewitz, M., Ghirardi, M., Schulten, K., Seibert, M., and King, P. (2005) Molecular dynamics and experimental investigation of H-2 and O-2 diffusion in [Fe]-hydrogenase, *Biochem Soc T 33*, 80-82.

96. Boyd, E. S., Spear, J. R., and Peters, J. W. (2009) [FeFe] Hydrogenase Genetic Diversity Provides Insight into Molecular Adaptation in a Saline Microbial Mat Community, *Appl Environ Microb 75*, 4620-4623.

97. Rees, D. C. (2002) GREAT METALLOCLUSTERS IN ENZYMOLOGY, *Annual Review of Biochemistry 71*, 221-246.

98. Meyer, J. (2008) Iron-sulfur protein folds, iron-sulfur chemistry, and evolution, *J. Biol. Inorg. Chem. 13*, 157-170.

99. McKinlay, J. B., and Harwood, C. S. (2010) Photobiological production of hydrogen gas as a biofuel, *Curr. Opin. Biotech. 21*, 244-251.

100. Baffert, C., Demuez, M., Cournac, L., Burlat, B., Guigliarelli, B., Bertrand, P., Girbal, L., and Léger, C. (2008) Hydrogen-Activating Enzymes: Activity Does Not Correlate with Oxygen Sensitivity, *Angew. Chem. Int. Edit 47*, 2052-2054.

101. Goldet, G., Brandmayr, C., Stripp, S. T., Happe, T., Cavazza, C., Fontecilla-Camps, J. C., and Armstrong, F. A. (2009) Electrochemical Kinetic Investigations of the Reactions of [FeFe]-Hydrogenases with Carbon Monoxide and Oxygen: Comparing the Importance of Gas Tunnels and Active-Site Electronic/Redox Effects, *J. Am. Chem. Soc. 131*, 14979-14989.

102. Stripp, S. T., Goldet, G., Brandmayr, C., Sanganas, O., Vincent, K. A., Haumann, M., Armstrong, F. A., and Happe, T. (2009) How oxygen attacks [FeFe] hydrogenases from photosynthetic organisms, *P. Natl. Acad. Sci. U.S.A. 106*, 17331-17336.

103. King, P. W., Svedruzic, D., Cohen, J., Schulten, K., Seibert, M., and Ghirardi, M. L. (2006) Structural and functional investigations of biological catalysts for optimization of solar-driven H2 production systems, pp 63400Y-63400Y-63409.

104. Lautier, T., Ezanno, P., Baffert, C., Fourmond, V., Cournac, L., Fontecilla-Camps, J. C., Soucaille, P., Bertrand, P., Meynial-Salles, I., and Leger, C. (2011) The quest for a functional substrate access tunnel in FeFe hydrogenase, *Faraday Discuss. 148*, 385-407.

105. Bingham, A. S., Smith, P. R., and Swartz, J. R. (2012) Evolution of an [FeFe] hydrogenase with decreased oxygen sensitivity, *Int. J. Hydrogen Energ. 37*, 2965-2976.

106. Bruska, M. K., Stiebritz, M. T., and Reiher, M. (2011) Regioselectivity of H Cluster Oxidation, *J. Am. Chem. Soc. 133*, 20588-20603.

107. Stiebritz, M. T., Finkelmann, A. R., and Reiher, M. (2011) Oxygen Coordination to the Active Site of Hmd in Relation to [FeFe] Hydrogenase, *Eur. J. Inorg. Chem. 2011*, 1163-1171.

108. Stiebritz, M. T., and Reiher, M. (2012) Hydrogenases and oxygen, *Chem. Sci. 3*, 1739-1751.

109. Kubas, A., De Sancho, D., Best, R. B., and Blumberger, J. (2014) Aerobic Damage to [FeFe]-Hydrogenases: Activation Barriers for the Chemical Attachment of O2, *Angew. Chem. 126*, 4165-4168.

110. Fourmond, V., Greco, C., Sybirna, K., Baffert, C., Wang, P.-H., Ezanno, P., Montefiori, M., Bruschi, M., Meynial-Salles, I., Soucaille, P., Blumberger, J., Bottin, H., De Gioia, L., and Léger, C. (2014) The oxidative inactivation of FeFe hydrogenase reveals the flexibility of the H-cluster, *Nat Chem 6*, 336-342.

111. Liebgott, P.-P., Leroux, F., Burlat, B., Dementin, S., Baffert, C., Lautier, T., Fourmond, V., Ceccaldi, P., Cavazza, C., Meynial-Salles, I., Soucaille, P., Fontecilla-Camps, J. C., Guigliarelli, B., Bertrand, P., Rousset, M., and Léger, C. (2010) Relating diffusion along the substrate tunnel and oxygen sensitivity in hydrogenase, *Nat. Chem. Biol. 6*, 63-70.

112. Lambertz, C., Leidel, N., Havelius, K. G. V., Noth, J., Chernev, P., Winkler, M., Happe, T., and Haumann, M. (2011) O2-reactions at the six-iron activesite (H-cluster) in [FeFe]-hydrogenase, *J. Biol. Chem. 286*, 40614.

113. Kowal, A. T., Adams, M. W., and Johnson, M. K. (1989) Electron paramagnetic resonance studies of the low temperature photolytic behavior of oxidized hydrogenase I from Clostridium pasteurianum, *Journal of Biological Chemistry 264*, 4342-4348.

114. Albracht, S. P. J., Roseboom, W., and Hatchikian, E. C. (2006) The active site of the [FeFe]-hydrogenase from *Desulfovibrio desulfuricans*. I. Light sensitivity and magnetic hyperfine interactions as observed by electron paramagnetic resonance, *JBIC Journal of Biological Inorganic Chemistry 11*, 88-101.

115. Roseboom, W., De Lacey, A. L., Fernandez, V. M., Hatchikian, E. C., and Albracht, S. P. J. (2006) The active site of the [FeFe]-hydrogenase from Desulfovibrio desulfuricans. II. Redox properties, light sensitivity and CO-ligand exchange as observed by infrared spectroscopy, *J. Biol. Inorg. Chem. 11*, 102-118.

116. Kabsch, W. (2010) XDS, *Acta Acta Crystallogr D 66*, 125-132.

117. Evans, P. (2006) Scaling and assessment of data quality, *Acta Crystallogr D 62*, 72-82.

118. Vagin, A., and Teplyakov, A. (1997) MOLREP: an Automated Program for Molecular Replacement, *J. Appl. Crystallogr. 30*, 1022-1025.

119. Chen, Z. J., Lemon, B. J., Huang, S., Swartz, D. J., Peters, J. W., and Bagley, K. A. (2002) Infrared studies of the CO-inhibited form of the Fe-only hydrogenase from Clostridium pasteurianum I: Examination of its light sensitivity at cryogenic temperatures, *Biochemistry 41*, 2036-2043.

120. Bennett, B., Lemon, B. J., and Peters, J. W. (2000) Reversible Carbon Monoxide Binding and Inhibition at the Active Site of the Fe-Only Hydrogenase†, *Biochemistry 39*, 7455-7460.

121. Adamska, A., Silakov, A., Lambertz, C., Rüdiger, O., Happe, T., Reijerse, E., and Lubitz, W. (2012) Identification and Characterization of the "Super-Reduced" State of the H-Cluster in [FeFe] Hydrogenase: A New Building Block for the Catalytic Cycle?, *Angew. Chem. Int. Edit. 51*, 11458-11462.

122. Silakov, A., Kamp, C., Reijerse, E., Happe, T., and Lubitz, W. (2009) Spectroelectrochemical Characterization of the Active Site of the [FeFe] Hydrogenase HydA1 from Chlamydomonas reinhardtii, *Biochemistry 48*, 7780-7786.

123. Nicolet, Y., Rohac, R., Martin, L., and Fontecilla-Camps, J. C. (2013) X-ray snapshots of possible intermediates in the time course of synthesis and degradation of protein-bound Fe4S4 clusters, *P. Natl. Acad. Sci. U.S.A. 110*, 7188-7192.

124. Cornish, A. J., Gärtner, K., Yang, H., Peters, J. W., and Hegg, E. L. (2011) Mechanism of Proton Transfer in [FeFe]-Hydrogenase from Clostridium pasteurianum, *J. Biol. Inorg. Chem. 286*, 38341-38347.

125. Kettenhofen, N. J., and Wood, M. J. (2010) Formation, Reactivity, and Detection of Protein Sulfenic Acids, *Chem. Res. Toxicol. 23*, 1633-1646.

APPENDICES

APPENDIX A

CONSENSUS SEQUENCES FROM CHAPTER 3

>Consensus 1
GTELLTRLKKALVEKKDVALPMFTSCSPGWIKFAEHYYPEFLDNLSTCKSPQQM
FGALAK
TYYAEKIGVKPEDMVVVSIMPCTAKKFEAQRPEMNDSGVKDVDYVLTTRELAR
MIKQAGI
DFNSLPDEKFDSPLGESSGAAVIFGA
>Consensus 2
GSEFVQRFVHKKGELPLITSCCPAWVDFMEKYHEDMIPHFSTAKSPQEMMGVM
TKTYYAE
KLGKKPSEICMVSVMPCTAKKYELSRSDEMFASGAQDIDVSITTRELSRMIKQAG
IDFGT
LPDEEADSPLGMYTGAGTIFGA
>Consensus 3
AHEFLERLEKNENLPLLTSCSSGWIKFLEHFYPELIPNASTCKSPMSMMSTLLKTY
YAEK
QNIDPEKIYSVAIMPCVAKKFEAARPEHLTDEGAPYTDAVLTTRELAWMIKAYGI
DLTNL
PPEDFDTPLGFSSGAADIFGT
>Consensus 4
GTEFLKRVEKGGPFPMITTCCPAWIKMMEHFHHDLFPNMSSCKSPHEMLGILTKT
YYSKN
EGIDPKDIVVVSIMPCTAKKFESAREEMESDVDYVLTTREAARLIKDHKTDFVNL
PDGEF
DDPLGVSTGAGVIFGA

APPENDIX B

SUPPLEMENTAL MATERIAL CHAPTER 4

Figure s1. FTIR spectra of CrHydA1 H_{ox}-CO before (a), and after (b) 2 h exposure to 24.2% O_2 at 4 °C. CrHydA1 concentration 70 mg^{-1} ml^{-1}. The principle *ν*CO peaks are colored as Hox-CO (black), H_{ox} (red), O_2 damaged (purple), unassigned (cyan).

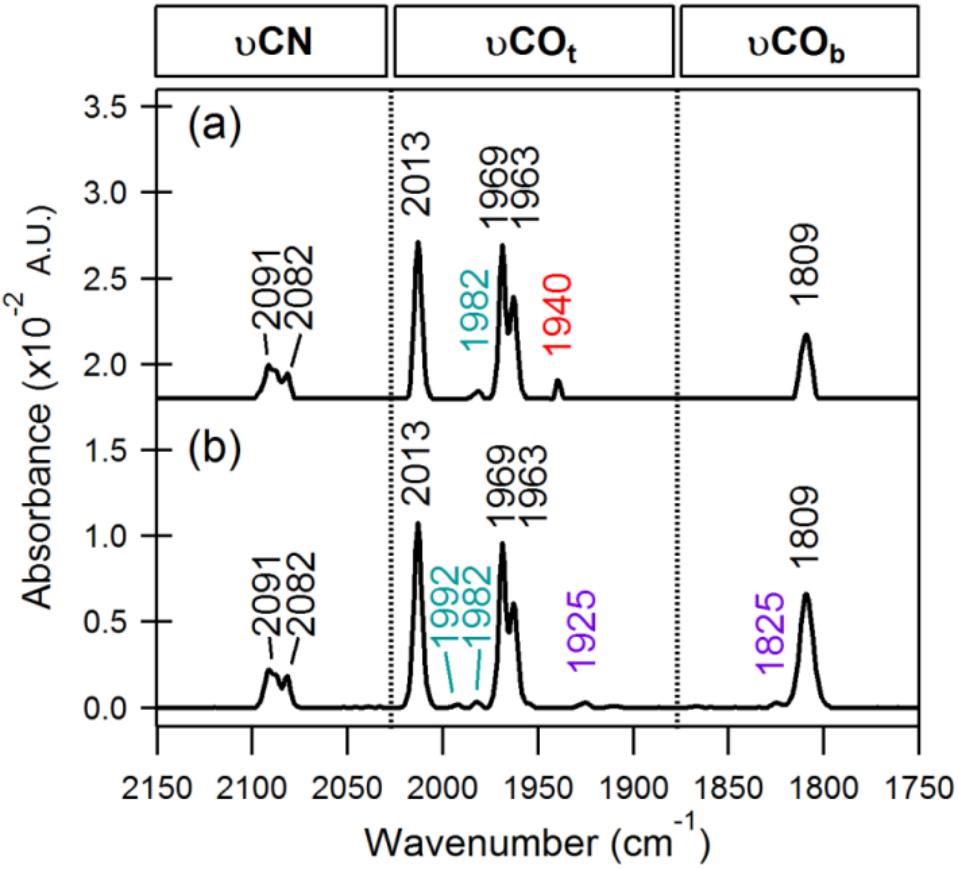

Figure S2. FTIR spectra of O_2 titration of NaDT-treated CrHydA1. (a) After 2 h of exposure to 0.002% O_2. (b) After 2 h exposure to 2% O_2. While there are additional features that may be a result of the interaction of NaDT and O_2, similar trends are observed here as seen in H_{ox} experiments. The growth of H_{ox}-CO and of signals assigned to O_2 damage, (1825 and/or 2025 cm^{-1}) are seen here. The *ν*CO and *ν*CN peaks are color-coded as; H_{ox}-CO (black), H_{ox} (red), H_{red}-DT (magenta) O_2 damaged (purple), unassigned (cyan).

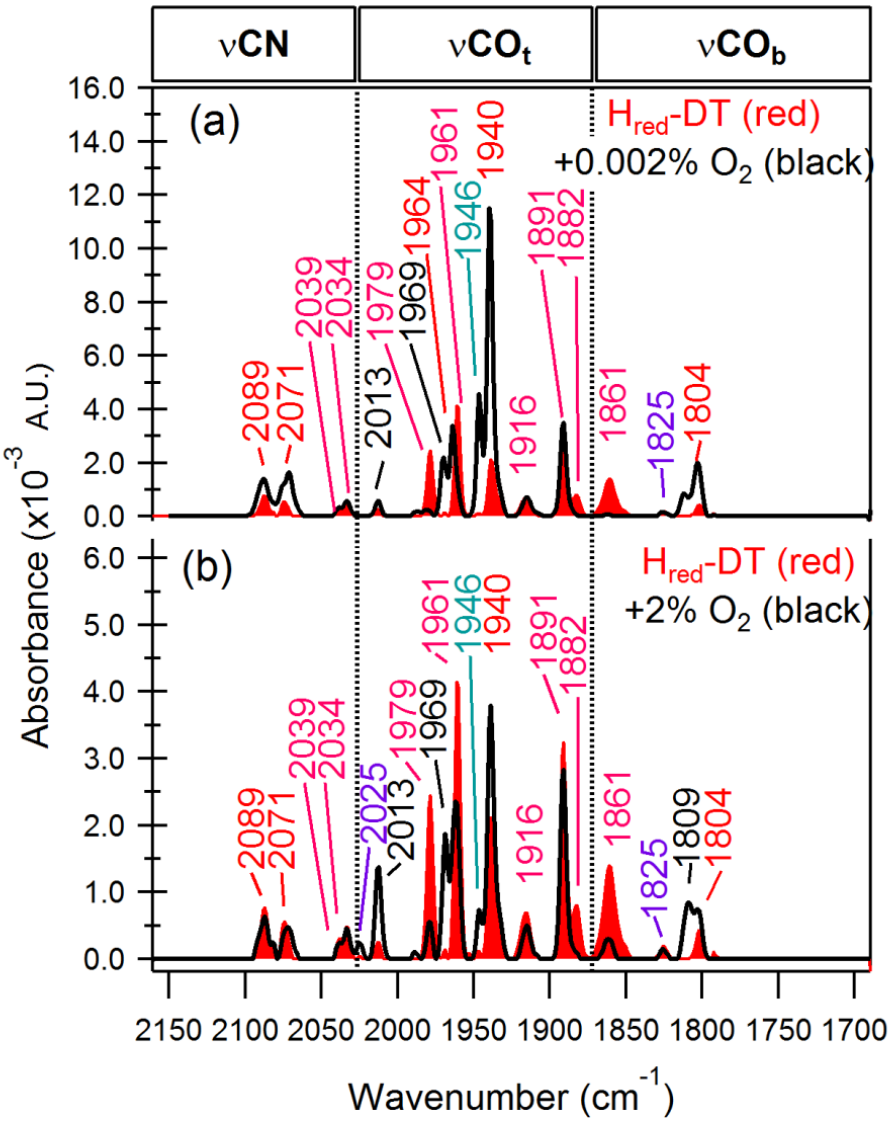

Figure S3. FTIR time-course of non-O_2 treated CrHydA1 under N2 atmosphere. CrHydA1 (59 mg mL^{-1}) was buffer exchanged by G-25 into NaDT-free buffer as described in the Experimental Section, but minus the O_2 injection. Time (min) is indicated on the right of the spectra. The increase in the H_{ox} specific 1940 cm^{-1} νCO peak along with the decrease in the H_{red} νCO peaks at 1891 and 1933 cm^{-1} indicates auto-oxidation of a small fraction of residual H_{red}.4

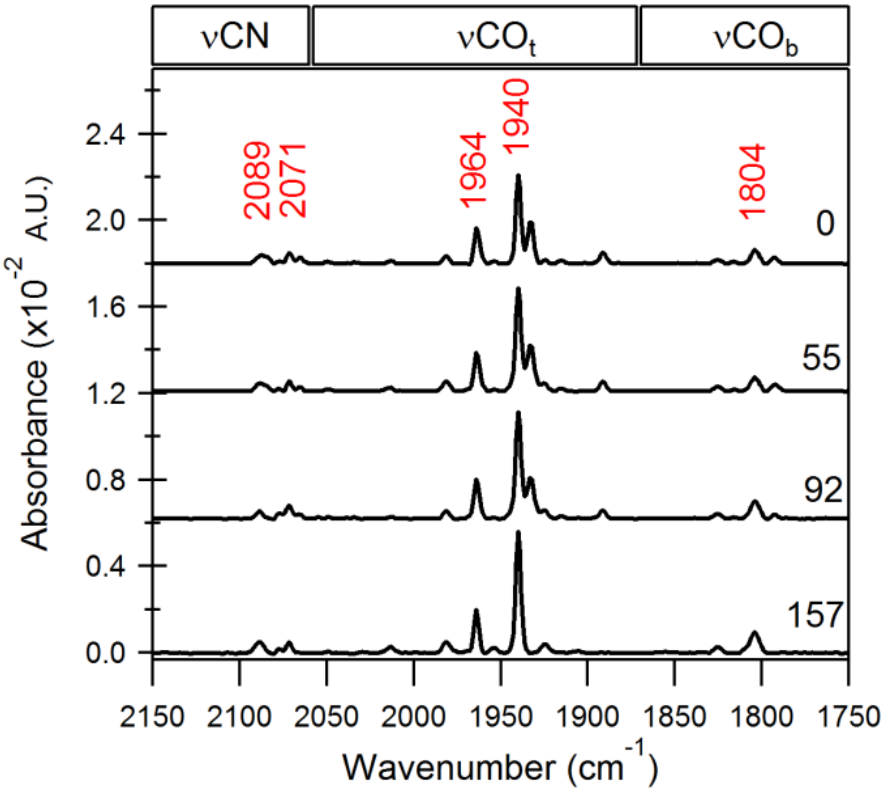

Figure S4. FTIR spectra of O_2 titration of H_{ox} CrHydA1. (a) H_{ox} CrHydA1 at 45 mg mL^{-1} (red) and after 133 min exposure to 0.01% O_2 (black), (b) H_{ox} CrHydA1 at 40 mg mL^{-1} (red) and after 120 min exposure to 1% O_2 (black), (c) H_{ox} CrHydA1 at 40 mg mL^{-1} (red) and after 120 min exposure to 10% O_2 (black).

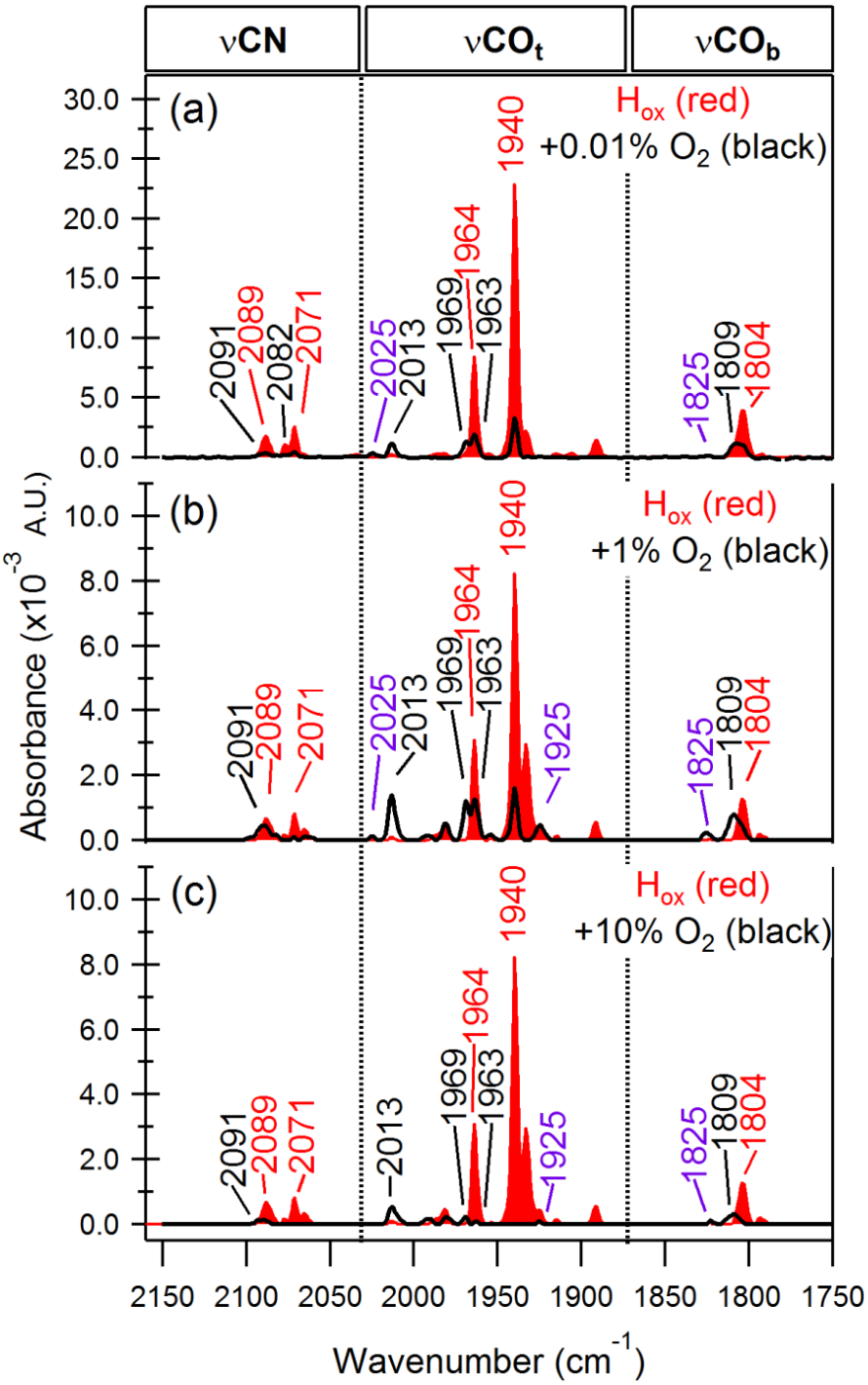

Figure S5. FTIR spectral time course of the 2Fe subcluster in CaI that was exposed to 0.28% O_2. CaI was prepared in the H_{ox} state and exposed to 0.28% O_2 at 4 °C with magnetic stirring. Aliquots were removed at the time intervals indicated on the right (in min, with increasing time from bottom to top), and analyzed by FTIR. The red dashed lines and arrows indicate the appearance of *ν*CO peaks assigned to the H_{ox}-CO state of CaI (2016 and 1807 cm^{-1}).

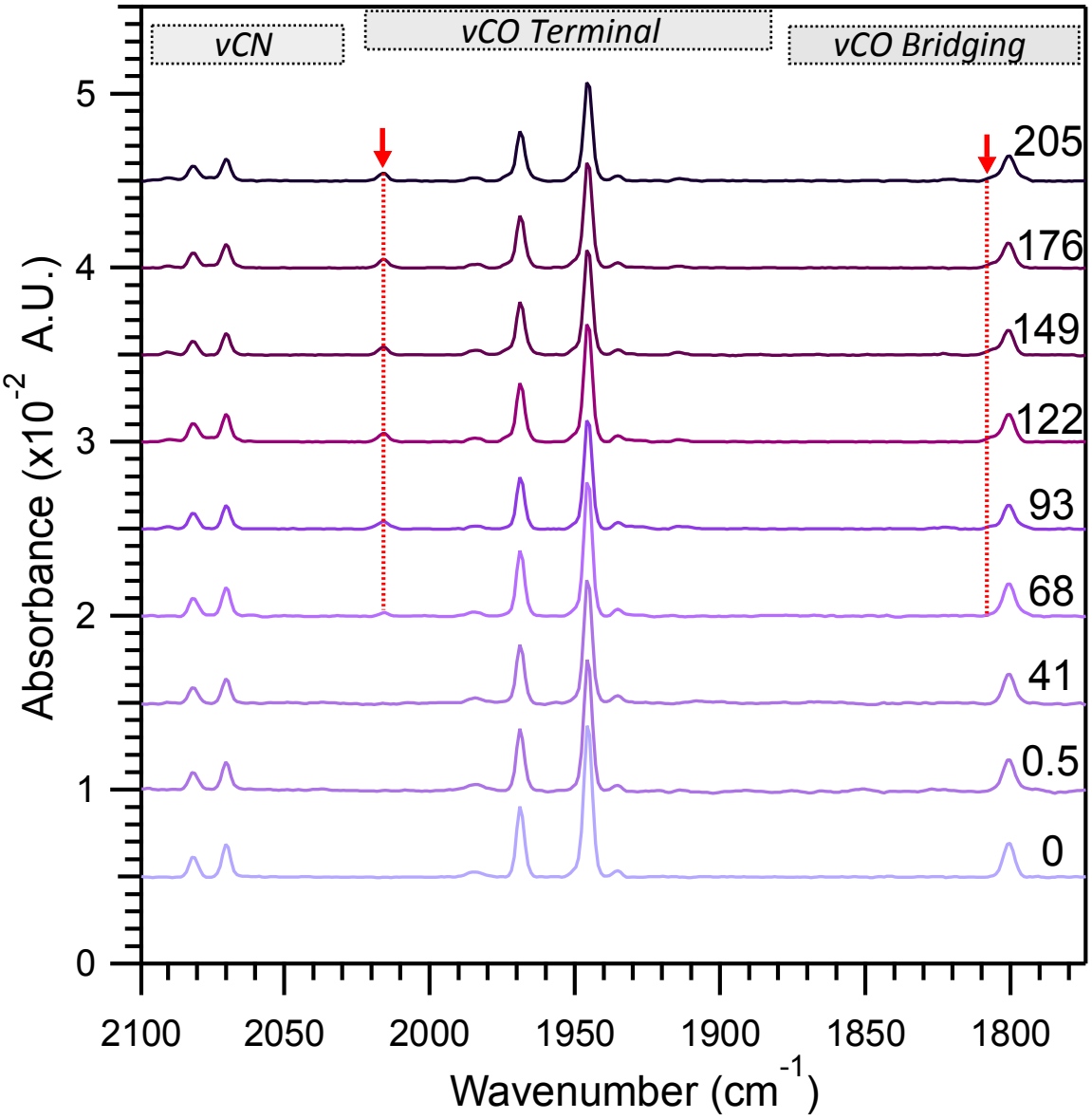

Figure S6 CrHydA1 (1o mg mL^{-1}) was exposed to ~0.1% O_2 for 2 h. The enzyme activity was monitored by gas chromatography, after the activity decayed to 50 µmol min^{-1} mg^{-1} the sample was allowed to equilibrate in an anaerobic Coy chamber for 30 min. The enzyme was then subjected to a trypsin digest and analyzed by mass spectrometry as described in the Experimental Section of the manuscript. Peptides were searched for by nonspecific cleavage, which increased coverage, likely due to fragmentation during HPLC and ionization.[1] No peptides were identified when using a nonspecific cleavage search against a non-CrHydA1 protein sequence. (a) Sequence coverage of CrHydA1 (60%) with modifications indicated at the bottom right of the coverage map. (b) Mass spectra of the peptide fragment that corresponds to sulfenic acid and site 169. (c) Annotated spectrum with alignment.

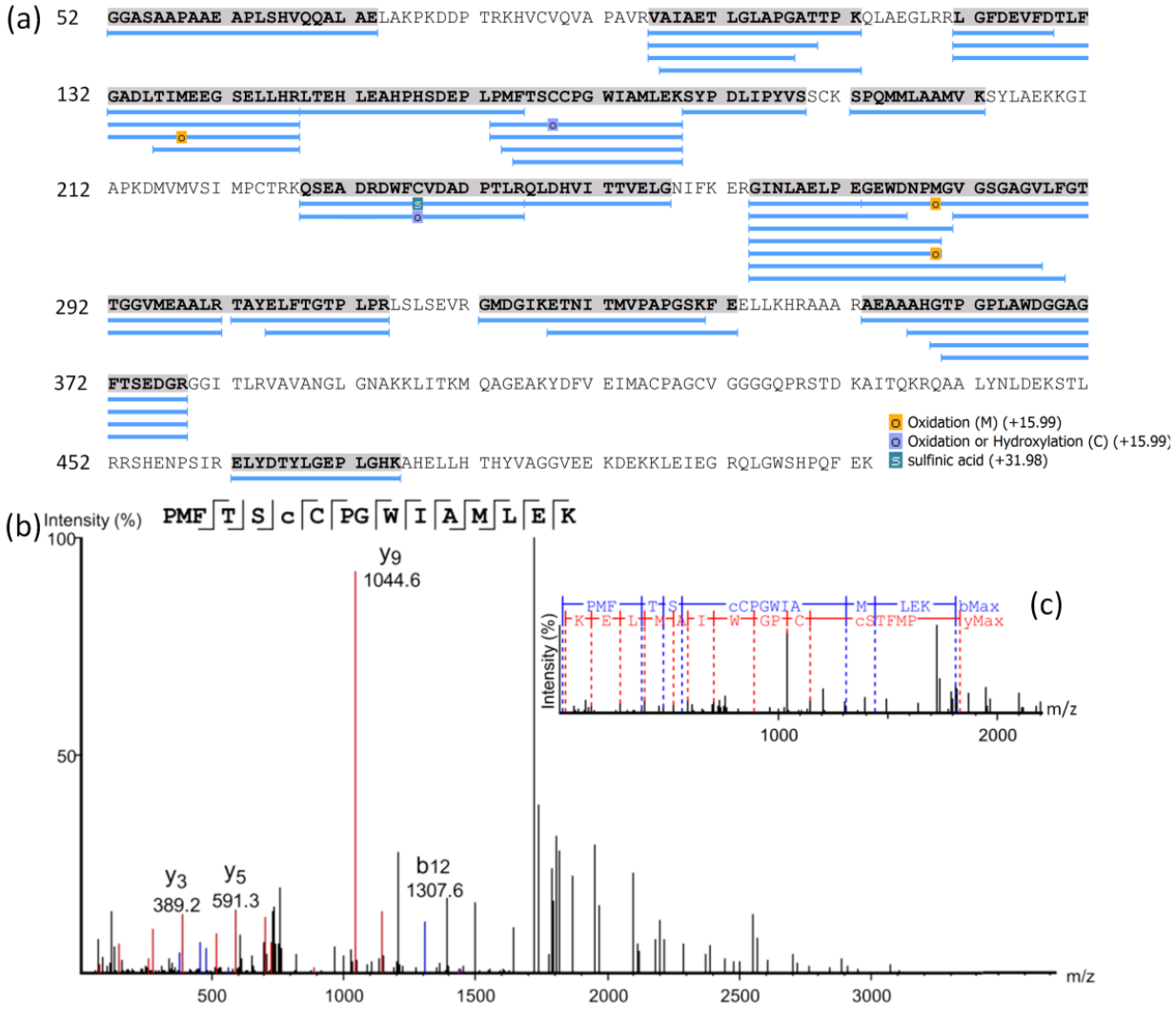

(1) König S., Zeller M., Peter-Katalinic J., Roth J., Sorg C., Vogl T. *J. Am. Chem. Soc. Mass Spectrom.* **2001**, 12, 1180

Figure s7. Titration of CrHydA1 (labeled as "HydA") with $HydF^{EG}$. Poor incorporation of 2Fe subcluster into HydF during heterologous expression in *E. coli* results in the need for large ratios of HydF to CrHydA1 to reach full activation.

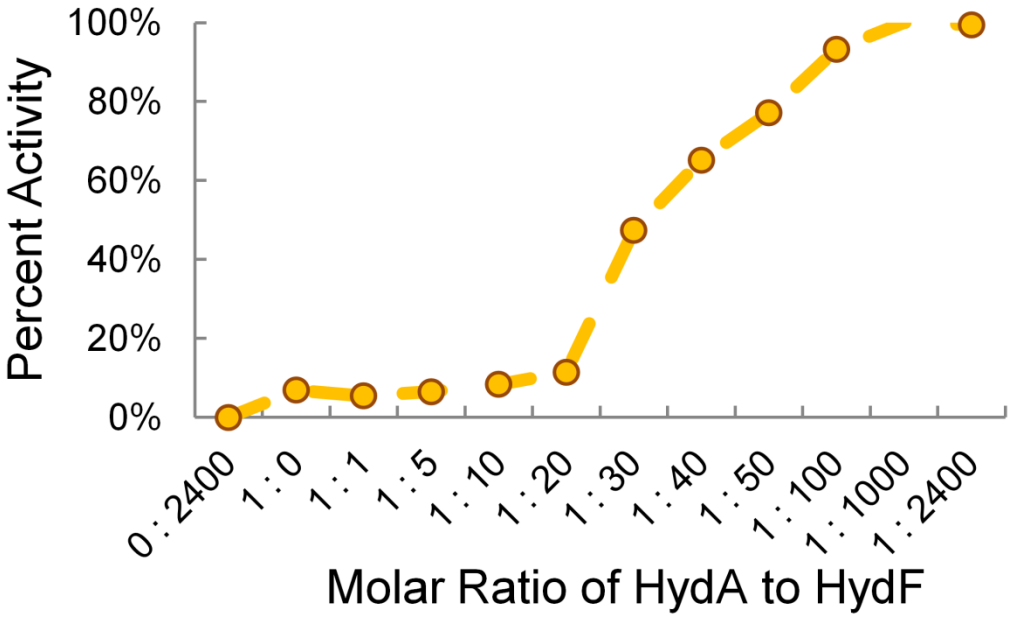

Table S1. Summary of O_2 concentrations and O2:CrHydA1 molar ratios for FTIR experiments.

Treatment	Mole ratio (O_2:CrHydA1)	Final O2 Headspace (%, SD = +/- 0.15*%)	Time (min)	Figure	Experiment
H_{ox}	0.06	0.01	133	Figures 4.2a and 4.3	FTIR
	5.07	1.02	120	Figure S4	FTIR
	50.43	10.15	120	Figure S4	FTIR
H_{ox}-CO	39.3	2.47	120	Figure 4.2b	FTIR
	392.99	24.69	120	Figure S1	FTIR
H_{red}-H_2	1.25	0.02	120	Figure 4.2c	FTIR
H_{red}-DT	0.06	0.002	120	Figure S2	FTIR
	1.25	0.05	120	Figure 4.2d	FTIR
	51.05	2.06	120	Figure S2	FTIR
H_{ox}	0.06	0.001	120	Figures 4.5b and 4.5c	UV-Vis
	1000	17	120	Figures 4.5b and 4.5c	UV-Vis
	17,647	300	180	Figures 4.5b and 4.5c	UV-Vis

Table S2. Average and standard deviation values of $\%O_2$ used for O2 treatments.

Vial	Injection volume (μ L)	[a]O2 (nmol)	[b]Molarity (mol^{-1} L^{-1} O2)	[c]pO_2 (atm)	[d]O2 %
1	50	14	3 E-04	0.0069	0.84
2	50	15	3 E-04	0.0072	0.88
3	50	12	2.4 E-04	0.0059	0.71
4	50	15	3 E-04	0.0070	0.85
5	50	19	4 E-04	0.0090	1.10
Average ± SD		15 ± 2			0.88 ± 0.14

[a] The O_2 peak area from GC was converted to nmol O2 based on a O_2 standard curve.
[b] Molarity=O2 (nmol)/injection volume (µL).
[c] pO2=nRT/V, where n/V is "molarity", T=298K.
[d] %O2=pO2/barometric pressure. Barometric pressure was 0.82 atm in Golden, CO.

Table S3. FTIR time-course fits and experimental conditions used to calculate O2 induced transitions in CaI and CrHydA1.

Enzyme	T (K)	Barometric Pressure (atm)	[a][O2]		[b]k (s^{-1})		k_{Hox} (s^{-1} µM O_2^{-1})
			%	µM	Δ1945 cm^{-1}	Δ1940 cm^{-1}	
CaI	277	0.82	0.28	3.2	1.2 x 10^{-3}		7.0 x 10^{-6}
CrHydA1	277	0.82	0.010	0.11		2.0 x 10^{-3}	3.0 x 10^{-4}
CrHydA1	277	0.82	0.13	1.49		2.1 x 10^{-2}	2.4 x 10^{-4}

[a] molar concentration = [% O_2*barometric pressure(atm)/(T(K)*0.082056)]*0.03181
[b] k (s^{-1}) = -[ln(A)/A_0)]/t (s). "A" is taken as the H_{ox} specific peak at 1945 cm^{-1} for CaI, and at 1940 cm^{-1} for CrHydA1.

Table S4. Data collection and refinement statistics for O2 exposed CrHydA1

Data Collection	**CrHydA1**
Wavelength (Å)	1.734
Unit cell parameters a, b, c (Å) α, β, γ (°)	 77.6, 71.0, 94.7 90.0, 91.9, 90.0
Space group	P 1 21 1
Resolution range (Å)	34.73-2.29 (2.241-2.29*)
Total reflections	288694
Unique reflections	45032
R-merge(%)	11 (40*)
I/σ (I)	6.6 (3.1*)
Completeness (%)	96 (87*)
Redundancy	6.4 (5.9*)

Refinement

Resolution limits (Å)	35-2.3
No of used reflections	39011
No of protein atoms	6282
R factor (%)	20.9
R free (%)	25.2
Ramachandran Favorite regions (%)	95.9
Ramachandran Allowed regions (%)	4.1
Ramachandran Outliers (%)	0.0
R.m.s. deviations from ideal values, bond lengths of refined atoms(Å)	0.019
Angels (Å)	2.09
Average B, all atoms (A^2)	49.48
Wilson B-factor (A^2)	25.6

* Values in parentheses are for the highest resolution shell.